Origin of optical properties of brown carbon aerosols

by

Sabrina Michelle Phillips

(Under the Direction of Geoffrey D. Smith)

Abstract

Light-absorbing organic material, or "brown carbon", can significantly influence the effect that aerosols have on climate, yet, the mechanism of light absorption in brown carbon aerosols is still poorly understood. In this work, charge transfer (CT) complexes are identified as a significant source of light absorption by organic compounds in aerosols. A dense manifold of these complexes, formed from interactions between alcohol and carbonyl moieties, accounts for approximately 50% of the absorption observed for water-extracted ambient particulate matter. Most likely a wide variety of CT complexes are formed as a result of a supramolecular association of self-assembling, smaller molecules, just as they are in natural humic substances, and that this gives rise to absorption that extends to red wavelengths where no other potential chromophores absorb. Bulk optical measurements were performed with difference extractions solvents, before and after chemical reduction with $NaBH_4$, pH adjustments, and photobleaching in a laboratory and with solar irradiation. Additional indices quantified the extent of similarities between brown carbon aerosols

and natural humic substances. These findings imply that light absorption by organic aerosols is governed by an interaction model, with independent and interacting chromophores both contributing to optical absorption and fluorescence. Furthermore, the environment of brown carbon chromophores can affect light absorption, and should be measured or controlled to best estimate its effect on global climate.

INDEX WORDS: organic aerosol, brown carbon, optical properties, UV-visible, absorption, fluorescence, charge transfer, reduction, $NaBH_4$, humic substances, radiative forcing, pH dependence, photobleaching

Origin of optical properties of brown carbon aerosols

by

Sabrina Michelle Phillips

University of San Diego, 2012

A Dissertation Submitted to the Graduate Faculty
of The University of Georgia in Partial Fulfillment
of the Requirements for the Degree

Doctor of Philosophy

Athens, Georgia

2017

Origin of optical properties of brown carbon aerosols

by

Sabrina Michelle Phillips

Approved:

Major Professor: Geoffrey D. Smith

Committee: I. Jon Amster
William Miller

Electronic Version Approved:

Suzanne Barbour
Dean of the Graduate School
The University of Georgia
May 2017

Acknowledgments

For their wonderful support and vested interest in my success, I thank my parents. I also wish to acknowledge several high school teachers I found particularly inspirational: my chemistry teacher Mrs. Goldsmith, English teacher Mr. McFerren, and my band instructor Mr. Nelson.

For academic advice and assistance at the University of San Diego, I thank, in particular, my research advisor, Dr. Kimberly Matulef, as well as Dr. Jeremy Kua, Dr. Debbie Tahmassebi, and Dr. Tammy Dwyer. I decided to pursue graduate studies because of their encouragement.

To my advisor, Dr. Geoff Smith, I am grateful for your trust and guidance as I pursued research at UGA. I also acknowledge my group members for their support, in particular, Joe Wiegand and Al Fischer.

Lastly, I'd like to thank my boyfriend, Dr. Justin Czerniawski. He provided endless encouragement throughout graduate school, and was always willing to edit my papers and keep me company in the lab.

Table of Contents

Chapter 1

Introduction and Literature Review

1.1 Introduction to atmospheric chemistry

The Earth's atmosphere protects life as we know it, and each layer provides a unique contribution to a global climate system. The troposphere, the lowest layer in the atmosphere, contains essentially all of the Earth's water vapor, clouds, and precipitation, which provide an important mechanism for scavenging pollutants. Stratospheric ozone is essential for life, as it shields the earth from the harmful UV rays ($\lambda < 290$ nm) of the sun and keeps the Earth warm. The Earth's climate may be affected by phenomena that occur in the troposphere and stratosphere, and thus these layers of the atmosphere are of particular interest in experimental study and climate modeling.

Certain atmospheric species can shift the balance of energy in the atmosphere. These can be naturally occurring, biogenic, or man-made, anthropogenic. Radiative forcing describes the difference in this energy balance due to the presence of clouds, gaseous compounds, and aerosol particles.[1] Positive radiative forcing represents a

warming effect resulting from an increase in energy due to absorption of irradiation, whereas negative radiative forcing represents a cooling effect caused when radiation is reflected out of the atmosphere. The current scientific understanding of perturbing species in the atmosphere is represented in Figure 1.1, which depicts the major radiative forcers in the atmosphere that arise from anthropogenic sources. CO_2, an anthropogenic greenhouse gas absorber, is the single largest contributor to climate change[2] and has a large positive radiative forcing value. Importantly, the error bars on CO_2 are small compared to the magnitude, demonstrating the high level of certainty associated with these measurements. Similarly, the uncertainties associated with other greenhouse gases are very low or negligible compared to their warming effects. This is in stark contrast to the forcing contributions of aerosols, where error associated with measurements can be as large as or even larger than the measurements themselves. In the case of mineral dust and organic carbon, these errors can make the difference between an overall warming and cooling effect.

1.2 Aerosols perturb the atmosphere

Atmospheric aerosols comprise solid and liquid particles suspended in our lower atmosphere. Their sources can be either natural or anthropogenic, and their presence has far-reaching effects on human health, climate, and environmental issues.[3] Aerosols can arise from particles directly emitted into the atmosphere or from chemical reactions that occur in the atmosphere; these are referred to as primary and secondary aerosols, respectively.[1] These particles range in diameter between ∼0.002 and ∼100 μm. The upper end of this range corresponds to the size of very fine sand, which is so

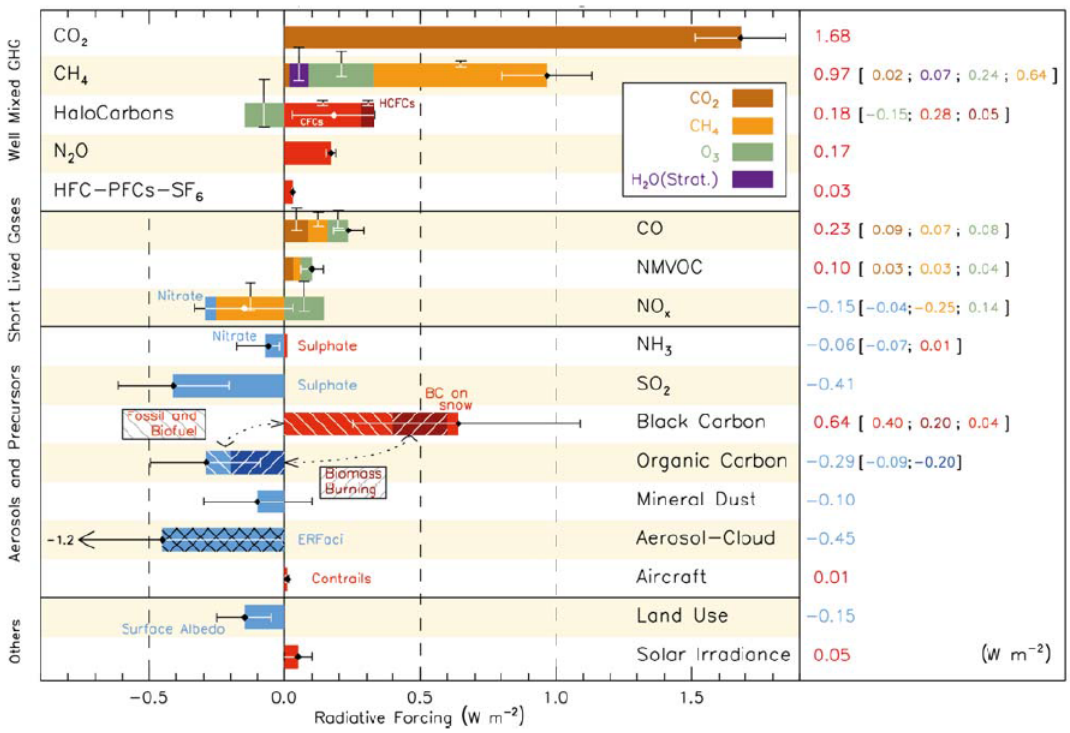

Figure 1.1: Radiative forcing bar chart: AR5 version. Reprinted from *Climate Change 2013: Physical Basis*, associated with the International Panel on Climate Change.[2]

large that these particles quickly fall out of the atmosphere and hence do not remain suspended for significant periods of time. Consequently, the most important particles with respect to atmospheric chemistry and physics are in the 0.002- to 10-μm range.[1]

Atmospheric aerosols play an important role in determining radiative forcing, the extent to which the Earth's energy budget is out of balance. Aerosol particles can both scatter and absorb UV-visible sunlight, directly affecting radiative forcing, as well as influence cloud formation, indirectly altering radiative forcing. The chemical composition of particles plays a big role in determining the magnitude, and sometimes the sign, of the effects on radiative forcing.[4] As a result, there is a need to characterize more completely the constituents responsible for scattering and, in particular, absorption.[5]

Atmospheric soot, or black carbon (BC), is a carbonaceous aerosol that has been thought of as the archetypical light absorbing aerosol for years. It originates from high temperature combustion and internal combustion engines, and it is composed of near-elemental carbon with a graphite-like structure.[6,7] Black carbon is emitted at levels of 4.3–22 Tg/yr[8] and is one of the most impactful human emissions contributing to global climate warming, with some evaluations suggesting that its impact on radiative forcing is second only to carbon dioxide.[9] Some climate models even suggest that its warming capabilities may rival those of the greenhouse gas methane.[10] Thus, there has been extensive research to assess the origins of and mechanism of absorptivity by black carbon.

1.2.1 The presence of brown carbon makes organic aerosols light absorbing

It has long been recognized that black carbon and mineral dust particles can absorb sunlight, however, internal mixing of organic constituents can alter this effect.[11] Some organic species also absorb light, further complicating estimates of radiative transfer in the atmosphere. It is clear that black carbon (BC) particles are very efficient absorbers of solar radiation, however, the role of organic carbon (OC) is much less well understood, and many climate models ignore light absorption by this fraction even though it has recently become clear that some OC does absorb light. The fraction of organic molecules that absorbs light, termed "brown carbon" (BrC), has a much more pronounced dependence on wavelength than does black carbon, absorbing UV and blue light preferentially.[4,12]

Field studies indicate that this brown carbon could be responsible for half or more of light absorption by aerosol particles at UV wavelengths[13] and could alter local gas-phase photochemistry as well as perturb radiative balance in the atmosphere. While black carbon particles are known to originate from high-temperature combustion of diesel and other fuels,[9] brown carbon particles can be formed both directly from low-temperature and incomplete combustion of biomass and fuels[13,14] and indirectly from combustion sources and biogenic organic compounds.[15–21]

Many laboratory studies have also elucidated mechanisms for the creation of light-absorbing organic species from aqueous reactions of small ketones and aldehydes with amines and ammonium salts.[20–23] Despite its importance, the chemical nature of BrC is still unclear, and the identification of specific chromophores in sam-

ples of ambient particulate matter remains incomplete, as discussed by Laskin et al.[24] and references therein. The organic aerosol fraction comprises hundreds of different species, and identifying specific chromophores responsible for the absorption exhibited by brown carbon has been challenging. Some studies have isolated nitrophenols as an important class of chromophores, though these have only accounted for 4% of measured BrC absorption.[25–27] Lin et al. were able to attribute as much as 25% of solvent-extractable absorption to nitrophenols and their derivatives and another 25% to PAH derivatives in particulate matter collected from controlled combustion of various biofuels,[28] and Desyaterik et al. attributed 48% of absorption in collected cloud water samples impacted by biomass burning to a collection of nitrophenols and aromatic carbonyls.[25] However, each of these types of chromophores exhibits little to no absorption at wavelengths longer than 450 nm whereas brown carbon absorption extends to at least 600 nm. Thus, the molecular origin of how the organic fraction absorbs light is an outstanding area of interest.

1.2.2 Brown carbon light absorption is affected by its environment

Without a more complete molecular characterization of the organic molecules constituting BrC, it is difficult to predict how its absorption spectrum might evolve in the atmosphere. For example, it may change as the particles photochemically age, the chromophores photobleach, the identities and concentrations of inorganic salts in the particles change, or the pH of the particles changes. The effect of pH, in particular, could be important as it is known to influence the physical and optical properties of humic substances,[29–34] which some fractions of ambient aerosol are

known to resemble.[35] Despite the fact that estimates of aerosol pH vary from 0 to 9 in atmospheric particles,[36–40] the effect of pH changes on BrC absorption has not been studied very much at all, and most studies do not measure, much less control, the pH of solvent-extracted filter samples.

Light absorption due to chromophores or charge transfer interactions can induce a number of photochemical intermediates and products.[41,42] The formation of these species can lead to the destruction of chromophores, and consequently charge transfer (CT) complexes, thus destroying the absorption associated with them.[43–46] This 'photobleaching' phenomenon can destroy chromophores in light-absorbing aerosols, potentially acting as a sink for brown carbon aerosols in the atmosphere.[47,48] The rate of brown carbon photobleaching has important implications in climate modeling. The absorptivity of these aerosols, and their effect on radiative forcing, can change drastically throughout their atmospheric lifetime. Photobleaching of brown carbon can be assessed through absorbance and fluorescence spectroscopy by measuring the effects of different light sources (monochromatic and polychromatic) on the spectral absorbance and light emission of collected ambient aerosols.

1.2.3 Brown carbon is like humic substances

Organic species in aerosols are diverse and complex; hundreds or thousands of organic compounds in aerosols have been identified by GCMS but these can account for only a small fraction of total organic matter in aerosols.[25–27,49–51] A substantial component of organic aerosols comprise polyacidic compounds similar to aquatic and terrestrial

humic substances (HS).[35] In fact, these aerosol species are so similar to HS that they've been called HULIS (humic-like substances).

Humic substance standards have been well studied and categorized by a number of different indices used to describe and differentiate HS by source (microbial or terrestrial in orgin) and chemical characteristics of sample.[52–59] Because of the inherent chemical complexity of dissolved organic matter (DOM) in HS, there are historically few simple chemical analyses to readily characterize samples, and consequently the aquatic community has employed absorbance and fluorescence spectra as indicators of general source and chemical characteristic of absorbing species in HS, or chromophoric dissolved organic matter (CDOM).[51,52,54–56,58–60] Variations in HS can arise from differences in precursor organic material and geochemical processes acting on HS, and these indices describe samples in terms of microbial and aromatic content, their relative molecular weight and their level of oxidation and irradiation.

1.3 Goals of this work

In chapter 2, we demonstrate for the first time that CT complexes are responsible for much of the observed absorption by the water-soluble fraction of ambient particulate matter. These complexes, which are formed from weak associations between molecules or separate parts of a single molecule, give rise to electronic transitions in the UV-visible spectrum which cannot be attributed to individual, isolated chromophores. Through a transfer of charge from a donor group, such as the hydroxyl of a hydroxy-aromatic, to an acceptor group, such as the carbonyl of a ketone or aldehyde, these complexes lead to optical transitions of lower energy than are associated

with either of the constituent groups individually. Consequently, they contribute to the long-wavelength tail of the absorption spectrum that defines brown carbon.

Chapter 3 provides further evidence for the presence of CT complexes in brown carbon using excitation-emission matrix (EEM) fluorescence spectroscopy to probe the excited states both before and after chemical reduction. We demonstrate that the observed fluorescence spectra of ambient particulate matter extracts are inconsistent with a model consisting solely of a superposition of independent chromophores. Instead, we find that a model including both direct and indirect excitation of CT complexes can explain the fluorescence spectral features. Furthermore, we find that a significant fraction of the observed fluorescence originates from the CT complexes. Finally, the data indicate that the CT complexes are not removed entirely by chemical reduction suggesting that their contribution to ambient aerosol optical properties may be even larger than previously thought.

Chapter 4 systematically examines the effect of changing pH on the magnitude and spectral shape of UV-visible absorption by water-soluble ambient brown carbon. We draw on observed similarities with the pH dependent absorption of humic substances to motivate a few plausible explanations including a link between structural changes induced by changing pH and observed absorption changes. We also explore the potential impacts of the pH dependence for the climate through simplified estimates of radiative forcing efficiency.

Chapter 5 analyzes a collection of ambient particulate matter samples using a split-filter approach in which we extract half of each filter in water and the other half in methanol. Most commonly, water is used as the extraction solvent, but it does

not extract all BrC. Organic solvents, and methanol in particular, have been found to extract even more absorption than water does, and it is believed that the water-soluble (WS) fraction of BrC is a subset of the methanol-soluble (MS) fraction.[18,61] Some studies have suggested that differences in the wavelength dependence of the two extracts indicate different classes of chromophores present.[18,27] However, relatively few studies have extracted in both solvents much less compared them systematically. Through such direct comparison we find that the WS and MS BrC spectra display many similarities but also with some important differences, including extinction by suspended insoluble particles in MS extracts, which has not previously been reported.

In Chapter 6, room-temperature absorption spectroscopy and laser photobleaching experiments provide additional evidence that brown carbon cannot arise from a superposition of the spectra of numerous independent chromophores. Photobleaching experiments have been previously conducted on SRFA and SRHA by Del Vecchio and coworkers to establish the contribution of charge-transfer complexes in the absorption spectra of HS.[62] They found that reciprocity of absorption loss was clearly violated for the HS studied. Here, ambient brown carbon samples were irradiated with a laser to selectively destroy species absorbing at specific wavelengths across the UV-visible wavelengths, using absorption spectroscopy to quantify the extent of photobleaching. These preliminary photobleaching experiments of SRFA and brown carbon showed a violation of absorption loss "reciprocity" and as such their absorption spectra must arise from a more complex mechanism.

Chapter 7 is a preliminary study of how ambient water-soluble brown carbon aerosols from Athens, GA compare to humic and fulvic acid standards using sev-

eral of the established absorbance and fluorescence indices in the humic community. This is the first time atmospheric HULIS has yet to be described by the indices created by the humic community, despite its extensive similarities to HS. Additionally, $NaBH_4$ reductions were performed on all samples to determine relative contribution of charge-transfer complexes to the UV-visible absorption of each sample.

Bibliography

[1] Finlayson-Pitts, B. J.; Pitts Jr, J. N. *Chemistry of the upper and lower atmosphere: theory, experiments, and applications*; Academic press, 1999.

[2] Stocker, T. F.; Qin, D.; Plattner, G. K.; Tignor, M.; Allen, S. K.; Boschung, J.; Nauels, A.; Xia, Y.; Bex, B.; Midgley, B. M. IPCC, 2013: Climate Change 2013: the Physical Science Basis. Contribution of working group I to the fifth assessment report of the intergovernmental panel on climate change. 2013.

[3] Jacobson, M.; Hansson, H. *Reviews of Geophysics* **2000**, 267–294.

[4] Andreae, M. O.; Gelencsér, A. *Atmospheric Chemistry and Physics* **2006**, *6*, 3131–3148.

[5] Bahadur, R.; Praveen, P. S.; Xu, Y.; Ramanathan, V. *Proceedings of the National Academy of Sciences of the United States of America* **2012**, *109*, 17366–71.

[6] Medalia, A.; Rivin, D.; Sanders, D. *Science of the total environment* **1983**, *31*.

[7] Grisdale, R. O. *Journal of Applied Physics* **1953**, *24*, 1082–1091.

[8] Bond, T. C.; Streets, D. G.; Yarber, K. F.; Nelson, S. M.; Woo, J.-H.; Klimont, Z. *Journal of Geophysical Research* **2004**, *109*, D14203.

[9] Bond, T. C. et al. *Journal of Geophysical Research: Atmospheres* **2013**, *118*, 5380–5552.

[10] Jacobson, M. Z. *Journal of Geophysical Research* **2004**, *109*, D21201.

[11] Lack, D. A.; Cappa, C. D. *Atmospheric Chemistry and Physics* **2010**, *10*, 4207–4220.

[12] Sun, H.; Biedermann, L.; Bond, T. C. *Geophysical Research Letters* **2007**, *34*, L17813.

[13] Kirchstetter, T. W.; Thatcher, T. L. *Atmospheric Chemistry and Physics* **2012**, *12*, 6067–6072.

[14] Lack, D. a.; Bahreni, R.; Langridge, J. M.; Gilman, J. B.; Middlebrook, a. M. *Atmospheric Chemistry and Physics* **2013**, *13*, 2415–2422.

[15] Hecobian, A.; Zhang, X.; Zheng, M.; Frank, N.; Edgerton, E. S.; Weber, R. J. *Atmospheric Chemistry and Physics* **2010**, *10*, 5965–5977.

[16] Nozière, B.; Dziedzic, P.; Córdova, A. *Geophysical Research Letters* **2007**, *34*, 1–5.

[17] Shapiro, E. L.; Szprengiel, J.; Sareen, N.; Jen, C. N.; Giordano, M. R.; McNeill, V. F. *Atmospheric Chemistry and Physics Discussions* **2009**, *9*, 59–80.

[18] Chen, Y.; Bond, T. C. *Atmospheric Chemistry and Physics* **2010**, 1773–1787.

[19] Zarzana, K. J.; De Haan, D. O.; Freedman, M. A.; Hasenkopf, C. A.; Tolbert, M. A. *Environmental Science & Technology* **2012**, *46*, 4845–4851.

[20] Updyke, K. M.; Nguyen, T. B.; Nizkorodov, S. a. *Atmospheric Environment* **2012**, *63*, 22–31.

[21] Powelson, M. H.; Espelien, B. M.; Hawkins, L. N.; Galloway, M. M.; De Haan, D. O. *Environmental science & technology* **2014**, *48*, 985–993.

[22] Sareen, N.; Schwier, A. N.; Shapiro, E. L.; Mitroo, D.; McNeill, V. F. *Atmospheric Chemistry and Physics* **2010**, *10*, 997–1016.

[23] De Haan, D. O.; Tolbert, M. a.; Jimenez, J. L. *Geophysical Research Letters* **2009**, *36*, L11819.

[24] Laskin, A.; Laskin, J.; Nizkorodov, S. A. *Chemical Reviews* **2015**, *115*, 4335–4382.

[25] Desyaterik, Y.; Sun, Y.; Shen, X.; Lee, T.; Wang, X.; Wang, T.; Collett, J. L. *Journal of Geophysical Research: Atmospheres* **2013**, *118*, 7389–7399.

[26] Mohr, C. et al. *Environmental science & technology* **2013**, *47*, 6316–24.

[27] Zhang, X.; Lin, Y.-H.; Surratt, J. D.; Weber, R. J. *Environmental Science & Technology* **2013**, *47*, 3685–93.

[28] Lin, P.; Aiona, P. K.; Li, Y.; Shiraiwa, M.; Laskin, J.; Nizkorodov, S. A.; Laskin, A. *Environmental Science & Technology* **2016**, *50*, 11815–11824.

[29] Ghosh, K.; Schnitzer, M. *Journal of Soil Science* **1979**, *30*, 735–745.

[30] Baes, A. U.; Bloom, P. R. *Soil Science Society of America Journal* **1990**, *54*, 1248–1254.

[31] Pinheiro, J. P.; Mota, A. M.; d'Oliveira, J. M. R.; Martinho, J. M. G. *Analytica Chimica Acta* **1996**, *329*, 15–24.

[32] Wang, Y.; Combe, C.; Clark, M. M. *Journal of Membrane Science* **2001**, *183*, 49–60.

[33] Brigante, M.; Zanini, G.; Avena, M. *Colloids and Surfaces A: Physicochemical and Engineering Aspects* **2007**, *294*, 64–70.

[34] Dryer, D.; Korshin, G.; Fabbricino, M. *Environmental Science and Technology* **2008**, *42*, 6644–6649.

[35] Graber, E.; Rudich, Y. *Atmospheric Chemistry and Physics* **2006**, 729–753.

[36] Fridlind, A. M.; Jacobson, M. Z. *Journal of Geophysical Research: Atmospheres* **2000**, *105*, 17325–17340.

[37] Keene, W. C.; Pszenny, A. A. P.; Maben, J. R.; Sander, R. *Geophysical research letters* **2002**, *29*, 1–4.

[38] Pszenny, A. A. P.; Moldanová, J.; Keene, W. C.; Sander, R.; Maben, J. R.; Martinez, M.; Crutzen, P. J.; Perner, D.; Prinn, R. G. *Atmospheric Chemistry and Physics* **2004**, *4*, 147–168.

[39] Guo, H.; Xu, L.; Bougiatioti, A.; Cerully, K. M.; Capps, S. L.; Hite Jr, J. R.; Carlton, A. G.; Lee, S. H.; Bergin, M. H.; Ng, N. L. *Atmos. Chem. Phys* **2015**, *15*, 5211–5228.

[40] Weber, R. J.; Guo, H.; Russell, A. G.; Nenes, A. *Nature Geoscience* **2016**, *9*, 1–5.

[41] Moran, M.; Zepp, R. *Limnology and Oceanography* **1997**, *42*, 1307–1316.

[42] Vecchio, R. D.; Blough, N. *Marine Chemistry* **2002**, *78*, 231–253.

[43] Moran, M.; Sheldon, W.; Zepp, R. *Limnology and Oceanography* **2000**, *45*, 1254–1264.

[44] Whitehead, R. F.; de Mora, S.; Demers, S.; Gosselin, M.; Monfort, P.; Mostajir, B. *Limnology and Oceanography* **2000**, *45*, 278–291.

[45] Reche, I.; Pace, M.; Cole, J. *Biogeochemistry* **1999**, 259–280.

[46] Skoog, A.; Wedborg, M.; Fogelqvist, E. *Marine chemistry* **1996**, *55*, 333–345.

[47] De Haan, H. *Limnology and Oceanography* **1993**, *250*, 665–669.

[48] Frimmel, F.; Bauer, H. *Science of the Total Environment* **1987**, *62*, 139–148.

[49] Liu, J.; Scheuer, E.; Dibb, J.; Ziemba, L. D.; Thornhill, K.; Anderson, B. E.; Wisthaler, A.; Mikoviny, T.; Devi, J. J.; Bergin, M. *Geophysical Research Letters* **2014**, *41*, 2191–2195.

[50] Jacobson, M. Z. *Journal of Geophysical Research* **1999**, *104*, 3527–3542.

[51] Lee, H. J. J.; Laskin, A.; Laskin, J.; Nizkorodov, S. a. *Environmental science & technology* **2013**, *47*, 5763–70.

[52] Chen, Y.; Senesi, N.; Schnitzer, M. *Soil science society of america journal* **1977**, *41*, 352–358.

[53] Mobed, J.; Hemmingsen, S.; Autry, J.; McGown, L. *Environmental science & technology* **1996**, *30*, 3061–3065.

[54] Mignone, R. a.; Martin, M. V.; Vieyra, F. E. M.; Palazzi, V. I.; de Mishima, B. L.; Mártire, D. O.; Borsarelli, C. D. *Photochemistry and photobiology* **2012**, *88*, 792–800.

[55] McKnight, D. M.; Boyer, E. W.; Westerhoff, P. K.; Doran, P. T.; Kulbe, T.; Andersen, D. T. *Limnology and Oceanography* **2001**, *46*, 38–48.

[56] Zsolnay, A.; Baigar, E.; Jimenez, M.; Steinweg, B.; Saccomandi, F. *Chemosphere* **1999**, *38*, 45–50.

[57] Korak, J. a.; Dotson, A. D.; Summers, R. S.; Rosario-Ortiz, F. L. *Water research* **2014**, *49*, 327–38.

[58] Huguet, a.; Vacher, L.; Relexans, S.; Saubusse, S.; Froidefond, J.; Parlanti, E. *Organic Geochemistry* **2009**, *40*, 706–719.

[59] Helms, J. R.; Stubbins, A.; Ritchie, J. D.; Minor, E. C.; Kieber, D. J.; Mopper, K. *Limnology and Oceanography* **2008**, *53*, 955–969.

[60] Birdwell, J. E.; Valsaraj, K. T. *Atmospheric Environment* **2010**, *44*, 3246–3253.

[61] Liu, J.; Bergin, M.; Guo, H.; King, L.; Kotra, N.; Edgerton, E.; Weber, R. J. *Atmospheric Chemistry and Physics Discussions* **2013**, *13*, 18233–18276.

[62] Vecchio, R. D.; Blough, N. *Environmental science & technology* **2004**, 3885–3891.

Chapter 2

Light Absorption by Charge Transfer Complexes in Brown Carbon Aerosols[1]

[1]Sabrina M. Phillips, and Smith, Geoffrey D. *Environ. Sci. Technol. Lett.*, **2014**, 1, 382-386. Reproduced with permission from The American Chemical Society.

2.1 Abstract

Recently it has become apparent that the organic fraction of ambient aerosols absorbs UV-visible light with a potential impact on climate. It is believed that this light-absorbing, sometimes called "brown", carbon originates from biomass and biofuel burning and could be formed through secondary processes in particles or clouds. Here, we identify for the first time charge transfer (CT) complexes as a significant source of light absorption by organic compounds in aerosols. A dense manifold of these complexes, formed from interactions between alcohol and carbonyl moieties, accounts for approximately 50% of the absorption (300 nm - 600 nm) observed for water-extracted ambient particulate matter. Corresponding fluorescence emission spectra with broad, overlapping long-wavelength tails are consistent with efficient energy transfer amongst a near-continuum of such coupled excited states. We postulate that a wide variety of CT complexes are formed as a result of a supramolecular association of self-assembling, smaller molecules, just as they are in natural humic substances, and that this gives rise to absorption that extends to red wavelengths where no other potential chromophores absorb. These findings imply that light absorption by organic aerosols is governed by a combination of independent as well as interacting chromophores and that both must be included in an accurate representation of aerosol optical properties.

2.2 Introduction

Organic molecules in atmospheric aerosol particles can be significant absorbers of ultraviolet (UV) and visible light.[1,2] Unlike black carbon particles which absorb strongly throughout the UV-visible spectrum, the organic fraction of aerosols has a much more pronounced wavelength dependence increasing exponentially with decreasing wavelength giving rise to the term "brown carbon."[3] Field studies indicate that this brown carbon could be responsible for half or more of light absorption by aerosol particles at UV wavelengths[4] and could alter local gas-phase photochemistry as well as perturb radiative balance in the atmosphere.[5] While black carbon particles are known to originate from high-temperature combustion of diesel and other fuels,[6] brown carbon particles can be formed both directly from low-temperature and incomplete combustion of biomass and fuels[4,7] and indirectly from combustion sources and biogenic organic compounds.[2,8–13]

The chemical characterization of brown carbon has proven to be difficult and remains incomplete.[14] The organic aerosol fraction comprises hundreds of different species, and identifying specific chromophores responsible for the absorption exhibited by brown carbon has been challenging. Jacobson suggested that nitroaromatic species in aerosols could absorb light,[15] and several groups have since detected them[16–18] and been able to attribute as much as 4% of observed brown carbon absorption to them as a class.[17,18] Others have demonstrated that condensation reactions involving ammonia, amines or amino acids, and various aldehydes produce products that could be responsible for as much as 10% of brown carbon UV-visible

absorption.[13,19] However, each of these types of chromophores exhibits little to no absorption at wavelengths longer than 450 nm,[13,17–19] whereas brown carbon absorption extends to at least 600 nm.[1,2] Thus, the molecular origin of how brown carbon absorbs light is an outstanding area of interest.

Here, we demonstrate for the first time that charge transfer (CT) complexes are responsible for much of the observed absorption by the water-soluble fraction of ambient particulate matter. This fraction has been found to constitute approximately $20 - 50\%$ of the total (methanol-extracted) BrC absorption depending on wavelength.[17] These CT complexes, which are formed from weak associations between molecules or separate parts of a single molecule, give rise to electronic transitions in the UV-visible spectrum that cannot be attributed to individual, isolated chromophores. Through a transfer of charge from a donor group, such as the hydroxyl of a hydroxy-aromatic, to an acceptor group, such as the carbonyl of a ketone or aldehyde (Figure 2.1), these complexes lead to optical transitions with energies lower than those of the transitions of the individual constituent groups. Consequently, they contribute to the long-wavelength tail of the absorption spectrum that defines brown carbon.

2.3 Materials and Methods

2.3.1 Aerosol Collection

Ambient aerosols were collected out of a window in the Chemistry Building at the University of Georgia (∼20 m above ground level) in Athens, GA (33.9488°N, 83.3747°W) from January 2014 to March 2014. A total of 10 samples were collected

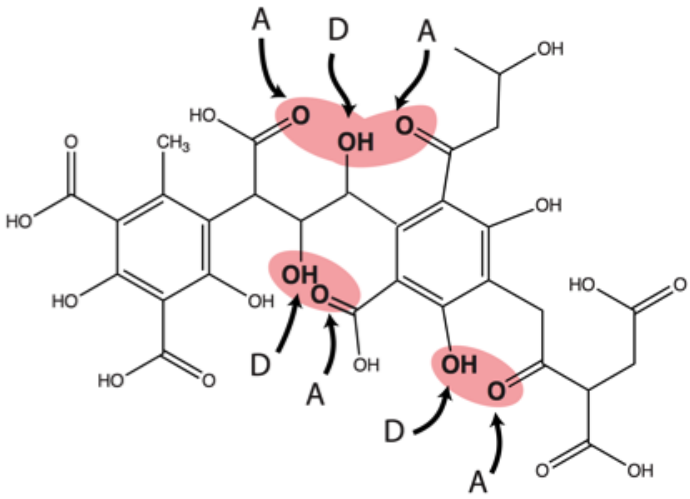

Figure 2.1: Hypothetical structure for a representative humic acid molecule or fragment. Charge transfer complexes formed from interactions between donor (D) and acceptor (A) groups are indicated by the red shaded regions.

on polytetrafluoroethylene (PTFE, Teflon) filters (0.2 μm pore size, Sterlitech) at a rate of 16.7 L/min for 10 separate 24 h ($\pm$1 h) periods. A very sharp cut cyclone inlet (BGI, Inc.) was employed to size select for particles with diameters of $< 2.5\mu$m. Water-soluble organic species were then extracted in a manner similar to that described by Hecobian et al.[2] by sonication of the filter for 20 min in 10 mL of Milli-Q water ($< 18.2M\Omega \cdot cm$). Extracted solutions were filtered using a 0.45 μm PTFE disposable syringe filter and adjusted to pH 7 with NaOH because the magnitude of the absorption spectra was pH-dependent (Figure 2.6). More details about the samples collected, including calculated back trajectories, are included in Table 2.1.

2.3.2 Summary of Ambient Samples

Despite the largely rural environment surrounding Athens, GA, the air masses sampled were probably influenced by sources typical of both urban and rural sites as Athens is only 70 miles east (and often downwind) of Atlanta. Of the 10 samples collected in this work, seven arrived in Athens from a westwardly direction (see Table 2.1) as determined from back trajectory analysis conducted using the NOAA Air Resources Laboratory's HYSPLIT model online . Also shown in Table 2.1 are the absorbance measured at 365 nm (extracted in 10 mL of water), the absorption Ångström exponent (AAE) derived from a power law fit to the extract absorption spectrum and the percentage absorption loss measured after reduction by $NaBH_4$ over the 300-600 nm region. These AAE values are lower than those measured by Hecobian et al.[2] for sites in Atlanta, GA in which AAE ranged from 6 to 8, though no obvious reason for the difference could be determined. PM 2.5 mass concentra-

Table 2.1: Summary of aerosols samples collected and Suwannee River Fulvic Acid (SRFA) standards. All aerosol samples were taken in Athens, GA at a volume flow rate of 16.7 SLPM (standard liters per minute).

Date	Abs (365 nm) (cm^{-1})	AAE (300-600 nm)	R^2 (AAE fit)	% Abs loss (300-600 nm)	PM 2.5 ($\mu g/m^3$)	Air mass source direction
1/20/2014 - 1/21/2014	0.0085	4.38	0.997	47.8	7.3	WSW
1/21/2014 - 1/22/2014	0.0034	6.36	0.988	31.3	7.0	NNW
2/2/2014 - 2/3/2014	0.0224	4.38	0.996	62.8	3.2	SSW
2/6/2014 - 2/7/2014	0.0525	4.07	0.987	56.6	13.0	N
2/9/2014 - 2/10/2014	0.0400	5.21	0.996	38.7	10.5	WNW
2/13/2014 - 2/14/2014	0.0318	4.17	0.997	57.5	6.7	W
2/16/2014 - 2/17/2014	0.0195	4.70	0.997	83.0	6.1	NW
2/17/2014 - 2/18/2014	0.0200	4.57	0.999	64.8	8.6	NW
2/20/2014 - 2/21/2014	0.0304	4.91	0.992	52.0	15.5	S
3/6/2014 - 3/7/2014	0.1385	4.96	0.999	49.0	6.2	NE
SRFA 1	0.1882	5.90	0.991	40.4	N/A	N/A
SRFA 2	0.1925	5.89	0.992	40.4	N/A	N/A

tions for a site three miles away as reported by the Georgia Department of Natural Resources (http://www.air.dnr.state.ga.us/amp/) are also listed.

2.3.3 Reduction

Reductions were adapted from the protocol detailed by Ma et al.[20] Extracted aerosol solutions and 50 mg/L aqueous Suwannee River fulvic acid (SRFA) (International Humic Substances Society) solutions were reduced in a 1 cm quartz cuvette (3 mL) by

adding approximately 5 mg of solid $NaBH_4$ and dissolving it by stirring. Reduction proceeded until no further change in absorbance was noticed (25 min). Because of an excess of $NaBH_4$, the pH of the solution increased to 10. The solution was readjusted to pH 7 with HCl before optical absorption spectra were recorded on a Cary 60 spectrophotometer (Agilent) over a range of 200-800 nm. Fluorescence spectra were recorded on a FluoroLog 2 fluorometer (Horiba) over an excitation range of 280-450 nm scanned in 10 nm steps.

The $NaBH_4$ reduction procedure was assessed for reproducibility on standardized SRFA to isolate for variability in ambient aerosol samples (Figure 2.2). Averaged absorbance loss for five SRFA samples after reduction was 35.85 $\pm$ 4.19 (300-600 nm).

2.4 Results and Discussion

2.4.1 Absorption Loss Accompanies Removal of Charge Transfer Complexes

While CT complexes have never before been identified in ambient aerosols, they have been suggested to be responsible for the absorption observed in a model aerosol system[21] as well as in aquatic and terrestrial humic substances.[22,23] In particular, Blough and co-workers have used a variety of methods to confirm the presence of CT complexes in aquatic humic substances, including chemical reduction to eliminate them[20] and excitation-emission matrix (EEM) fluorescence spectroscopy to learn more about the CT states.[20,22,24] Here, we use these same methods with ambient aerosol extracts.

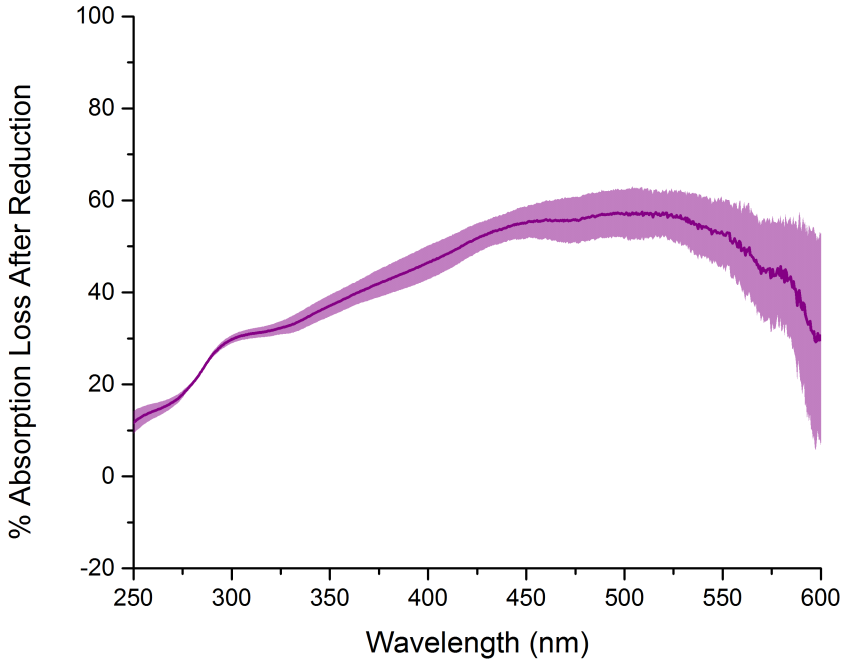

Figure 2.2: $NaBH_4$ reduction on five averaged SRFA samples with the shaded region representing standard deviation.

We used $NaBH_4$ to reduce carbonyl functional groups in ketones and aldehydes, likely electron acceptors in CT complexes, to the corresponding alcohols. Importantly, $NaBH_4$ does not reduce other moieties that have been proposed to be responsible for absorption of visible light, including extended aromatic or highly conjugated systems as well as heteroaromatic structures.[20] Absorption spectra of a typical aqueous extract of ambient particulate matter before and after reduction are shown in Figure 2.3a, with the absorbance loss in the inset representing the collective absorption spectrum of the CT complexes removed upon reduction. For comparison, we performed the same reduction on Suwannee River fulvic acid (SRFA), a standard commonly used to represent natural humic substances (Figure 2.3b). The similarities in the near-exponential shapes of the spectra and the absorbance losses after reduction suggest that these two different types of substances, one atmospheric and one aquatic, could share a common chemical explanation for light absorption, i.e., CT complex formation.

Figure 2.4 shows the average percent absorption loss spectrum for ambient aerosol samples collected on 10 different days over 7 weeks showing that absorption loss starts abruptly at $\sim$275 nm, increases to $\sim$65% at 450 nm, and then decreases to 40% at 600 nm. Despite the small absorption at wavelengths above 500 nm, a sizable fractional loss due to reduction is observed. Over the 300-600 nm region of the spectrum, there is an average loss of 53% of the absorption by water-soluble ambient particulate matter that can be attributed to CT complexes. We postulate that there is a near continuum of such CT states that gives rise to the observed monotonically decreasing

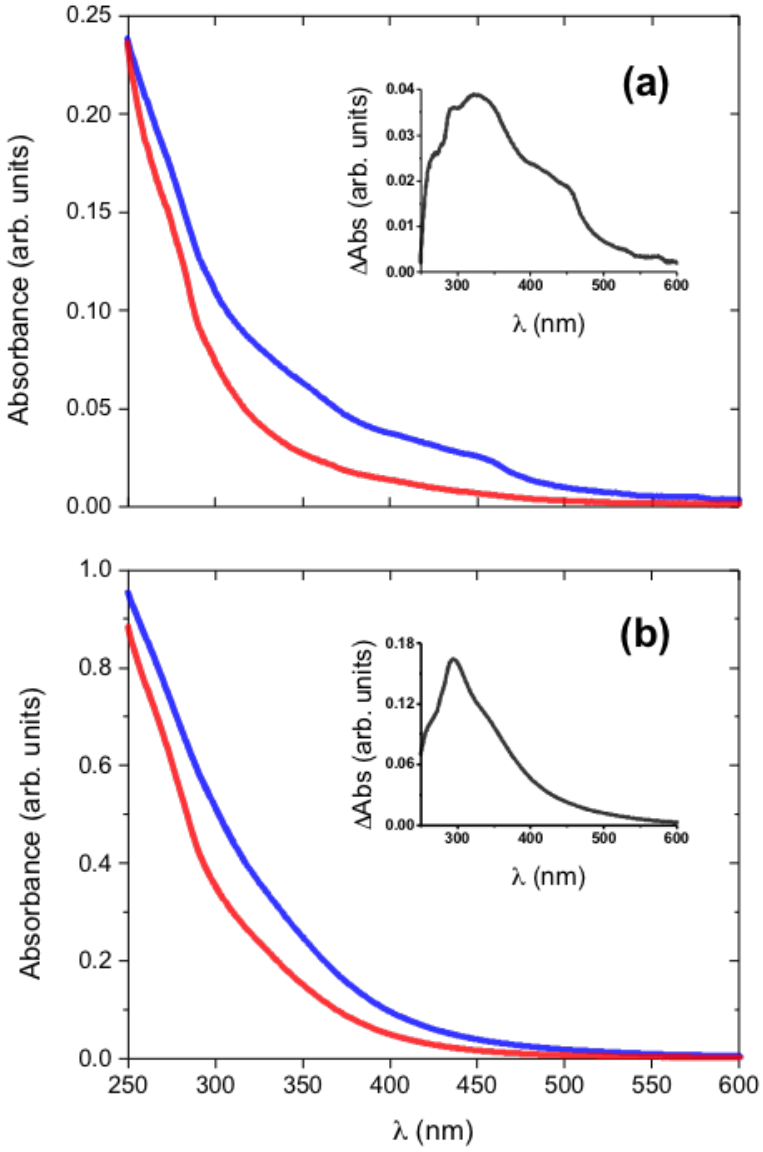

Figure 2.3: Absorption spectra of aqueous solutions of (a) an ambient aerosol extract and (b) Suwannee River Fulvic Acid prior to (blue lines) and after (red lines) reduction by $NaBH_4$. Insets show absorption loss after reduction as a function of wavelength.

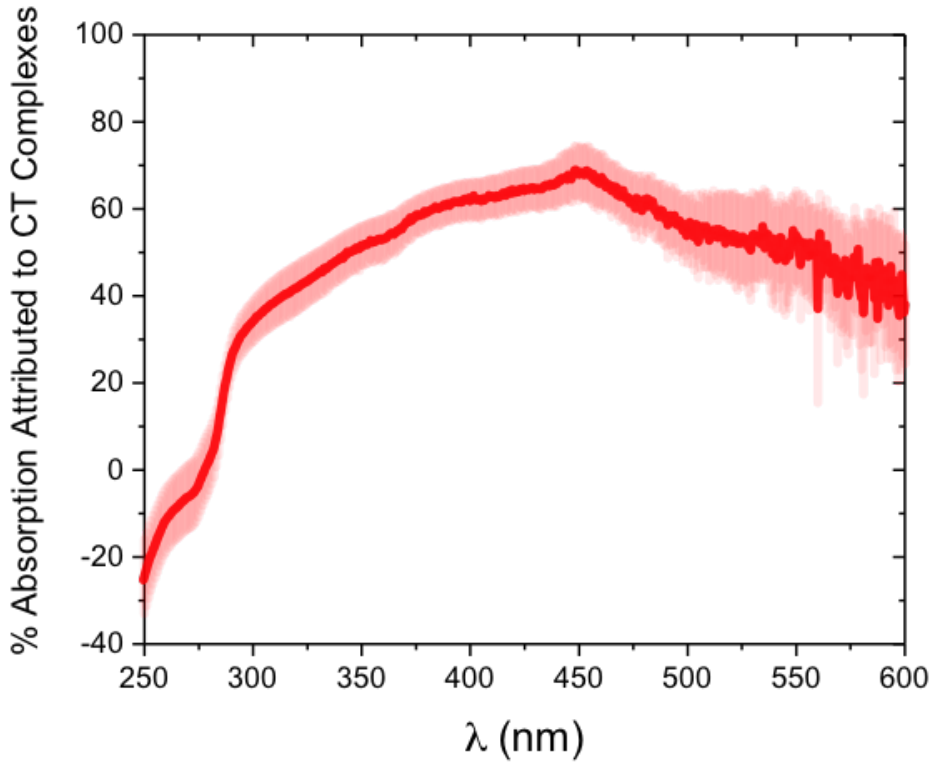

Figure 2.4: The average percentage absorption loss of ten ambient aerosol extracts after reduction by $NaBH_4$. The light red area represents the uncertainty as ± the standard error of the mean.

absorption spectra extending to the red wavelengths, just as Blough and co-workers have suggested for natural humic substances.[20,22,24]

2.4.2 Fluorescence Spectra Indicate a Large Number of Coupled Excited States

We also recorded EEM fluorescence spectra of the ambient samples and SRFA (Figure 2.5). In each case, we observed broad, unstructured emission with substantial Stokes shifts of ∼100 nm. Also of note is the fact that the long-wavelength tails of the emission spectra all fall within a single envelope independent of excitation wavelength, λ_{exc}, which is evident in the insets of Figure 2.5. Such overlap suggests that there is a dense set of excited (fluorescing) states that are coupled to each other,[21,22] allowing the lower-energy excited states to be reached by excitation of a variety of higher-energy excited states followed by energy transfer.

It is also interesting to note that the peak emission wavelength, λ_{em}^{max}, is nearly constant (430 nm for the ambient sample, 450 nm for SRFA) for short-wavelength excitation and then increases at longer-wavelength excitation (λ_{exc} <330 nm for the ambient sample and λ_{exc} <350 nm for SRFA). These two regions are represented by the arrows in the EEM plots of Figure 2.5. The correlation between λ_{em}^{max} and λ_{exc} is unusual because fluorescence generally originates from emission by the lowest-energy excited state, and therefore, the wavelength of emission is not determined by the wavelength of excitation as long as $\lambda_{em} \geq \lambda_{exc}$. The continuous red shift of λ_{em}^{max} indicates the existence of a large number of fluorescing states with an increasingly smaller subset of states accessible as λ_{exc} increases. We interpret this near continuum of states as likely to consist of a variety of excited CT complexes just as Blough and co-workers did in their studies of SRFA and other natural humic substances.[22]

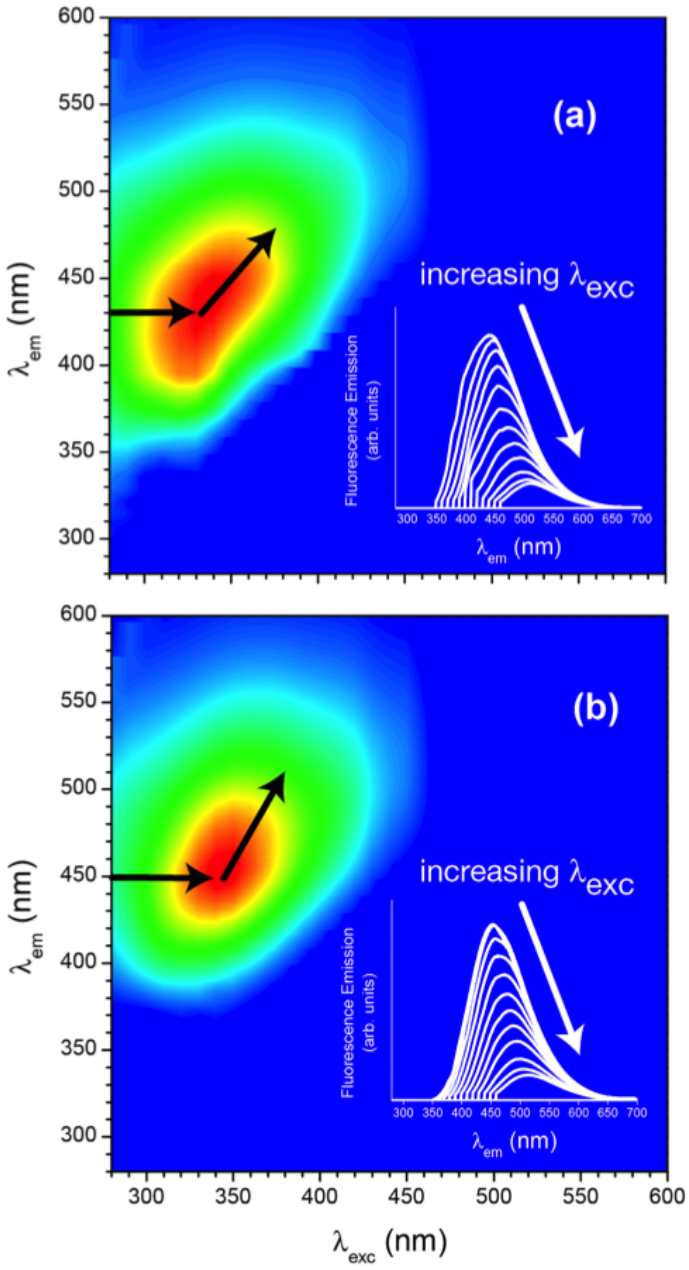

Figure 2.5: Fluorescence excitation-emission matrix (EEM) spectra of (a) an aqueous ambient aerosol extract and (b) an aqueous solution of Suwannee River Fulvic Acid. Arrows indicate the trends of constant and then increasing λ_{em}^{max} with increasing λ_{exc}. Insets show fluorescence spectra with λ_{exc} = 340 nm 450 nm (every 10 nm).

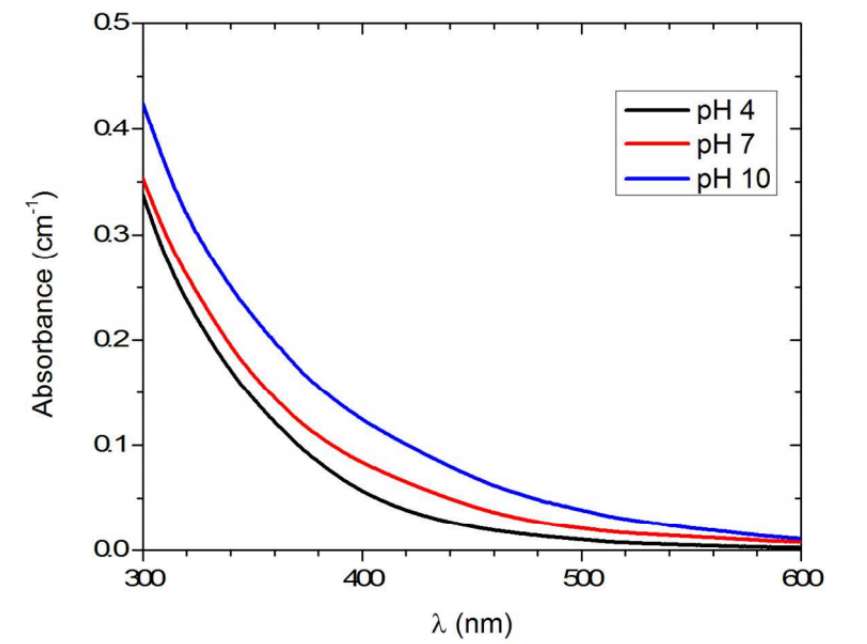

Figure 2.6: Absorption spectra of water extracts of ambient particulate matter collected 3/6/14 - 3/7/14 in Athens, GA at pH 4, pH 7 and pH 10.

2.4.3 pH Dependence of Particulate Matter Absorption

We found that the absorption spectra of the collected ambient particulate matter extracted in water were dependent on pH (example shown in Figure 2.6). Therefore, in order to make comparisons of absorption before and after reduction by $NaBH_4$ meaningful, we adjusted the pH to 7 using NaOH (to raise it) and HCl (to lower it). Also, the pH increases to approximately 10 when the $NaBH_4$ is added, thereby necessitating a readjustment.

The origin for the observed increase in absorbance when the pH is raised is not obvious. However, it is consistent with the potential strengthening of CT complexes as a result of phenol deprotonation, as has been pointed out by Sharpless and Blough[25] for aquatic humic substances. They argue that phenolate ions formed at higher pH values are better electron donors than their phenol analogues.[26] With a pKa of ∼10 for many phenols and substituted phenols,[27] it seems plausible that our ambient particulate extracts might also contain CT complexes containing phenol moieties as electron donors. And, as Sharpless and Blough pointed out, the pH effect on the spectrum is not simply a result of a red shift accompanying the deprotonation of the phenol because that effect would be limited to the UV portion of the spectrum.[25] Additionally, such pH dependence is not expected for conjugated systems, quinones or extended aromatic systems, other possible chromophores.

2.4.4 Effect of $NaBH_4$ on nitroaromatic species

The $NaBH_4$ used to carry out the reductions of ambient aerosol extracts is not expected to react with many of the functional groups and classes of molecules suspected as being responsible for light absorption by brown carbon. In particular, it should not react with nitroaromatic species which have been found to contribute to ambient aerosol absorption.[16–18] To confirm this lack of reactivity, we added $NaBH_4$ to aqueous solutions of three nitroaromatic species which have been identified in ambient samples by Zhang et al.,[17] Mohr et al.[18] and Desyaterik et al.[16]: 4-nitrophenol, 4-nitrosalicylic acid and 4-nitrocatechol. The absorption spectra of these compounds with and without addition of $NaBH_4$ are shown in Figure 2.7.

Neither the 4-nitrophenol spectrum (Fig. 2.7a) nor the 4-nitrosalicylic acid spectrum (Fig. 2.7b) show a significant change in the presence of $NaBH_4$. However, the 4-nitrocatechol spectrum shows what appears as a decrease in absorption of approximately 50% at λ >400 nm after addition of $NaBH_4$. This decrease could be interpreted as resulting from reaction with the $NaBH_4$, though it is not clear how the two species would react. Alternatively, the $NaBH_4$ may be inducing a blue shift of the 4-nitrocatechol spectrum with the peak shifting from 425 nm to 380 nm. In fact, such a shift has been noted for 4-nitrocatechol in a Borax buffer (disodium tetraborate, $Na_2B_4O_7$).[28] To test this possibility, we added Borax to the 4-nitrocatechol solution (Fig. 2.8) and observed a blue shift of the spectrum (peak shift from 425 nm to 385 nm) in almost exactly the same manner observed upon addition of $NaBH_4$ (Fig. 2.7c).

We believe that the similar effects observed for the Borax and the $NaBH_4$ solutions result from the similarity in the hydrated species; $NaBH_4$ reacts with water to form boron oxides[29] which are similar to the hydrated form of Borax, $Na_2[B_4O_5(OH)_4](8H_2O)$. These boron oxides can interact with the 4-nitrocatechol thereby shifting the absorption spectrum (Fig. 2.7c). Why, then, aren't the spectra of 4-nitrophenol (Fig. 2.7a) and 4-nitrosalicylic acid (Fig. 2.7b) affected similarly? The answer likely lies in the fact that at pH = 7 a significant fraction of the 4-nitrocatechol exists in its singly-deprotonated form since its pKa = 6.78[30]. This 4-nitrocatecholate ion possesses an intramolecular hydrogen bond involving the -O- and -OH moieties[31] that is destabilized in the presence of the boron oxides present from the addition of either $NaBH_4$ or Borax. This disruption of the hydrogen bond results in a blue shift of the absorption.

No such hydrogen bond is formed by deprotonated 4-nitrophenol or 4-nitrosalicylic acid, and consequently no effect from the addition of $NaBH_4$ is observed in those spectra (Figs. 2.7a,b).

To what extent, then, could the boron oxides affect the absorption spectra of our collected ambient aerosols? We added Borax to several of the filter samples and found that there was a negligible influence on the spectra (Fig. 2.9). Consequently, we conclude that the decrease in absorption of the ambient samples we observe (Figs. 2.3, 2.4) does not result from the boron oxides formed when $NaBH_4$ reacts with water. Therefore, the decrease is, in fact, due to the reduction of the sample. Furthermore, since we observed a sizable shift in the absorption spectrum of 4-nitrocatechol (Fig. 2.7c) upon addition of Borax but not of the ambient samples, we conclude that little, if any, of the ambient sample absorption can be attributed to 4-nitrocatechol. Its possible that other nitro-aromatic species contribute to the ambient sample absorption, but these are not reduced by $NaBH_4$ and therefore are not responsible for the decrease in absorption upon reduction.

2.4.5 CT Model for Aerosol Absorption and Atmospheric Implications

Given the observed similarities between ambient aerosol extracts and SRFA, it seems reasonable that they would share a common origin of light absorption. Furthermore, the ubiquitous nature of humic-like substances in aerosols[32,33] and the prevalence of functional groups (carbonyls and alcohols) responsible for CT complex formation in them suggest that the CT model put forth by Blough and co-workers to explain

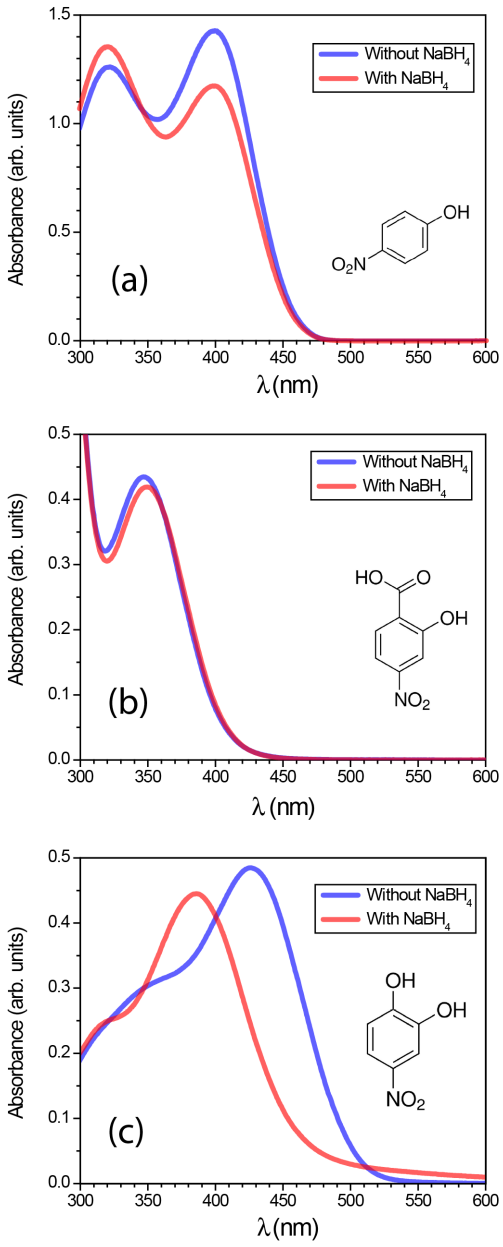

Figure 2.7: Absorption spectra of aqueous solutions of nitro-aromatic compounds with (red curves) and without (blue curves) addition of NaBH4: (a) 4-nitrophenol, (b) 4-nitrosalicylic acid, (c) 4-nitrocatechol.

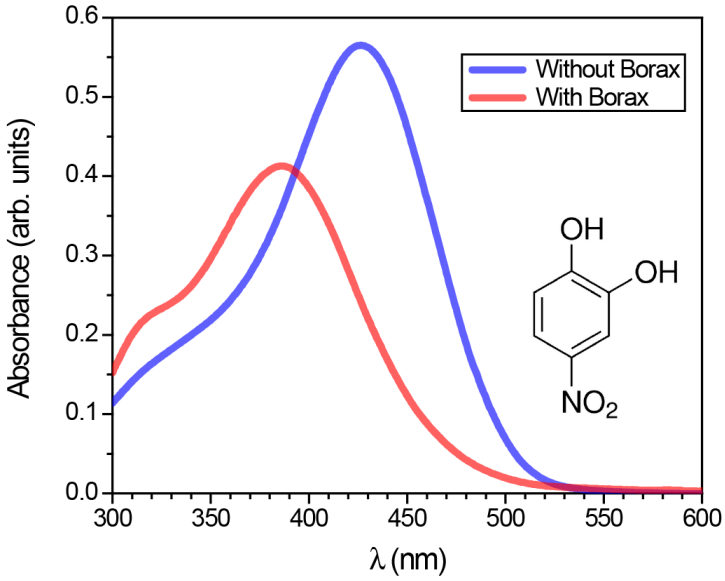

Figure 2.8: Absorption spectrum of 4-nitrocatechol with (red curve) and without (blue curve) addition of Borax.

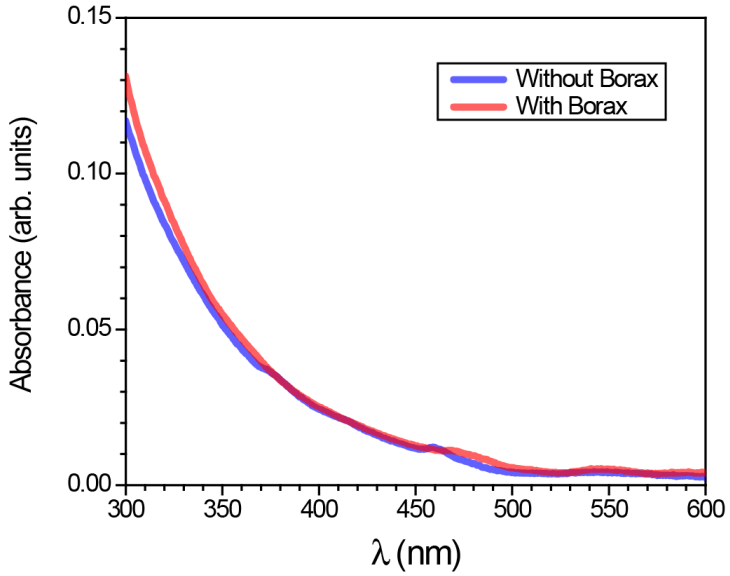

Figure 2.9: Absorption spectrum of a water extract of an ambient particulate matter filter sample with (red curve) and without (blue curve) addition of Borax.

humic substance absorption[22] could also apply to aerosols. This model consists of independent chromophores that are coupled to a dense manifold of CT complexes (Figure 2.10).

At shorter wavelengths, absorption and fluorescence are dominated by the independent chromophores that may, but do not necessarily include, the donor and acceptor species that form the CT complexes. Coupling to the dense manifold of CT complexes gives rise to the long-wavelength tails in the fluorescence emission spectra. At longer wavelengths, these CT complexes can be excited directly, too, and the maximal fluorescence emission shifts to longer and longer wavelengths as the lower-energy CT states are preferentially populated. This model is consistent with the $NaBH_4$ reduction results, as well, because the carbonyl groups are reduced to alcohols, thereby eliminating the CT complexes and decreasing the long-wavelength absorption attributed to them. The fact that not all absorption is removed upon reduction, however, indicates that chromophores other than CT complexes are also present.

Certainly other chromophores exist in ambient aerosols, but none seems to be as consistent with all of the observations as CT complexes are. As mentioned previously, possible chromophores such as extended aromatic or highly conjugated systems will not be reduced by $NaBH_4$ and therefore cannot explain the decreased absorption. Incorporation of carbonyl groups into those systems would make them susceptible to reaction with $NaBH_4$, but such species are still not likely or are not consistent with observations. For example, extended conjugated systems containing carbonyl groups in resonance could absorb into the visible region of the spectrum, but as mentioned

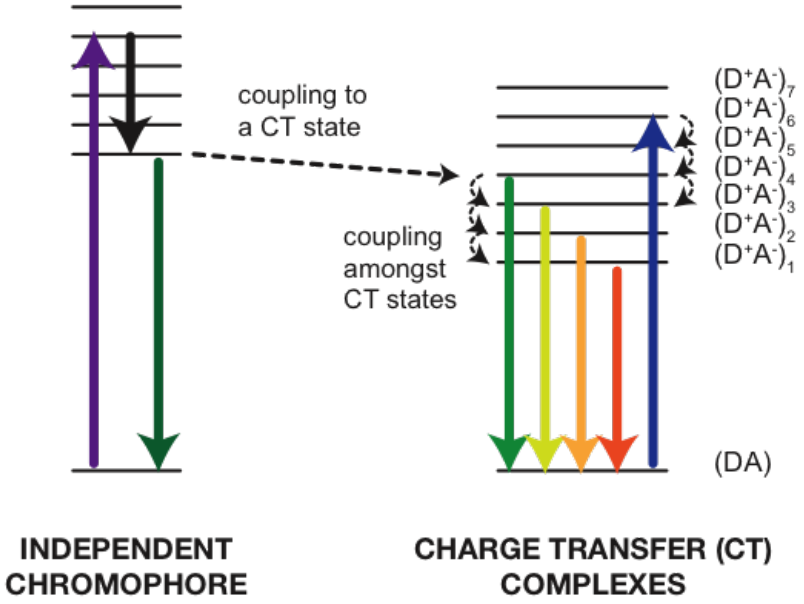

Figure 2.10: Energy level schematic showing absorption and fluorescence of independent chromophores (left) and charge transfer (CT) complexes (right). A near-continuum of CT states gives rise to the observed monotonic wavelength dependence in the absorption spectrum. Coupling between the chromophores and the CT complexes and amongst the CT complexes (dashed arrows) leads to the common emission tail at longer wavelengths observed in the fluorescence spectra.

by others,[16] extended conjugated systems are unlikely to be present in appreciable amounts in ambient aerosols because ozone reacts with the double bonds. Systems containing quinoid groups could be responsible for some absorption at UV and blue wavelengths; however, in general, they do not absorb red wavelengths,[20] and though they are reduced by $NaBH_4$, that reaction is reversible in the presence of O_2,[34] as is the case in our experiments. Extended aromatic systems containing conjugated carbonyls could also contribute to absorption and would be reactive toward $NaBH_4$, but an unlikely and coincidental superposition of many different such systems would be necessary to reproduce the absorption spectra (Figure 2.3) and the observed continuous red shift in peak fluorescence wavelength and the overlapping "tails" (Figure 2.5). Furthermore, the fluorescence quantum yields for our ambient samples ($\sim$0.02) are much lower than those typical of extended aromatics; for example, the quantum yield for anthracene ($C_{14}H_{10}$) is 0.22-0.33 (depending on solvent), while it is 0.87-0.89 for perylene ($C_{20}H_{12}$), an even larger polyaromatic species.[35]

The existence of CT complexes in ambient aerosols could have implications for how brown carbon particles are studied and understood. Beyond the fact that these complexes determine the brown color of these particles to a large extent, they also influence the wavelength dependence of the aerosol absorption spectrum that is often used to infer properties and sources. For example, the absorption Ångström exponent (AAE), the exponent in a power law fit to the absorption spectrum absorbance $\propto \lambda^{-AAE}$, is used to summarize wavelength dependence with a value of 1 for particles dominated by freshly emitted black carbon and values substantially larger than 1 indicating the contribution from BrC.[1,36] These values have also been

used to differentiate sources such as motor vehicles from biomass smoke.[1,4] The steep wavelength dependence of the CT complex absorption spectrum (Figure 2.3, inset) could, therefore, contribute to making overall AAE values larger than 1 and may even indicate a link to biomass smoke.

The wavelength dependence has also been noted to be remarkably different depending on whether particles are extracted in water or methanol,[17] and it seems likely that solvent-dependent CT complex formation might be, in part, responsible. In analogy to humic substances, these complexes may form from the aggregation of smaller units that could be affected by the nature of the solvent. The link between CT complex formation and aggregation might also explain why it has proven difficult to identify specific chromophores in ambient aerosols; for example, even relatively gentle techniques such as electrospray ionization (ESI) mass spectrometry may dissociate the aggregates,[37] leaving no evidence of the CT complexes responsible for absorption. The weak forces holding these complexes together suggest that particular attention must be paid to solvent properties such as polarity, pH, and temperature when extracting and analyzing particulate matter and that it may be difficult to compare the optical properties of samples extracted in different solvents.

While the extent to which CT complexes are formed in ambient aerosols is not known, in general, the necessary components, namely, ketones or aldehydes and alcohols, can originate from oxidation and low-temperature combustion of biogenic species including lignin.[38] Perhaps, then, these complexes provide a link between biomass burning and the formation of BrC. Our findings also intimate that these complexes could be responsible for a significant fraction of aerosol direct radiative

forcing. For example, recent measurements by Liu et al.[14] indicate that BrC constitutes 25% of aerosol absorption (at 365 nm), half of which could originate from CT complexes if we assume that our findings for water-soluble BrC represent the total BrC. Clearly, that assumption needs to be validated, and correlations between CT complex formation and specific sources need to be explored to determine how prevalent they are.

2.5 Acknowledgements

We gratefully acknowledge support for this research from the National Science Foundation (AGS-1241621) and from the Henry Luce Foundations Clare Boothe Luce Program. We also acknowledge Prof. Jeff Urbauer and Ramona Urbauer for use of and assistance with the fluorometer for some of the fluorescence experiments.

Bibliography

[1] Kirchstetter, T. W.; Novakov, T.; Hobbs, P. V. *Journal of Geophysical Research: Atmospheres* **2004**, *109*, D21208.

[2] Hecobian, A.; Zhang, X.; Zheng, M.; Frank, N.; Edgerton, E. S.; Weber, R. J. *Atmospheric Chemistry and Physics* **2010**, *10*, 5965–5977.

[3] Andreae, M. O.; Gelencsér, A. *Atmospheric Chemistry and Physics* **2006**, *6*, 3131–3148.

[4] Kirchstetter, T. W.; Thatcher, T. L. *Atmospheric Chemistry and Physics* **2012**, *12*, 6067–6072.

[5] Feng, Y.; Ramanathan, V.; Kotamarthi, V. R. *Atmospheric Chemistry and Physics* **2013**, *13*, 8607–8621.

[6] Bond, T. C. et al. *Journal of Geophysical Research: Atmospheres* **2013**, *118*, 5380–5552.

[7] Lack, D. a.; Bahreni, R.; Langridge, J. M.; Gilman, J. B.; Middlebrook, a. M. *Atmospheric Chemistry and Physics* **2013**, *13*, 2415–2422.

[8] Nozière, B.; Dziedzic, P.; Córdova, A. *Geophysical Research Letters* **2007**, *34*, 1–5.

[9] Shapiro, E. L.; Szprengiel, J.; Sareen, N.; Jen, C. N.; Giordano, M. R.; McNeill, V. F. *Atmospheric Chemistry and Physics Discussions* **2009**, *9*, 59–80.

[10] Chen, Y.; Bond, T. C. *Atmospheric Chemistry and Physics* **2010**, 1773–1787.

[11] Zarzana, K. J.; De Haan, D. O.; Freedman, M. A.; Hasenkopf, C. A.; Tolbert, M. A. *Environmental Science & Technology* **2012**, *46*, 4845–4851.

[12] Updyke, K. M.; Nguyen, T. B.; Nizkorodov, S. a. *Atmospheric Environment* **2012**, *63*, 22–31.

[13] Powelson, M. H.; Espelien, B. M.; Hawkins, L. N.; Galloway, M. M.; De Haan, D. O. *Environmental science & technology* **2014**, *48*, 985–993.

[14] Liu, J.; Scheuer, E.; Dibb, J.; Ziemba, L. D.; Thornhill, K.; Anderson, B. E.; Wisthaler, A.; Mikoviny, T.; Devi, J. J.; Bergin, M. *Geophysical Research Letters* **2014**, *41*, 2191–2195.

[15] Jacobson, M. Z. *Journal of Geophysical Research* **1999**, *104*, 3527–3542.

[16] Desyaterik, Y.; Sun, Y.; Shen, X.; Lee, T.; Wang, X.; Wang, T.; Collett, J. L. *Journal of Geophysical Research: Atmospheres* **2013**, *118*, 7389–7399.

[17] Zhang, X.; Lin, Y.-H.; Surratt, J. D.; Weber, R. J. *Environmental Science & Technology* **2013**, *47*, 3685–93.

[18] Mohr, C. et al. *Environmental science & technology* **2013**, *47*, 6316–24.

[19] Lee, H. J. J.; Laskin, A.; Laskin, J.; Nizkorodov, S. a. *Environmental science & technology* **2013**, *47*, 5763–70.

[20] Ma, J.; Del Vecchio, R.; Golanoski, K. S.; Boyle, E. S.; Blough, N. V. *Environmental science & technology* **2010**, *44*, 5395–5402.

[21] Rincón, A.; Guzmán, M. *The Journal of Physical Chemistry. A* **2009**, 10512–10520.

[22] Vecchio, R. D.; Blough, N. *Environmental science & technology* **2004**, 3885–3891.

[23] Guo, R.; Ma, J. *RSC Advances* **2014**, *4*, 25880–25885.

[24] Boyle, E. S.; Guerriero, N.; Thiallet, A. *Environmental Science & Technology* **2009**, *43*, 2262–2268.

[25] Sharpless, C. M.; Blough, N. V. *Environmental science. Processes & impacts* **2014**, *16*, 654–71.

[26] Li, C.; Hoffman, M. Z. *The Journal of Physical Chemistry B* **1999**, *103*, 6653–6656.

[27] Stradins, J.; Hasanli, B. *Journal of Electroanalytical Chemistry* **1993**, *353*, 57–69.

[28] Nothnagel, E.; Zitter, R. *The Journal of Physical Chemistry* **1976**, 722–727.

[29] Stepanov, N.; Uvarov, V.; Popov, I.; Sasson, Y. *International Journal of Hydrogen Energy* **2008**, *33*, 7378–7384.

[30] Hakoila, E. J.; Kankare, J. J.; Skarp, T. *Analytical chemistry* **1972**, *44*, 1857–1860.

[31] Cornard, J.-p.; Rasmiwetti,; Merlin, J.-c. *Chemical Physics* **2005**, *309*, 239–249.

[32] Gelencsér, A.; Hoffer, A.; Krivacsy, Z.; Kiss, G.; Molnar, A.; Meszaros, E. *Journal of Geophysical Research: Atmospheres* **2002**, *107*, 4137.

[33] Graber, E.; Rudich, Y. *Atmospheric Chemistry and Physics* **2006**, 729–753.

[34] Golanoski, K. S.; Fang, S.; Del Vecchio, R.; Blough, N. V. *Environmental science & technology* **2012**, *46*, 3912–20.

[35] Birks, J. B. **1970**, *74*, 1294–1295.

[36] Hoffer, a.; Gelencsér, A.; Guyon, P.; Kiss, G.; Schmid, O.; Frank, G.; Artaxo, P.; Andreae, M. O. *Atmospheric Chemistry and Physics Discussions* **2006**, *6*, 3563–3570.

[37] Stenson, A. C.; Landing, W. M.; Marshall, A. G.; Cooper, W. T. *Analytical Chemistry* **2002**, *74*, 4397–4409.

[38] Baluha, D. R.; Blough, N. V.; Del Vecchio, R. *Environmental Science & Technology* **2013**, *47*, 9891–9897.

Chapter 3

Further Evidence for Charge Transfer Complexes in Brown Carbon Aerosols from Excitation-Emission Matrix Fluorescence Spectroscopy[1]

[1]Sabrina M. Phillips, and Geoffrey D. Smith. *J. Phys. Chem. A*, **2014**, 119, 4545-4551. Reproduced with permission from The American Chemical Society.

3.1 Abstract

The light-absorbing fraction of organic molecules in ambient aerosols, known as "brown carbon," is an important yet poorly characterized component. Despite the fact that brown carbon could alter the radiative forcing of aerosols significantly, identification of specific chromophores has remained challenging. We recently demonstrated that charge transfer (CT) complexes formed in organic molecules could be responsible for a large fraction of absorption observed in water-extracted ambient particulate matter.[1] In the present study, we use excitation-emission matrix fluorescence spectroscopy to further corroborate the importance of CT complexes in defining aerosol optical properties. Monotonically increasing and decreasing quantum yields, decreasing Stokes shifts, and red-shifting emission maxima are observed from ambient particulate matter collected in Athens, Georgia strongly suggesting that a superposition of independent chromophores is not sufficient to explain brown carbon absorption and fluorescence. Instead, we show that a model in which such chromophores are energetically coupled to a dense manifold of CT complexes is consistent with all of the observations. Further, we suggest that a significant fraction of the observed fluorescence originates from CT complexes and that their contribution to brown carbon absorption is likely greater than we reported previously.

3.2 Introduction

Atmospheric aerosols play an important role in determining radiative forcing, the extent to which the Earth's energy budget is out of balance. Aerosol particles can both

scatter and absorb UV-visible sunlight, directly affecting radiative forcing, as well as influence cloud formation, indirectly altering radiative forcing. The chemical composition of particles plays a big role in determining the magnitude, and sometimes the sign, of the effects on radiative forcing.[2] As a result, there is a need to characterize more completely the constituents responsible for scattering and, in particular, absorption.[3]

It has long been recognized that black carbon and mineral dust particles can absorb sunlight, but only recently have measurements indicated that organic species within particles can also absorb light.[2,4,5] The fraction of organic molecules that absorbs light, termed "brown carbon" (BrC), has a much more pronounced dependence on wavelength than does black carbon, absorbing UV and blue light preferentially.[2,6] Brown carbon is thought to originate from low-temperature combustion, biomass burning and secondary organic aerosol[4,7–11] and has been estimated to contribute approximately a quarter as much warming as black carbon.[12] Despite its importance, the chemical nature of BrC is still unclear, though several potential classes of chromophores have been suggested, including nitro-aromatics[13–16] and condensation products involving ammonia, amines and amino acids and aldehydes.[17–20]

We recently demonstrated that a different class of chromophores, charge transfer (CT) complexes, are also present in ambient aerosols.[1] These complexes, formed through the interaction between carbonyl and alcohol moieties in organic molecules, are energetically coupled to one another and form a near-continuum of states that absorb light from 250 nm to 600 nm. By chemically reducing the carbonyls and thereby disrupting the complexes, we found that 53% of absorption (λ = 300 nm -

600 nm) exhibited by the water-soluble fraction of ambient particulate matter could be attributed to CT complexes.

In the present work, we provide further evidence for the presence of CT complexes in brown carbon using excitation-emission matrix (EEM) fluorescence spectroscopy to probe the excited states both before and after chemical reduction. We demonstrate that the observed fluorescence spectra of ambient particulate matter extracts are inconsistent with a model consisting solely of a superposition of independent chromophores. Instead, we find that a model including both direct and indirect excitation of CT complexes can explain the fluorescence spectral features. Furthermore, we find that a significant fraction of the observed fluorescence originates from the CT complexes. Finally, the data indicate that the CT complexes are not removed entirely by chemical reduction suggesting that their contribution to ambient aerosol optical properties may be even larger than previously thought.

3.3 Materials and Methods

3.3.1 Aerosol Collection

Ambient aerosols were collected out of a window in the Chemistry Building at the University of Georgia (∼20 m above ground level) in Athens, GA (33.9488°N, 83.3747°W) from January 2014 to March 2014. A total of 10 samples were collected on polytetrafluoroethylene (PTFE, Teflon) filters (0.2 μm pore size, Sterlitech) at a rate of 16.7 L/min for 10 separate 24 h ($\pm$1 h) periods. A very sharp cut cyclone inlet (BGI, Inc.) was employed to size select for particles with diameters of <2.5 μm. Water-soluble organic species were then extracted in a manner similar to that

described by Hecobian et al.[11] by sonication of the filter for 20 min in 10 mL of Milli-Q water ($< 18.2 M\Omega \cdot cm$). Extracted solutions were filtered using a 0.45 μm PTFE disposable syringe filter and adjusted to pH 7 with NaOH because the magnitude of the absorption spectra was pH-dependent.[1]

3.3.2 Reduction

Reduction protocols were adapted from the procedures detailed in Ma et al.[21] Extracted aerosol solutions were reduced in a 1-cm quartz cuvette (Thorlabs; volume = 3 mL) by adding approximately 5 mg of solid $NaBH_4$ and dissolved by stirring. Reduction proceeded until no further change in absorbance was noticed (25 min). Due to an excess of $NaBH_4$, the pH of the solution rose to 10, so the solution was readjusted to pH 7 with the addition of HCl. $NaBH_4$ is a convenient reducing agent for these experiments as it can be added directly to water unlike more aggressive reducing agents such as $LiAlH_4$. As a consequence, however, $NaBH_4$ reduces ketones and aldehydes to alcohols but it does not reduce carboxylic acids. Because of its selectivity, $NaBH_4$ will not react with other functional groups or moieties that have been proposed to be chromophores in particulate matter, including highly-conjugated systems and extended aromatic structures.[21]

3.3.3 Absorption and Fluorescence

Optical absorption spectra of extracts placed in a 1-cm quartz cuvette were collected on a Cary 60 (Agilent) over a range of 200 nm to 800 nm and with a scan rate of 600 nm/min. Fluorescence spectra (uncorrected) of extracts in the same cuvette were

collected on a FluoroLog II fluorometer (Horiba) over an excitation range of λ_{exc} = 280 nm - 450 nm in 10 nm steps, an emission range of λ_{em} = 280 nm - 700 nm in 1 nm steps, and at a scan rate of 300 nm/min.

3.3.4 Quantum Yields

Effective fluorescence quantum yields were calculated similarly to Lee et al.[22] using quinine sulfate (QS) in 0.05 M sulfuric acid as a reference compound. The emission intensity of QS integrated between 362 nm and 600 nm at an excitation wavelength of λ_{exc} = 349 nm was used to place the quantum yield values from the water-soluble fraction extracted from the filter ("BrC") on an absolute scale.[23] The value of Φ_{BrC} was calculated at each excitation wavelength by comparing the measured fluorescence emission intensities integrated over all emission wavelengths (I) and the absorption coefficients (α), as measured with the UV-visible spectrophotometer:

$$\Phi_{BrC}(\lambda_{ex}) \cong \Phi_{QS}(349nm) \cdot \frac{I_{BrC}(\lambda_{ex})}{I_{QS}(349nm)} \cdot \frac{\alpha_{QS}(349nm)}{\alpha_{BrC}(\lambda_{ex})} \tag{3.1}$$

The quantum yield values calculated in this way are approximate because it has been assumed that any instrumental factors affecting the fluorescence intensities (e.g. transmission efficiency and detector response) will be similar for the QS emission spectrum and the BrC emission spectrum. Such an assumption is commonly made in using a reference to place quantum yield measurements on an absolute scale.[22] However, in general these factors can be wavelength dependent and may not cancel exactly. Nonetheless, the conclusions that we are able to draw from the wavelength-

dependent quantum yield measurements are unlikely to be influenced by assuming that the instrumental factors cancel.

3.4 Results

Fluorescence emission spectra from all 10 water-extracted samples were individually normalized to the peak emission intensity and then averaged (Figure 3.1a). These spectra are also combined and displayed as an average excitation-emission matrix (EEM) spectrum (Figure 3.2a), a common format used in the analysis of fluorescence by aquatic organics.[24] The EEM spectrum for the ambient samples collected here is qualitatively similar to that presented by Duarte et al. for water-soluble ambient particulate matter[25] as well as EEM spectra for model organic aerosol systems.[19,22,26] Several of those spectra contain a peak in the region of λ_{ex} = 300 nm - 400 nm and λ_{em} = 400 nm - 450 nm, as observed in Figure 3.2a, though the exact locations and shapes of emission vary.

The fluorescence spectra in Figures 3.1a and 3.2a show long, overlapping emission tails that fall within a single emission envelope indicative of a dense manifold of emitting states such as those corresponding to an ensemble of CT complexes. These features are also present in the emission spectra after reduction by $NaBH_4$ (Figures 3.1b and 3.2b) suggesting that the fluorescing states after reduction may be a subset of those present before reduction. In fact, the fluorescence emission intensity increases after reduction, which is readily observed in the averaged EEM spectra before and after reduction (Figure 3.2). The largest increase in fluorescence intensity occurs at $\lambda_{ex} \sim 310$ nm where the absorption loss is also the greatest (Figure 3.7).

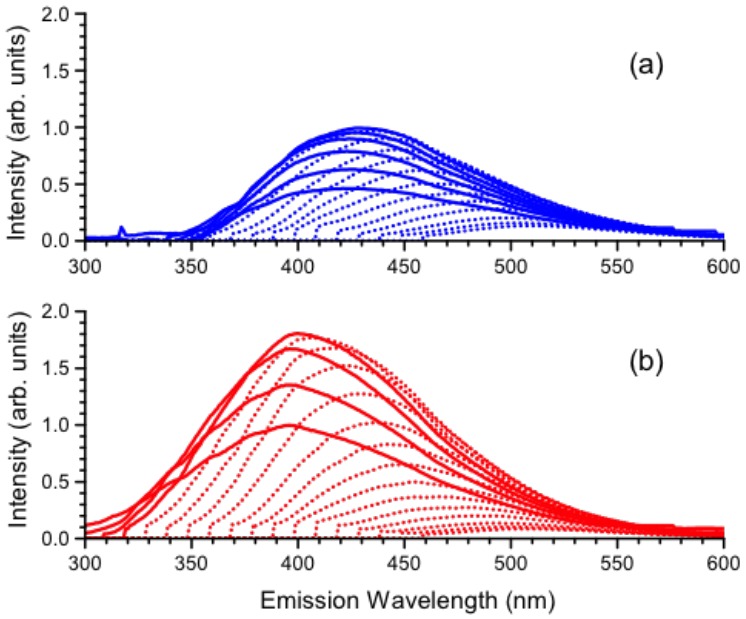

Figure 3.1: Average fluorescence emission spectra of ambient aerosol samples collected in Athens, GA: (a) before reduction and (b) after reduction. Solid curves represent excitation wavelengths in the UV with constant peak emission wavelengths, while dashed curves represent monotonically red-shifting peak emission wavelengths.

This correlation between fluorescence gain and absorption loss demonstrates that the increased fluorescence is unlikely to result from newly created absorbing species and thus likely results from previously existing species that are more strongly fluorescing after reduction.

Although the EEM spectrum constitutes the most complete representation of the entire set of fluorescence emission spectra, some of the notable features are more readily apparent when isolated individually. For example, fluorescence quantum yield (Φ) calculations (Equation 3.1) more clearly exhibit changes in fluorescence efficiency as they normalize fluorescence emission to absorption (Figure 3.3). The value of Φ increases from 0.004 at λ_{ex} = 280 nm to a maximum of 0.017 at λ_{ex} = 350 nm and then decreases with increasing λ_{ex}. These values are similar to fluorescence quantum yields of fulvic acid (Φ = 0.02[27]) and various natural water humic substances (Φ = 0.002 - 0.025[28]) as well as laboratory-generated secondary organic aerosol from limonene (Φ = 0.004) and -pinene (Φ = 0.008).[22] After reduction, the same pronounced wavelength dependence is observed indicating that the fluorescing species present both before and after reduction share some similar characteristics, perhaps because not all of the CT complexes are removed by reduction. The apparent quantum yields, however, are 2-3 times larger (Figure 3.4) suggesting that reduction decreases quenching.

The plots of the maximum wavelength of emission (λ_{em}^{max}) as a function of λ_{ex} also exhibit similar shapes before and after reduction (Figure 3.5). In each case, the value of λ_{em}^{max} is constant at short wavelengths with a monotonic red shift to longer wavelengths at $\lambda_{ex} \geq$ 310 nm. This red shift is indicative of the presence

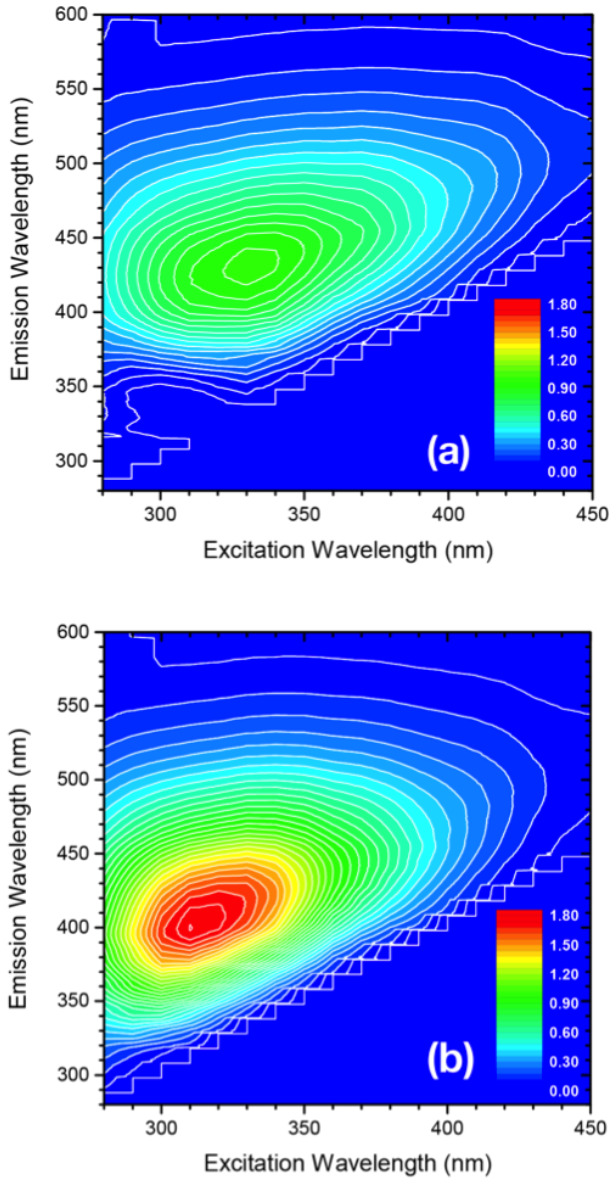

Figure 3.2: Average excitation-emission matrix (EEM) fluorescence spectra of ambient aerosol samples collected in Athens, GA: (a) before reduction and (b) after reduction. Increased and blue-shifted emission is observed after reduction.

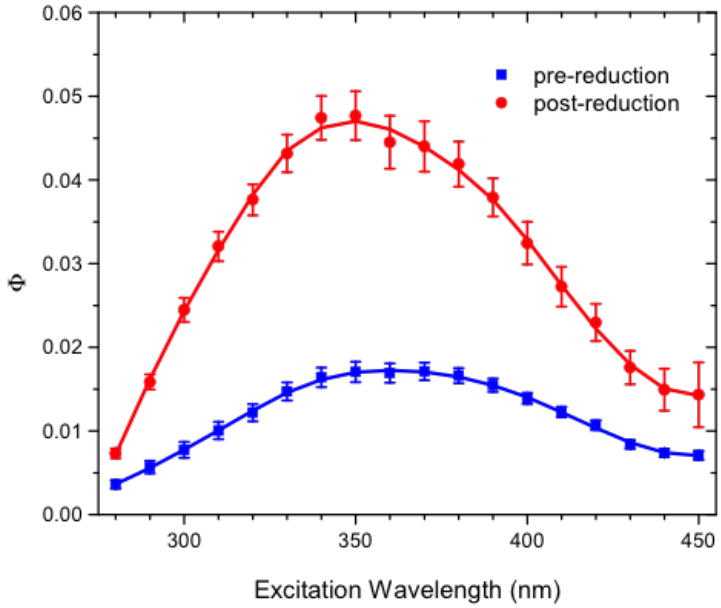

Figure 3.3: Average fluorescence quantum yields (Φ) before (blue squares) and after (red circles) reduction by $NaBH_4$ as functions of excitation wavelength.

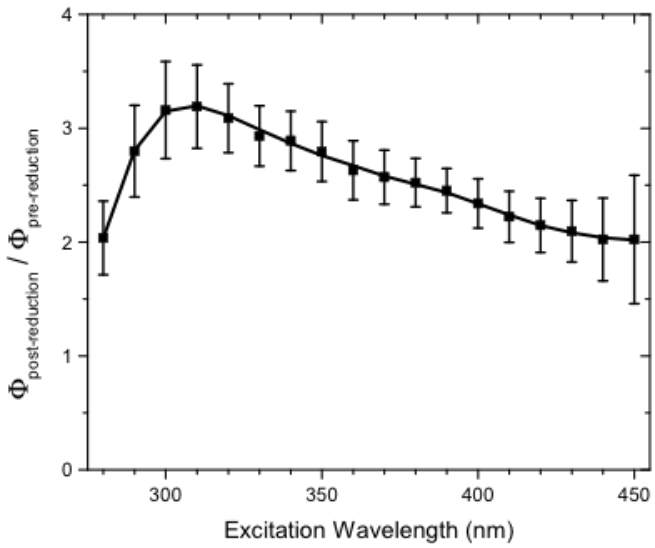

Figure 3.4: Ratio of average post- and pre-reduction quantum yields as a function of excitation wavelength.

of a densely-populated continuum of coupled fluorescing states. As with the quantum yield data, the similarities in the dependence on λ_{ex} before and after reduction suggest an incomplete removal of the molecules or moieties (perhaps CT complexes) responsible for fluorescence. The blue shift to shorter λ_{em}^{max} values after reduction, shown in the inset to Figure 3.5, also displays a montonic decrease with λ_{ex} and is suggestive of a large number of coupled states.

The observed Stokes shifts, the difference in λ_{em}^{max} and λ_{ex} (Figure 3.6), also provide some information about the extent of energetic relaxation between the absorption of light and the subsequent fluorescence by the excited state. For both pre- and post-reduction, the Stokes shift decreases monotonically with λ_{ex} while at the same time λ_{em}^{max} increases monotonically (Figure 3.5). The similar wavelength dependence observed for the Stokes shifts before and after reduction also suggest that the fluorescing species remaining after reduction are a subset of those present before reduction, just as the quantum yield (Figure 3.3) and λ_{em}^{max} (Figure 3.5) curves do. In the following discussion, we demonstrate how these observations are not readily explained by a collection of independent chromophores and that, instead, they are consistent with the existence of a large number of energetically coupled charge transfer complexes that are not removed entirely by reaction with $NaBH_4$.

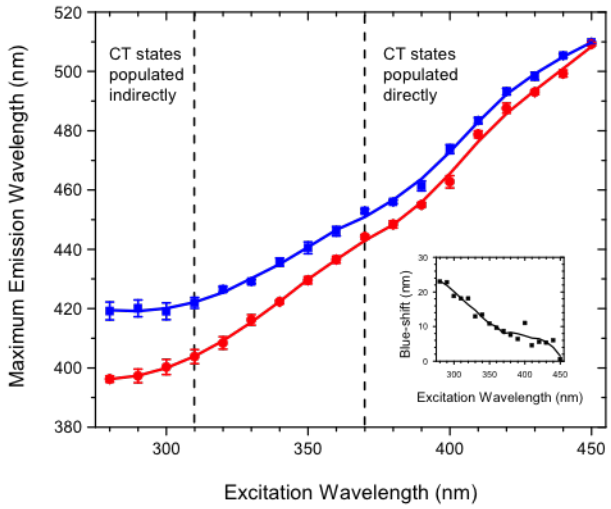

Figure 3.5: Average wavelength of maximum fluorescence emission as a function of excitation wavelength before (blue squares) and after (red circles) reduction by $NaBH_4$. Dashed lines show regions in which fluorescence arises primarily from charge transfer states populated indirectly through energy transfer from independent chromophores (left) and directly through absorption (right). Inset shows blue shift of wavelength of maximum emission as a function of excitation wavelength.

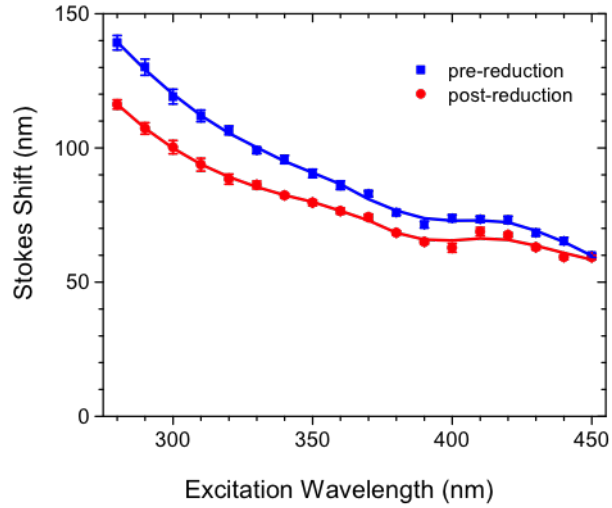

Figure 3.6: Average Stokes shift as a function of excitation wavelength before (blue squares) and after (red circles) reduction by $NaBH_4$.

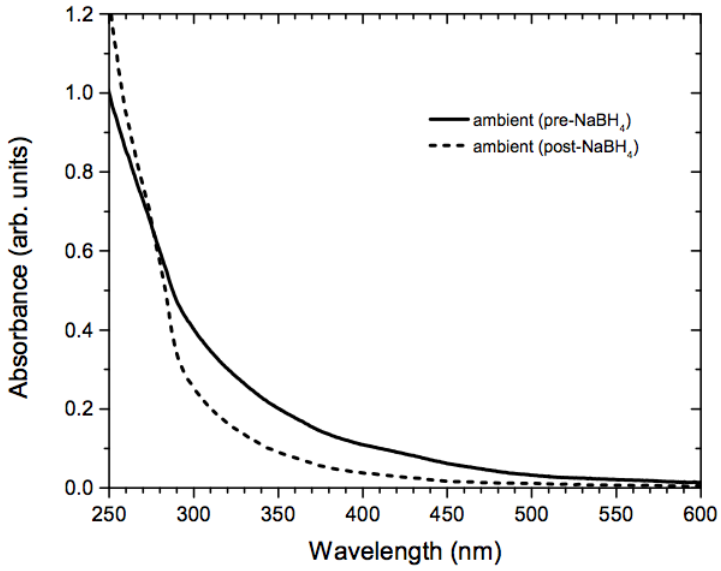

Figure 3.7: Average absorption spectrum of ambient aerosol water extract collected January, 2014 March, 2014 in Athens, GA before (solid line) and after (dashed line) reduction by $NaBH_4$. Decreased absorption after reduction is attributed to removal of charge transfer complexes.

3.5 Discussion

3.5.1 A superposition of independent chromophores does not explain observed fluorescence

As Blough and co-workers have found with aquatic colored dissolved organic matter (CDOM),[29] we have found that a model in which independent chromophores in ambient particulate matter absorb and emit light does not seem to be consistent with the observed fluorescence data. For one, the long-wavelength "tail" observed past ∼500 nm in the fluorescence emission spectra (Figure 3.1) is common to all excitation wavelengths from 280 nm to 450 nm. Such an overlap is unlikely, though not entirely impossible, for a collection of independent chromophores over such an extended range of excitation wavelengths. Also, the fact that the fluorescence intensity increases with increasing excitation wavelength for $\lambda_{ex} \leq 330$ nm (Figure 3.1) while at the same time the absorption decreases (Figure 3.7) results in an observed quantum yield that increases monotonically with increasing excitation wavelength (Figure 3.3). Such a trend would have to arise coincidentally for a collection of independent chromophores since, in general, there is no relationship between excitation wavelength and quantum yield. Instead, the data suggest that other fluorophores with larger quantum yields, which we posit below are charge transfer complexes, are increasingly excited. At the same time, the fact that the shapes of the emission spectra and the wavelengths of maximum emission (Figure 3.5) do not change suggests that they are determined more by these other fluorophores than by fluorescence from the independent chromophores.

At longer excitation wavelengths, the monotonically increasing λ_{em}^{max} (Figure 3.5) would require an improbable collection of independent chromophores with coincidental peak emission wavelengths that exhibit a continuous red shift dependent on the energy of excitation. This highly unlikely collection of independent chromophores would also have to possess fluorescence Stokes shifts that coincidentally decrease monotonically with excitation wavelength as observed in Figure 3.6. Additionally, the fluorescence quantum yields are seen to decrease monotonically with excitation wavelength longer than $\lambda_{ex} \sim 370$ nm (Figure 3.3); again, such a trend would have to be coincidental for a collection of independent chromophores since, in general, there is no relationship between excitation wavelength and quantum yield. Finally, the observed monotonic decrease in quantum yield enhancement upon reduction with excitation wavelength (Figure 3.4) would also have to result from a highly unlikely coincidence of independent chromophores that react with $NaBH_4$ to varying degrees correlated with excitation wavelength. Altogether, then, the trends displayed in the fluorescence data of Figures 3.1 to 3.6 appear to be inconsistent with a superposition of independent chromophores as the sole, or even primary, explanation for the observed fluorescence of ambient particulate matter extracts.

3.5.2 Brown carbon fluorescence originates from both direct and indirect excitation of charge transfer states

The trends with excitation wavelength observed in the fluorescence spectra and quantum yields implicate the existence of a large number of coupled states. Previously, we showed that CT complexes could form such states and, along with independent

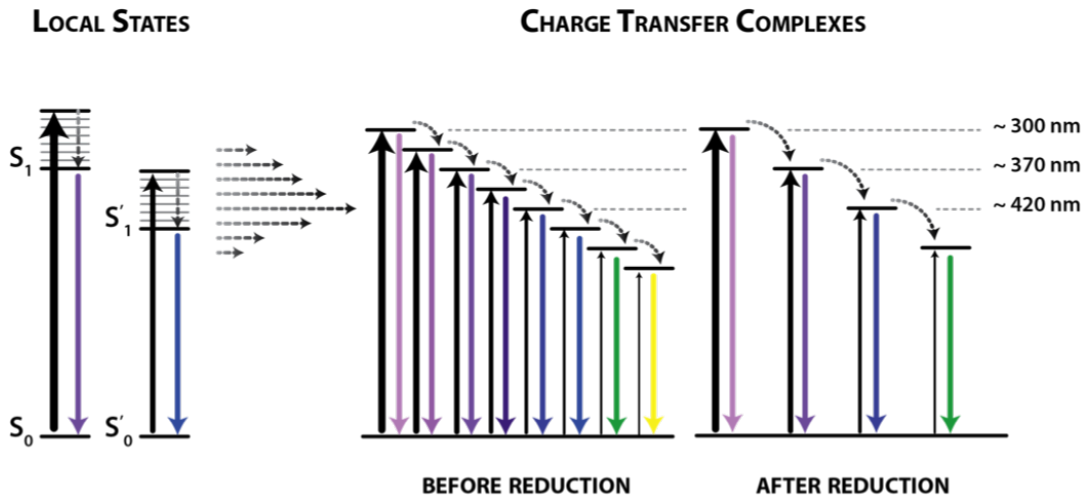

Figure 3.8: Diagram of proposed model in which local states and charge transfer complexes are coupled. Fluorescence originates from emission by excited charge transfer states populated indirectly through energy transfer from local states (horizontal arrows) or directly by absorption of longer-wavelength (λ ¿ 300 nm) light. Reduction by $NaBH_4$ eliminates some charge transfer complexes resulting in less efficient coupling amongst the remaining charge transfer complexes.

chromophores, be responsible for much of the absorption observed for ambient particulate matter extracts.[1] Here, we refine that picture (Figure 3.8) to incorporate all of the fluorescence measurements presented in this work, both before and after reduction with $NaBH_4$. The primary difference between the picture developed here and that presented earlier is that now we attribute a significant fraction of the observed fluorescence to the charge transfer states; previously, we had assumed that some of the fluorescence at short excitation wavelengths originated from independent chromophores consistent with the work of del Vecchio and Blough[29] on aquatic humic substances.

In the current picture (Figure 3.8), both independent chromophores ("local states") and charge transfer complexes can absorb light with the relative contributions from local states and CT complexes decreasing and increasing, respectively, with increasing wavelength. This transition appears to occur over a wavelength range of ∼300 nm - 370 nm and is evident in the absorption spectra (Figure 3.7) in which the fractional loss of absorption after reduction (indicating CT complex removal) becomes increasingly larger with increasing wavelength until about 370 nm. The effective quantum yields (Figure 3.3) also increase until a wavelength of about 370 nm, probably because the local states responsible for much of the absorption at the short wavelengths do not fluoresce efficiently; as the local state contribution to absorption decreases with increasing wavelength, the effective quantum yield increases. At the shortest wavelengths (e.g., 280 nm) where absorption appears to be dominated by local states (as indicated by the small fractional loss of absorption after reduction in Figure 3.7), the fluorescence quantum yield is very small indicating that the local states do not fluoresce efficiently. In fact, in additional fluorescence measurements extended to $\lambda_{ex} = 220$ nm (not shown) the quantum yield decreases even further with values less than 0.0004 at $\lambda_{ex} \leq 250$ nm.

The fluorescence emission spectra (Figure 3.1) suggest that excitation of the local states leads to fluorescence emission indirectly through energy transfer and population of excited CT states. Specifically, the common long-wavelength "tail" ($\lambda_{em} > 450$ nm) observed for both the short-wavelength excitation ($\lambda_{ex} \leq 300$ nm) of the local states and the longer-wavelength excitation ($\lambda_{ex} \geq 370$ nm) of the CT complexes indicates that they are energetically coupled. Such coupling is presumably

inefficient as the effective quantum yields are small (Figure 3.3). The similarities in the shapes of the emission spectra (Figure 3.1) and the peak emission wavelengths (Figure 3.5) for short excitation wavelengths ($\lambda_{ex} \leq 300$ nm) are also consistent with nearly all of the absorbance being attributed to the local states and much of the fluorescence originating from energy transfer from them to excited CT states. In essence, for shorter excitation wavelengths the local states dictate the population of the excited CT states, and the concomitant fluorescence emission spectra reflect the strength of coupling between them (horizontal arrows in Figure 3.8) with the result that the spectral shapes are independent of excitation wavelength.

At longer excitation wavelengths ($\lambda_{ex} > 300$ nm), direct excitation of the CT complexes becomes more significant and their population becomes less dictated by energy transfer from the local states. The more efficient population of those excited states can be seen in the larger effective quantum yields (Figure 3.3). Likewise, the peak emission wavelength, λ_{em}^{max}, increases monotonically as lower-energy excited CT states are populated more (Figure 3.5). The concurrent decrease in Stokes shift (Figure 3.6) reflects the smaller extent of coupling to lower-energy states because there are fewer such states and because the rate of non-radiative decay increases with the decreasing energy gap between the excited and ground states (i.e. the increasing emission wavelength).[30,31] The larger rate of non-radiative decay for the lower-lying CT states is also responsible for the decreasing trend in the quantum yield for fluorescence at $\lambda_{ex} > 370$ nm (Figure 3.3). In essence, energy transfer depopulates the higher-energy states replacing them with lower-lying states that have smaller quantum yields.

3.5.3 Reduction decreases coupling within a dense manifold of charge transfer states

As we have demonstrated previously,[1] reduction by $NaBH_4$ decreases the absorption by a substantial fraction throughout the UV-visible region of the spectrum (Figure 3.7) strongly suggesting that CT complexes are responsible for the absorption. Conversely, fluorescence intensity increases after reduction (Figures 3.1 and 3.2) suggesting that perhaps the CT complexes, or the carbonyl groups that were reduced, were quenching the fluorescence of independent chromophores. However, fluorescence by the independent chromophores is inconsistent with all of the observations (see discussion above). Instead, we posit that reaction with $NaBH_4$ does not eliminate all CT complexes and that the fluorescence observed after reduction originates from the remaining complexes. Perhaps these complexes involve carboxylic acids, which are known to be unreactive toward $NaBH_4$, or quinones which are reduced but are regenerated in the presence of O_2.[21,32] Consistent with this explanation, the fluorescence spectra (Figures 3.1 and 3.2), quantum yields (Figure 3.3), maximum emission wavelengths (Figure 3.5) and Stokes shifts (Figure 3.6) all show similar wavelength dependences after reduction as they do before reduction.

We hypothesize that the removal of some CT complexes inhibits energy transfer amongst the manifold of CT states by making it less dense (Figure 3.8). The remaining CT complexes still absorb light and could be responsible for some of the exponential shape of the absorption spectrum observed after reduction (Figure 3.7) but there are just fewer of them. Likewise, these complexes still fluoresce with long, overlapping tails at long wavelengths, just as was observed before reduction (Figures

3.1 and 3.2) indicating coupling amongst a large number of remaining excited states. The larger fluorescence intensity probably originates from less-efficient energy transfer to the longer-wavelength states that possess smaller fluorescence quantum yields. Consequently, the peak emission wavelengths blue shift, as seen in Figure 3.5 (and the accompanying inset). The monotonic decrease in the blue shift with excitation wavelength results from the fact that there are fewer and fewer CT states at lower energy thereby decreasing the extent of the cascade of energy transfer. For the same reason, the Stokes shift decreases after reduction (Figure 3.6).

The larger effective quantum yields (Figure 3.3) arise from the combination of increased fluorescence and decreased absorption; the CT complexes remaining after reduction still absorb light and in fact fluoresce more efficiently because there is less efficient energy coupling to low-lying CT states that have smaller effective quantum yields. Consequently, the enhancement in the quantum yield after reduction would be expected to be a function of wavelength since the extent to which energy transfer to low-lying CT states decreases at longer excitation wavelength. In fact, the enhancement does display a monotonic decrease from 3.2 times at $\lambda_{ex} = 310$ nm to 2.0 times at $\lambda_{ex} = 450$ nm (Figure 3.4). Taken together, all of these post-reduction fluorescence emission measurements are consistent with a coupled manifold of CT states that becomes less dense, but not eliminated, after reduction.

3.5.4 Conclusions

In this work we have demonstrated that the spectral characteristics of brown carbon fluorescence are consistent with a model consisting of individual chromophores

and a densely-populated ensemble of coupled charge transfer states. In this model, short-wavelength light primarily excites the individual chromophores that transfer energy to and excite charge transfer complexes while longer-wavelength light excites the charge transfer complexes directly. In both cases, a cascade of energy transfer amongst the near-continuum of charge transfer states populates a range of complexes that are responsible for the broad fluorescence emission observed. The overlapping tails of the fluorescence spectra, the observed wavelength dependence in the emission maxima and the quantum yields, and the more intense and blue-shifted emission after reduction all substantiate the hypothesis that charge transfer complexes are a major contributor to light absorption and fluorescence in brown carbon aerosols. Furthermore, we have shown that reduction by $NaBH_4$ results in incomplete removal of the charge transfer complexes suggesting that they may be responsible for even more than the 53% of UV-visible light absorption by water-soluble brown carbon that we reported previously.

3.5.5 Update

Since publication, several groups have similarly employed fluorescence-based methods to study ambient aerosols and SOA. Powelson et al.[19] previously used EEM's to measure highly fluorescent products generated by aqueous-phase reactions of small aldehydes with AS and amines. They recently expanded on this, comparing EEM's of several Maillard reaction systems to atmospheric WSOC collected from Portugal.[33,34]

Several groups have measured ambient aerosol EEM's and PARAFAC analysis to link fluorescence characteristics to seasonal variabilities and other water-soluble

chromophores. Matos et al.[35] attributed seasonal variations to degree of unsaturated π-bond systems as well as more significant atmospheric aging of urban aerosols in warmer seasons. Chen et al.[36,37] identified HULIS and PLOM (protein-like organic matter) in urban, forest, and marine aerosols. Their findings might be useful for evaluating reaction pathways involved in the formation or loss of organic chromophores in atmospheric aerosols.

3.6 Acknowledgements

The authors gratefully acknowledge support for this research from the National Science Foundation (AGS-1241621).

Bibliography

[1] Phillips, S.; Smith, G. *Environmental Science & Technology Letters* **2014**, *1*, 382–386.

[2] Andreae, M. O.; Gelencsér, A. *Atmospheric Chemistry and Physics* **2006**, *6*, 3131–3148.

[3] Bahadur, R.; Praveen, P. S.; Xu, Y.; Ramanathan, V. *Proceedings of the National Academy of Sciences of the United States of America* **2012**, *109*, 17366–71.

[4] Kirchstetter, T. W.; Novakov, T.; Hobbs, P. V. *Journal of Geophysical Research: Atmospheres* **2004**, *109*, D21208.

[5] Hoffer, a.; Gelencsér, A.; Guyon, P.; Kiss, G.; Schmid, O.; Frank, G.; Artaxo, P.; Andreae, M. O. *Atmospheric Chemistry and Physics Discussions* **2006**, *6*, 3563–3570.

[6] Sun, H.; Biedermann, L.; Bond, T. C. *Geophysical Research Letters* **2007**, *34*, L17813.

[7] Chen, J.; Venables, D. S. *Atmospheric Measurement Techniques* **2011**, *4*, 425–436.

[8] Lack, D. A.; Langridge, J. M.; Bahreini, R.; Cappa, C. D.; Middlebrook, A. M.; Schwarz, J. P. *Proceedings of the National Academy of Sciences of the United States of America* **2012**, *109*, 14802–14807.

[9] Saleh, R.; Hennigan, C. J.; McMeeking, G. R.; Chuang, W. K.; Robinson, E. S.; Coe, H.; Donahue, N. M.; Robinson, A. L. *Atmospheric Chemistry and Physics* **2013**, *13*, 7683–7693.

[10] Lukács, H.; Gelencsér, A.; Hammer, S.; Puxbaum, H.; Pio, C.; Legrand, M.; Kasper-Giebl, A.; Handler, M.; Limbeck, A.; Simpson, D.; Preunkert, S. *Journal of Geophysical Research* **2007**, *112*, D23S18.

[11] Hecobian, A.; Zhang, X.; Zheng, M.; Frank, N.; Edgerton, E. S.; Weber, R. J. *Atmospheric Chemistry and Physics* **2010**, *10*, 5965–5977.

[12] Feng, Y.; Ramanathan, V.; Kotamarthi, V. R. *Atmospheric Chemistry and Physics* **2013**, *13*, 8607–8621.

[13] Jacobson, M. Z. *Journal of Geophysical Research* **1999**, *104*, 3527–3542.

[14] Desyaterik, Y.; Sun, Y.; Shen, X.; Lee, T.; Wang, X.; Wang, T.; Collett, J. L. *Journal of Geophysical Research: Atmospheres* **2013**, *118*, 7389–7399.

[15] Zhang, X.; Lin, Y.-H.; Surratt, J. D.; Weber, R. J. *Environmental Science & Technology* **2013**, *47*, 3685–93.

[16] Mohr, C. et al. *Environmental science & technology* **2013**, *47*, 6316–24.

[17] Nozière, B.; Dziedzic, P.; Córdova, A. *Geophysical Research Letters* **2007**, *34*, 1–5.

[18] Shapiro, E. L.; Szprengiel, J.; Sareen, N.; Jen, C. N.; Giordano, M. R.; McNeill, V. F. *Atmospheric Chemistry and Physics Discussions* **2009**, *9*, 59–80.

[19] Powelson, M. H.; Espelien, B. M.; Hawkins, L. N.; Galloway, M. M.; De Haan, D. O. *Environmental science & technology* **2014**, *48*, 985–993.

[20] Updyke, K. M.; Nguyen, T. B.; Nizkorodov, S. a. *Atmospheric Environment* **2012**, *63*, 22–31.

[21] Ma, J.; Del Vecchio, R.; Golanoski, K. S.; Boyle, E. S.; Blough, N. V. *Environmental science & technology* **2010**, *44*, 5395–5402.

[22] Lee, H. J. J.; Laskin, A.; Laskin, J.; Nizkorodov, S. a. *Environmental science & technology* **2013**, *47*, 5763–70.

[23] Melhuish, W. *Journal of Physical Chemistry* **1961**, *65*, 229–235.

[24] Hudson, N.; Baker, A.; Reynolds, D. *River Research and Applications* **2007**, *23*, 631–649.

[25] Duarte, R. M. B. O.; Pio, C. A.; Duarte, A. C. *Analytica Chimica Acta* **2005**, *530*, 7–14.

[26] De Laurentiis, E.; Socorro, J.; Vione, D.; Quivet, E.; Brigante, M.; Mailhot, G.; Wortham, H.; Gligorovski, S. *Atmospheric environment* **2013**, *81*, 569–578.

[27] Gosteva, O. Y.; Izosimov, A. A.; Patsaeva, S. V.; Yuzhakov, V. I.; Yakimenko, O. S. *Journal of Applied Spectroscopy* **2012**, *78*, 884–891.

[28] Boyle, E. S.; Guerriero, N.; Thiallet, A. *Environmental Science & Technology* **2009**, *43*, 2262–2268.

[29] Vecchio, R. D.; Blough, N. *Environmental science & technology* **2004**, 3885–3891.

[30] Turro, N. J. *Modern Molecular Photochemistry*; The Benjamin/Cummings Publishing Co., Inc.: Menlo Park, CA,, 1978.

[31] Bixon, M.; Jortner, J.; Cortes, J.; Heitele, H.; Michel-Beyerle, M. E. *Journal of Physical Chemistry* **1994**, *98*, 7289–7299.

[32] Tinnacher, R. M.; Honeyman, B. D. *Environmental science & technology* **2007**, *41*, 6776–6782.

[33] Hawkins, L. N.; Lemire, A. N.; Galloway, M. M.; Corrigan, A. L.; Turley, J. J.; Espelien, B. M.; De Haan, D. O. *Environmental Science and Technology* **2016**, *50*, 7443–7452.

[34] Duarte, R. M.; Pio, C. A.; Duarte, A. C. *Journal of Atmospheric Chemistry* **2004**, *48*, 157–171.

[35] Matos, J. T.; Freire, S. M.; Duarte, R. M.; Duarte, A. C. *Atmospheric Environment* **2015**, *102*, 1–10.

[36] Chen, Q.; Miyazaki, Y.; Kawamura, K.; Matsumoto, K.; Coburn, S.; Volkamer, R.; Iwamoto, Y.; Kagami, S.; Deng, Y.; Ogawa, S.; Ramasamy, S.; Kato, S.; Ida, A.; Kajii, Y.; Mochida, M. *Environmental Science and Technology*; 2016; Vol. 50; pp 10351–10360.

[37] Chen, Q.; Ikemori, F.; Mochida, M. *Environmental Science and Technology* **2016**, *50*, 10859–10868.

Chapter 4

Brown Carbon Light Absorption is pH Dependent[1]

[1]Sabrina M. Phillips, and Geoffrey D. Smith. Submitted to *Environ. Sci. Technol.*, **2017**,

4.1 Abstract

Light-absorbing organic material, or "brown carbon" (BrC), can significantly influence the effect that aerosols have on climate. Here, we investigate how changing pH affects absorption spectra of water-soluble BrC from ambient particulate matter collected in Athens, Georgia. We find that absorption increases 10% per pH unit from pH = 2 to pH = 12 with a broad, featureless tail at visible wavelengths where the largest fractional increase is also observed. The resulting change in the spectral shape causes the absorption Ångström exponent to decrease by 0.18 per unit increase in pH. Strikingly similar behavior with humic substances suggests that they and BrC share a common physicochemical link between pH and absorption, which we propose is a consequence of changes in the supramolecular assemblies formed from organic molecules. Specifically, we hypothesize that a wider variety and larger number of absorbing charge transfer complexes are formed as carboxylic acid and phenol moieties in these molecules become deprotonated. These findings suggest that: 1) the pH of ambient particulate matter samples should be measured or controlled, and 2) radiative forcing by aerosols could be overestimated if pH dependent BrC absorption is not accounted for.

4.2 Introduction

Atmospheric aerosols affect radiative forcing both directly through their interaction with sunlight as well as indirectly through their influence on clouds. It is clear that black carbon (BC) particles are very efficient absorbers of solar radiation, with some

evaluations suggesting that its impact on radiative forcing is second only to carbon dioxide.[1] However, the role of organic carbon (OC) is much less well understood, and many climate models ignore light absorption by this fraction even though it has recently become clear that some OC does absorb light. This light-absorbing fraction, sometimes called "brown carbon" (BrC), generally has an absorption spectrum that varies much more strongly with wavelength than BC does. As a consequence, BrC is not believed to contribute substantially to aerosol absorption past 500 nm, though at UV wavelengths it can be comparable to BC[2] and can decrease OH production by up to 30%.[3]

There is substantial evidence that this BrC can originate from biomass burning,[4–8] and many laboratory studies have also elucidated mechanisms for the creation of light-absorbing organic species from aqueous reactions of small ketones and aldehydes with amines and ammonium salts.[9–12] However, the identification of specific chromophores in samples of ambient particulate matter has proven difficult, as discussed by Laskin et al.[13] and references therein. Some studies have isolated nitrophenols as an important class of chromophores, though these have only accounted for 4% of measured BrC absorption.[14–16] Lin et al. were able to attribute as much as 25% of solvent-extractable absorption to nitrophenols and their derivatives and another 25% to PAH derivatives in particulate matter collected from controlled combustion of various biofuels,[17] and Desyaterik et al. attributed 48% of absorption in collected cloud water samples impacted by biomass burning to a collection of nitrophenols and aromatic carbonyls.[14] Phillips and Smith have also found that as much as 50% of water-extracted BrC absorption from ambient samples can be attributed

to charge transfer complexes formed through the interaction between aromatic carbonyl species and phenolic species[18,19] in analogy to terrestrial and aquatic humic substances.[20,21]

Without a more complete molecular characterization of the organic molecules constituting BrC, it is difficult to predict how its absorption spectrum might evolve in the atmosphere. For example, it may change as the particles photochemically age, the chromophores photobleach, the identities and concentrations of inorganic salts in the particles change, or the pH of the particles changes. The effect of pH, in particular, could be important as it is known to influence the physical and optical properties of humic substances,[22–27] which some fractions of ambient aerosol are known to resemble.[28] Despite the fact that estimates of aerosol pH vary from 0 to 9 in atmospheric particles,[29–33] the effect of pH changes on BrC absorption has not been studied very much at all, and most studies do not measure, much less control, the pH of solvent-extracted filter samples. Lee et al.[34] did find an increase in absorption with increasing pH of water extracts of laboratory-generated naphthalene secondary organic aerosols, which they attributed to deprotonation of nitrophenols. Phillips and Smith[18] demonstrated a similar increase for water-extracted ambient particulate matter noting the similarities with humic substances.[21] Likewise, Teich et al.[35] very recently reported a 60% increase in 370 nm absorption of water-soluble ambient filter extracts when pH increased from 2 to 10, but there is no indication of how pH affects absorption at other wavelengths or pH values, and no physicochemical explanation for the effect was offered. In none of these studies was the role of pH the central focus.

Here, we systematically examine the effect of changing pH on the magnitude and spectral shape of UV-visible absorption by water-soluble ambient brown carbon. We draw on observed similarities with the pH dependent absorption of humic substances to motivate a few plausible explanations including a link between structural changes induced by changing pH and observed absorption changes. We also explore the potential impacts of the pH dependence for the climate through simplified estimates of radiative forcing efficiency.

4.3 Materials and Methods

4.3.1 Aerosol and fulvic acid samples

Ambient aerosols were collected out of a window in the Chemistry Building at the University of Georgia (∼20 m above ground level) in Athens, Georgia (33.9488°N, 83.3747°W), during the months of April, August, September, October, and November of 2016, including five days when the air quality in Athens, GA was heavily impacted by nearby forest fires burning over 100,000 acres across the southeastern United States.[36] A total of 15 (10 baseline ambient, five biomass burning-influenced) samples were collected on 47 mm diameter polytetrafluoroethylene (PTFE, Teflon) filters (0.2 μm pore size, Sterlitech) at 16.7 L/min for separate 24 h periods (shorter for days influenced by the wildfires). A Very Sharp Cut Cyclone inlet (BGI, Inc.) was employed to size select for particles with diameters less than 2.5 μm. Water-soluble organic species were extracted, similarly to Hecobian et al.,[37] by sonication of the filter for 20 min in 10 mL of Milli-Q water ($< 18.2 M\Omega \cdot cm$). Extracted solutions were filtered using a 13 mm, 0.45 μm PTFE disposable syringe filter (VWR 28145-493).

Suwannee River Fulvic Acid (SRFA) was purchased from the International Humic Substances Society and used without further purification or treatment. Solutions of SRFA in Milli-Q water were made at concentrations of 5 mg/L and 50 mg/L.

4.3.2 pH measurement and adjustment

The pH of each aqueous sample was measured using a pH meter (Omega, PHH222) with a gel-filled electrode (Omega, PHE-1332), which were calibrated daily with buffer solutions of pH = 4.01, 7.00, and 10.01. The initial pH of the baseline ambient samples taken before any adjustments were made was 4.20 ($\pm$ 0.38), while the initial pH of the biomass burning-influenced samples was 4.55 ($\pm$ 0.41). The initial pH of the SRFA samples was 3.90. The pH was continuously monitored in the 1 cm cuvette during titration.

The pH of extracts in the cuvette was adjusted through the addition of 1-5 μl of HCl or NaOH solutions of 0.01, 0.1, or 1 M concentration using a micropipette. To minimize hysteresis effects[38,39] the solution pH was cycled between 2 and 11 prior to analysis. The pH was adjusted in increments of approximately one pH unit in both the forward (increasing pH) and the backward (decreasing pH) directions, and the aqueous solutions were stirred continuously using a small magnetic stir bar.

4.3.3 Measurement of UV-visible spectra

UV-visible absorption spectra (200 - 800 nm) of the aqueous extracts were measured on a Cary 60 UV-vis spectrophotometer (Agilent). The absorption spectra were fit to a power law function over the range 300-500 nm according to:

$$A(\lambda) = a \cdot \lambda^{-AAE} \tag{4.1}$$

where A is absorbance, a is a scaling constant, and AAE is the Absorption Ångström Exponent, which describes the wavelength dependence.

4.4 Results

4.4.1 Water-soluble BrC absorption increases at all wavelengths with increasing pH

The absorption spectra of water-soluble (WS) BrC (Figure 4.1) exhibit featureless, near-exponential shapes. There is a clear increase in absorption at all wavelengths as pH increases, yet the shapes of the spectra remain largely the same. Specifically, they all display a power law dependence on wavelength (Equation 4.1) for wavelengths greater than 300 nm, as illustrated by the linearly decaying absorption displayed on the log-log plot in the inset to Figure 4.1. The systematic increase in absorption with pH is more clearly evident in the plot of integrated absorption (300-500 nm) vs. pH in Figure 4.2. On average, an increase of one unit in pH results in a 10% increase in integrated absorption. However, the samples clearly fall into two groups, with one showing a more pronounced pH dependence (with a 13% increase per pH unit) and the other a smaller one (with a 8% increase per pH unit), and in fact these slopes are statistically different at the $p < 0.01$ level. These groups may represent particles from different sources or of different photochemical age, but without chemical markers it is difficult to know.

Interestingly, we found that the magnitude of absorption from the biomass burning-influenced samples also increased with pH (orange open circles in Figure 4.2) with a dependence resembling the upper group of baseline ambient samples (blue squares in Figure 4.2) that were not influenced by biomass burning events. The similarity hints at a possible correlation, perhaps indicating that some of our baseline ambient samples originated from biomass burning events further away, though we stress that this is very speculative. The spectra from the biomass burning-impacted samples (Figure 4.3) are not fit well by a power law function, however, and demonstrate spectral features not evident in the baseline ambient samples. Also of note, the pH dependence of SRFA spectra (gray open triangles in Figure 4.2) is similar to the lower group of ambient samples (green squares in Figure 4.2) suggesting a potential resemblance between these samples and humic substances. The increase in absorption with pH observed in all samples suggests that this might be a feature common to ambient WS BrC spanning a wide range of sources and photochemical age.

4.4.2 Effect of pH on absorption is a function of wavelength

While increasing alkalinity increases WS BrC absorption at all wavelengths, the magnitude of this increase was found to be a function of wavelength. Specifically, absorption at longer wavelengths increases proportionately more than at shorter wavelengths. This trend is clear in Figure 4.4a in which the ratio of the average absorption at pH = 5, 7, and 10 relative to absorption at pH = 2 is plotted. The calculated ratio gets rather noisy at about 500 nm since the WS BrC spectra are very close to the detection limit at this point. By way of comparison, Teich et al.

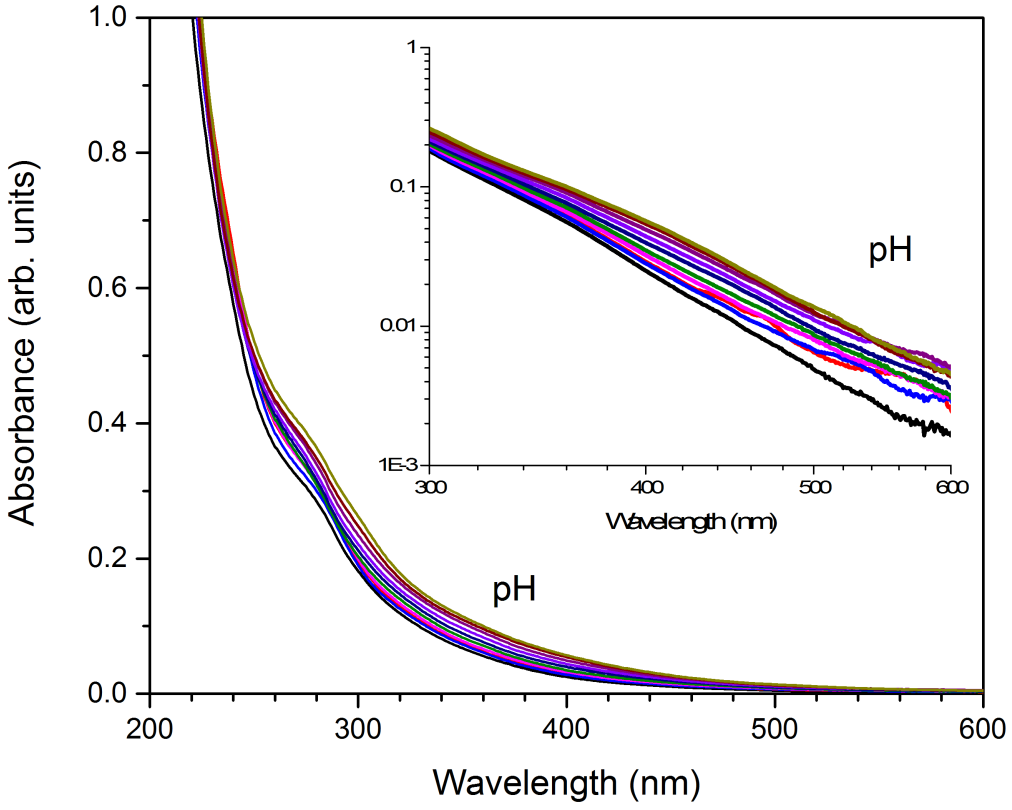

Figure 4.1: Averaged absorbance spectra as a function of pH for the baseline ambient samples. Each spectrum is normalized to the value at 225 nm and pH = 11 for that sample. The linearity of the log-transformed spectra (inset) indicates quality of fit to a power law function.

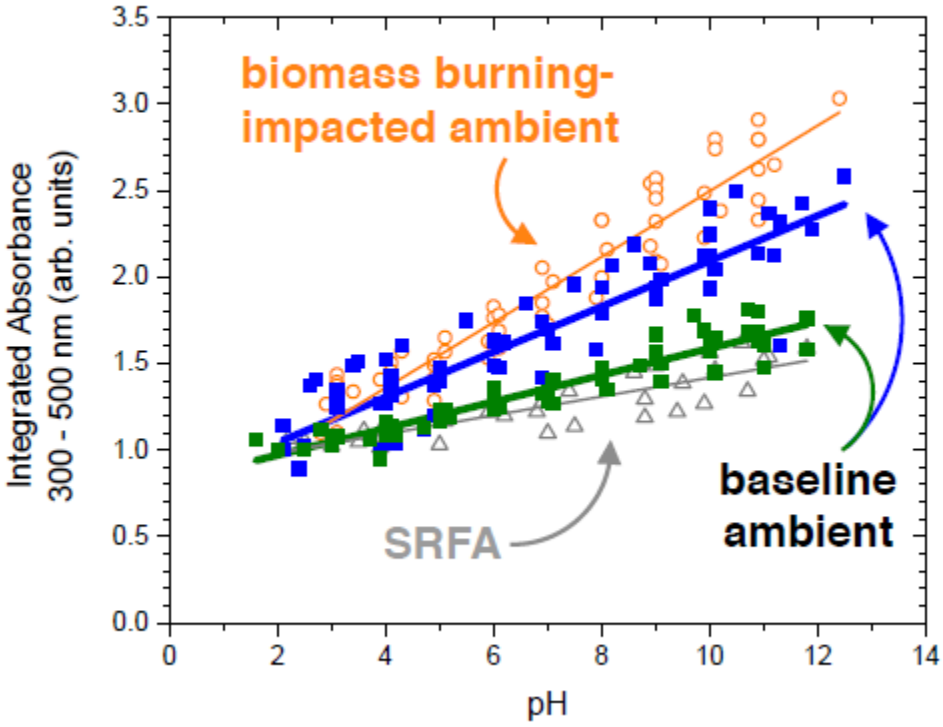

Figure 4.2: Integrated absorbance (300-500 nm) as a function of pH. Baseline ambient samples separate into two groups (blue and green squares), one of which resembles the SRFA samples (gray triangles), while the other resembles the biomass burning impacted samples (orange circles).

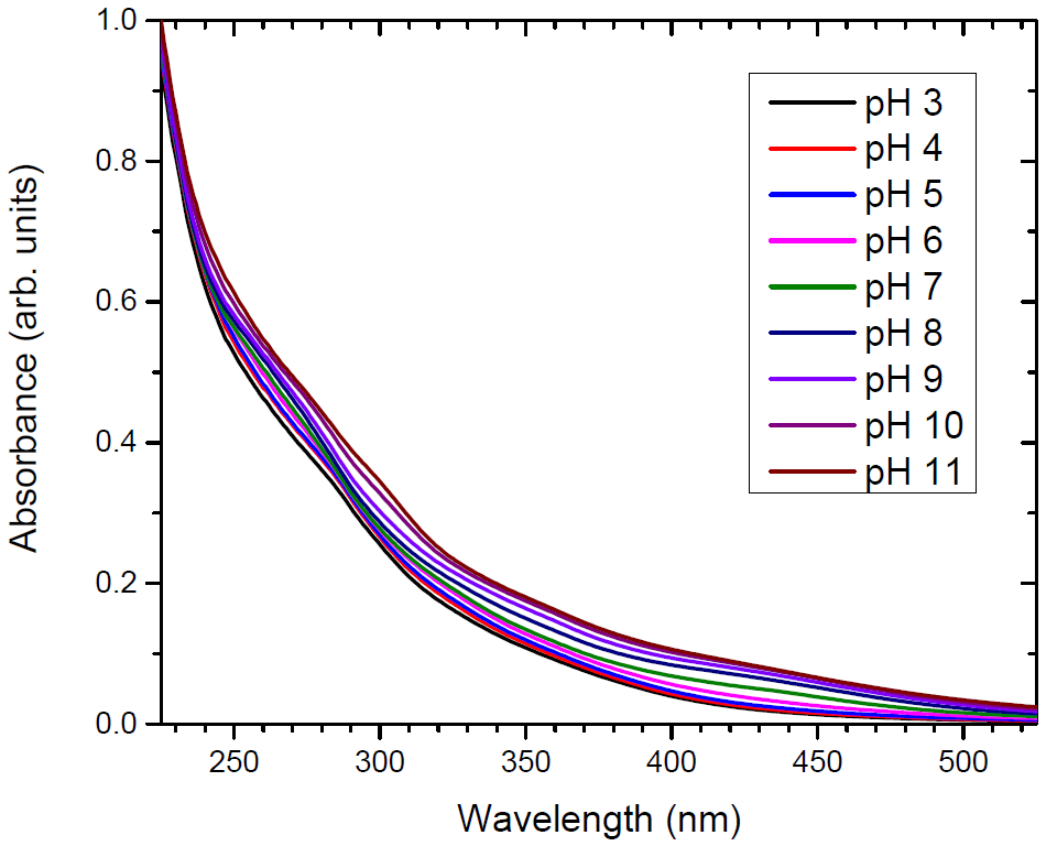

Figure 4.3: Averaged absorbance spectra of ambient Athens, GA samples affected by wildfires (November, 2016). The spectra are not fit by a power law function as well as the baseline ambient spectra are.

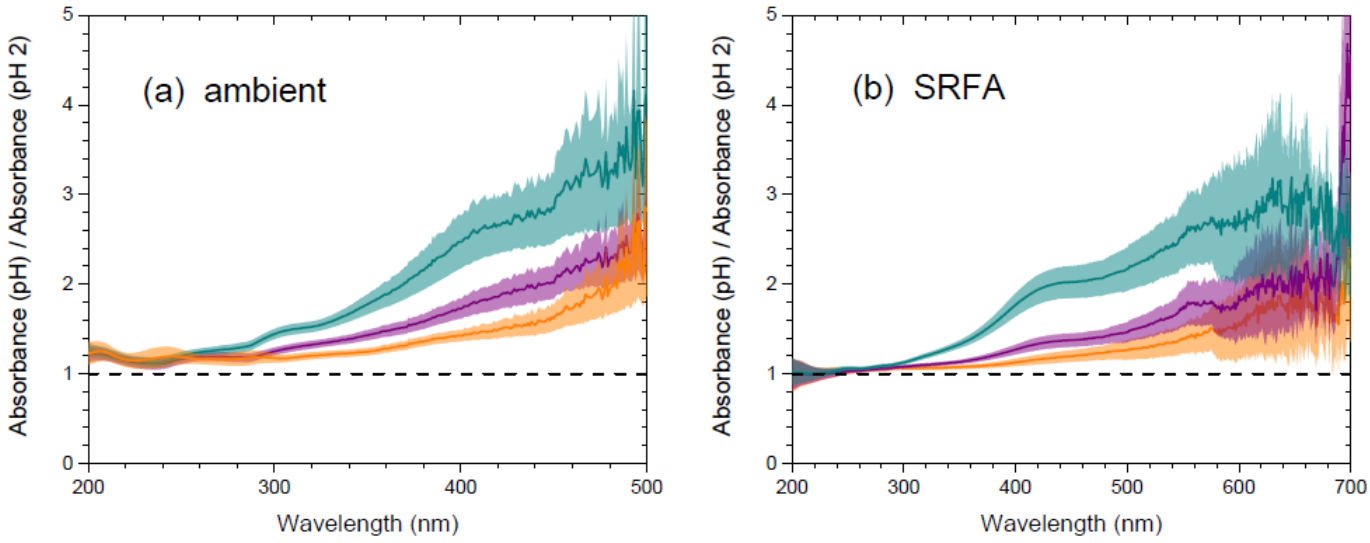

Figure 4.4: Ratio of absorbance at pH = 5 (orange), pH = 7 (purple), and pH = 10 (green) relative to pH = 2 as a function of wavelength for: (a) baseline ambient samples, and (b) SRFA samples.

report an increase in BrC absorption at 370 nm by a factor of 1.6 in going from pH = 2 to pH = 10 in Germany;[35] here, we observe an increase by a factor of 2.0 at the same wavelength. The spectra of the SRFA demonstrate a very similar dependence on pH and wavelength (Figure 4.4b), but with the larger signal-to-noise the trend is seen to persist to wavelengths up to at least 700 nm. Previous work with SRFA and other humic and fulvic substances have also reported more pronounced increase in absorption with increasing pH at longer wavelengths.[40]

Strikingly, the absorption ratio for both the WS BrC and the SRFA samples never falls below a value of unity as would be expected if chromophores were removed due to deprotonation. For example, the 350 nm absorption peak of 4-nitrocatechol, a

chromophore sometimes attributed to BrC,[16,41,42] disappears as pH is raised above its first pKa of 6.65[43] while another peak at 425 nm, corresponding to the deprotonated form, appears (see Figure 4.5). Any similar shifts in absorption occurring in the WS BrC samples would have to be coincidentally compensated for by shifts associated with other chromophores to explain the increase observed at all wavelengths. The unlikeliness of this coincidence occurring in all samples suggests the existence of some other pH-dependent mechanism that affects the whole host of chromophores. One such potential explanation involves the alteration of supramolecular assemblies of molecules[44,45] and is discussed in more detail in section 4.5.

The wavelength dependence of the pH effect on absorption results in a subtle yet measurable effect on the shape of the spectrum. As illustrated by the linear trends in the log-transformed spectra shown in the Figure 4.1 inset, a power law function fits the spectra well, though the corresponding AAE (reflected by the slope) does change. This trend is apparent in Figure 4.6 in which the AAE values from the power law fits are plotted as a function of pH. Each sample exhibits this decrease in AAE individually (shown in Figure 4.7), and on average the AAE decreases by 0.18 per unit pH increase. This systematic relationship between AAE and pH is also observed with the SRFA samples, which demonstrate a similar decrease of 0.16 per unit increase in pH, though the AAEs are on average 8% lower than for the WS BrC. This similarity in the pH dependence of the spectral shapes further supports a common underlying chemical explanation.

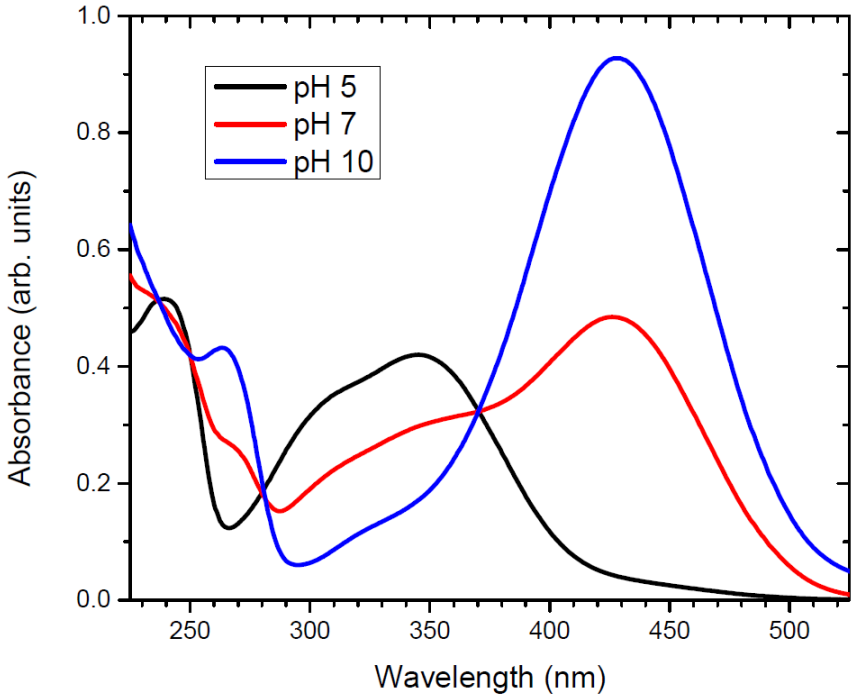

Figure 4.5: Absorbance spectra of a 50 mg/L aqueous 4-nitrocatechol solution at pH = 5, pH = 7, and pH = 10. The peak at 430 nm present at pH =7 and pH = 10 corresponds to the deprotonated phenolate form.

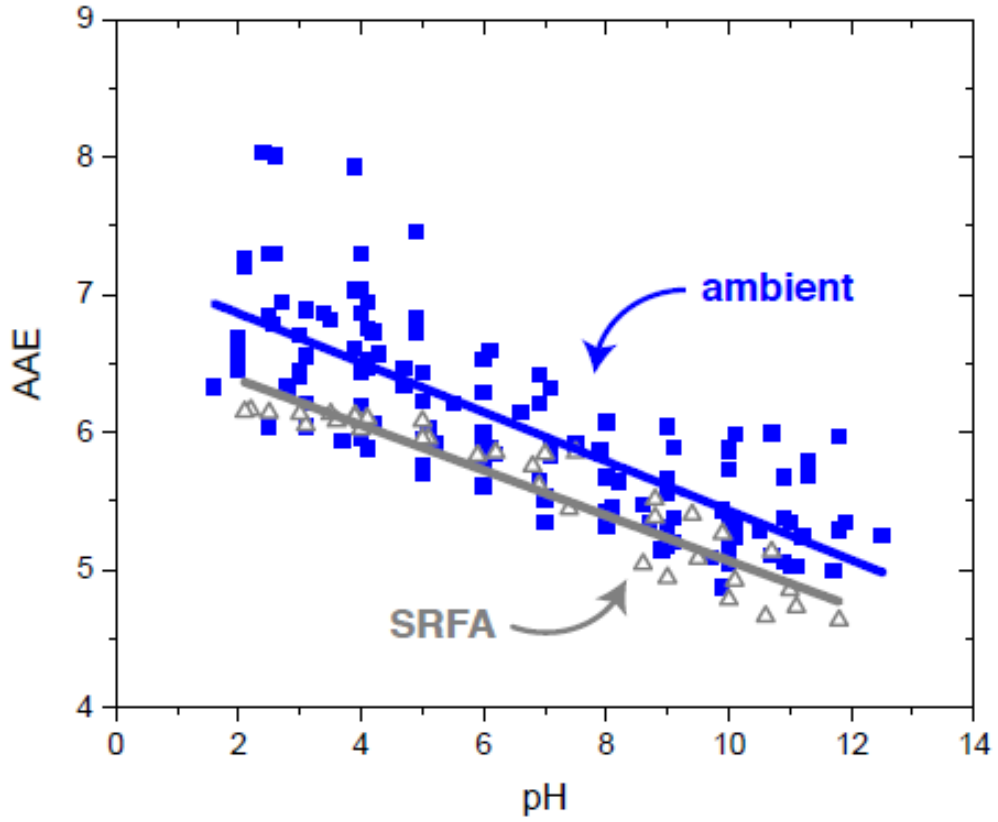

Figure 4.6: Absorption Ångström exponent as a function of pH for baseline ambient (blue squares) and SRFA (gray triangles) samples.

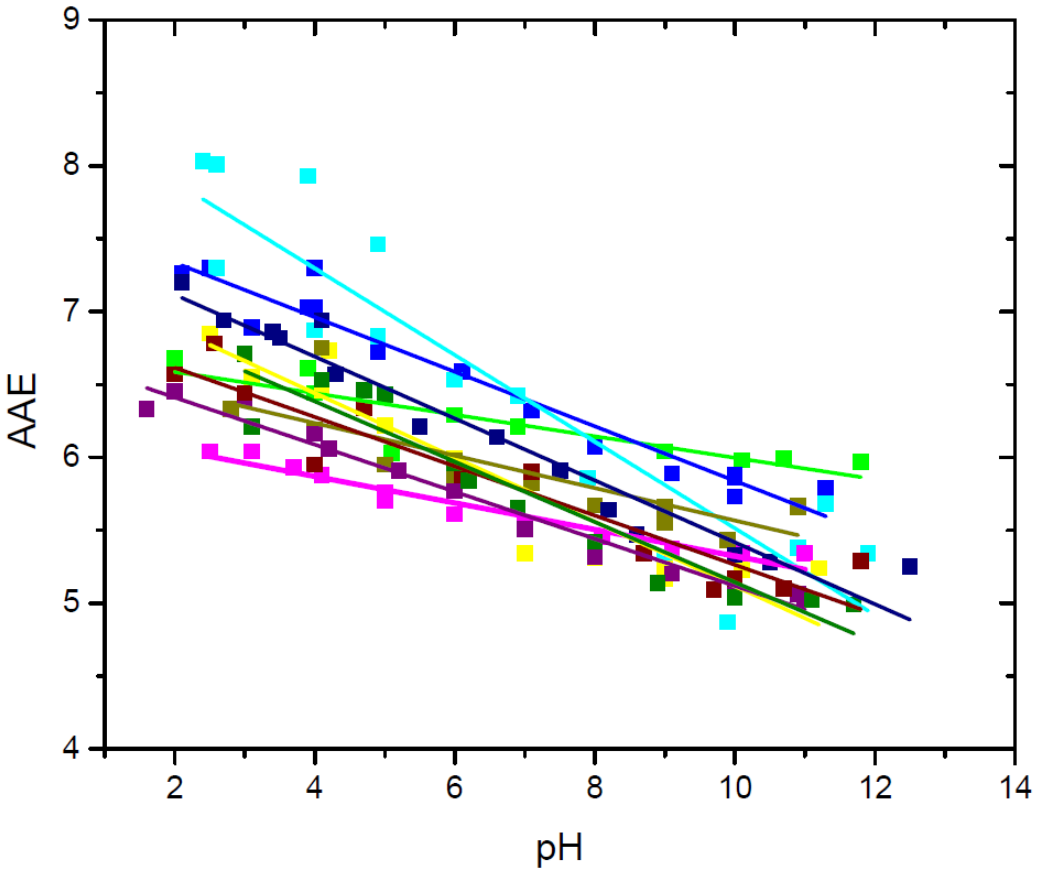

Figure 4.7: Absorption Ångström exponent (AAE) as a function of pH for individual baseline ambient Athens, GA filter samples. All samples show a similar trend of decreasing AAE with increasing pH.

4.4.3 Differential spectra reveal absorption features accompanying pH increase

To better resolve changes in spectral features associated with changing pH, we used differential absorbance spectroscopy (DAS). The DAS spectrum is calculated according to the equation:

$$\Delta A_{pH}(\lambda) = A_{pH}(\lambda) - A_{pH_{ref}}(\lambda) \tag{4.2}$$

where $\Delta A_{pH}(\lambda)$ is the difference between the absorbance, A, at a particular value of pH and at a reference pH, pH_{ref}. Here, pH_{ref} was chosen to be pH = 2, the lowest pH studied. Because DAS isolates differences in absorbance spectra, it is useful for detecting subtle changes accompanying changing physicochemical conditions; for example, it has been employed to investigate how absorption by humic and fulvic substances and dissolved organic matter are affected by pH.[27,46] That work has identified different DAS spectra at low pH values (pH < 6) and at high values (pH > 7) leading to the suggestion that the observed changes are correlated with the deprotonation of carboxylic acids at low pH and of phenols at high pH. These functional groups have previously been identified as being prevalent in humic and fulvic substances with effective pKas of $2.0 - 3.8$ and $7.2 - 10.9$ for carboxylic acids and phenols, respectively.[47] Similarly, carboxylic acids have been found to account for $10\% - 40\%$ of organic particulate matter from a variety of sources[48] and phenols arise from lignin burning and have been identified in ambient and biomass burning aerosols.[13,17,49,50]

The average DAS spectra (Figure 4.8) were calculated by first normalizing each individual DAS spectrum to the value at 370 nm and pH = 11; this was necessary to account for differences in magnitude of absorption from day to day amongst the samples. These DAS spectra reflect the increase in overall absorption with increasing pH observed in the spectra (Figure 4.1), but they also make it possible to identify specific bands that appear and grow as pH increases such as the peaks near 260 nm and 300 nm. It is possible that the peak at 260 nm could arise from aromatic species, which are known constituents of humic substances and humic-like substances in particulate matter,[28] and absorb near this wavelength. For example, benzene and many substituted benzene species have absorption peaks in the 250 nm − 270 nm range.[51] Likewise, the peak near 300 nm could originate from phenolate anions created from the deprotonation of phenols; for example, the phenol absorption peak shifts from 270 nm to 287 nm upon deprotonation.[51] The 300 nm peak can be seen to grow in intensity relative to the 260 nm peak at pH = 7 and higher, precisely in the range of pKas found for phenols in fulvic acids (pKa = $7.2 - 10.9$[47]).

The DAS spectra in Figure 4.8 also display what appears to be a broad continuum at wavelengths longer than 350 nm. This band decreases monotonically with increasing wavelength while the magnitude of absorption increases with pH at all wavelengths. Even more intriguing, this band looks nearly identical for all pH values when normalized to the value at 370 nm at each pH (Figure 4.9a). Such normalization makes it possible to view the spectral changes at different wavelengths relative to one another despite the different magnitudes in the DAS spectrum at different pH values. It is clear that the shape of the differential spectrum, that is how much

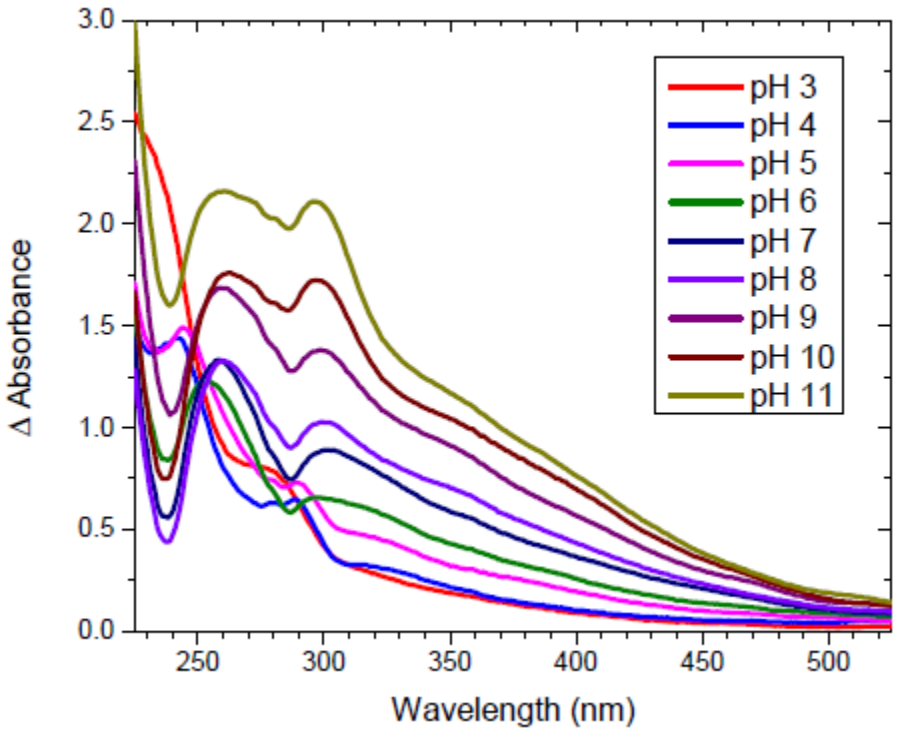

Figure 4.8: Average differential absorption spectra for pH = 3-11 relative to pH = 2 displaying the emergence of spectral features near 260 nm and 300 nm as well as a long wavelength tail. Each sample was normalized to the value at 370 nm and pH = 11.

absorption increases with pH as a function of wavelength, does not change over the wide range of pHs from pH = 3 to pH = 11. By contrast, the relative magnitudes of the peaks near 250 nm and 290 nm decrease dramatically with increasing pH. This behavior indicates that there is something about the increasing pH that systematically increases absorption at $\lambda > 350$ nm in a similar manner whether pH increases from 2 to 3 or from 2 to 11. This behavior is not consistent with a simple model of a superposition of chromophores that are deprotonated at successively higher pH values since that would involve a decrease in absorption by the chromophore at some wavelength accompanying an increase in absorption by the deprotonated form at another. In fact, no decrease is observed at any wavelengths over the entire range from 225 nm to 525 nm. Interestingly, the very same behavior is observed at wavelengths longer than 350 nm in the normalized DAS spectra of SRFA (Figure 4.9b). For both systems to demonstrate such a response to pH simply because of deprotonation of a superposition of chromophores would have to be so coincidental as to make it nearly impossible. Instead, we interpret the similarity as further support for a common explanation in which the increased absorption with increasing alkalinity by both ambient BrC and SRFA is attributed to a structural alteration of the aggregation of organic molecules. We discuss this hypothesis in more detail in section 4.5.

4.5 Discussion

The systematic absorption increase with increasing pH observed in all ambient samples, including those affected by biomass burning, as well as humic substances, suggests an underlying chemical cause linked to deprotonation. Elucidating this cause

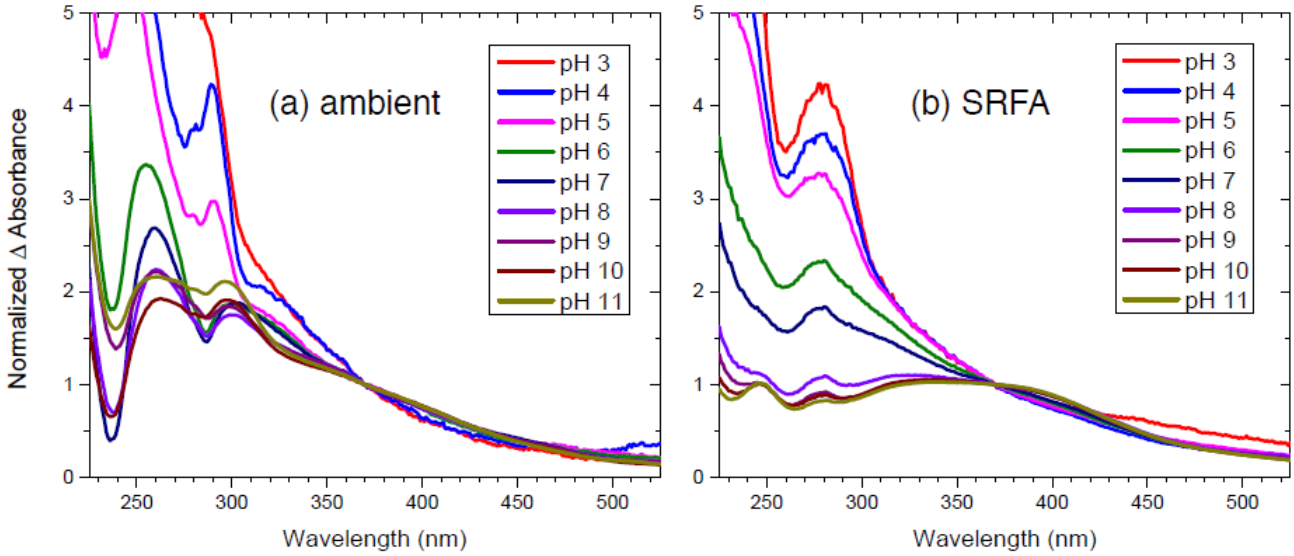

Figure 4.9: Normalized differential absorption spectra for pH = 3-11 relative to pH = 2 for (a) ambient and (b) SRFA samples. Each spectrum is normalized to the absorbance at 370 nm to allow relative changes in absorbance to be identified more clearly. Strikingly, the long wavelength tail ($\lambda > 370$ nm) is remarkably similar at all pH values and for both ambient and SRFA samples.

could be important for understanding how BrC absorption changes as particle composition evolves in the atmosphere, how to compare disparate BrC measurements made at a variety of sites with different sampling approaches and under different conditions, and how radiative transfer in the atmosphere is sensitive to the pH of particles. Despite the clear link between pH and BrC absorption, however, there is relatively little known about the chemical nature of this link. We believe that there are likely several explanations for why absorption increases with increasing pH, including both direct deprotonation of chromophores as well indirect modification of chromophores through structural changes of molecular assemblies accompanying deprotonation. We discuss each of these below.

4.5.1 Direct effects of deprotonation on chromophores: nitro-aromatics and phenols

Nitro-aromatic species

There is growing evidence that nitro-aromatic species are important chromophores in BrC[13] (and references therein), especially since it is one of only a few classes of molecules that absorb significantly into the visible region of the spectrum. The absorption spectra of nitro-aromatic species tend to shift to longer wavelengths upon deprotonation[34] and could explain some of the apparent increased absorption at longer wavelengths. For example, we show in Figure 4.5 the absorption spectrum of 4-nitrocatechol with a peak at 350 nm at pH = 5 that decreases in intensity as pH is raised and is replaced by one at 425 nm at pH = 10. Such a shift, however, could only explain part of the observed change because nitro-aromatics are thought

to account for only 4% of BrC absorption in ambient aerosols.[15,16] Curiously, there is no decrease in absorbance observed at shorter wavelengths as would be expected if nitro-aromatic species were replaced by their deprotonated analogs. What is more, these species generally dont absorb at wavelengths as long as 500 nm and therefore could not explain the increase in BrC absorption observed there. There would also need to be an unlikely coincidental superposition of many of these absorption spectra to account for the observed BrC spectra and their response to pH changes. So, while some of the pH dependence could be attributed to nitro-aromatic species, it is clear that other chromophores must contribute as well.

Phenols and charge transfer complexes

The differential absorption spectra (Figure 4.8) show a clear emergence of a peak near 300 nm as pH increases, which may correspond to the known absorption band of phenolate anions in the $285-293$ nm range.[52] What is more, this band appears at pHs in the range of pKas reported for substituted phenols ($4.7-11.6$[53]) and apparent pKa values attributed to phenolic groups in fulvic acids ($7.2-10.9$[47]). It seems likely, given the existence of phenols and phenol groups in ambient aerosols,[13,17,49,50] biomass pyrolysis products,[54,55] and humic substances,[56,57] that some of the increase observed in the UV region of the spectra could be attributed to the conversion of phenols to phenolate anions. However, the absorption increase at longer, visible wavelengths as well as at lower pH values cannot be attributed directly to phenol deprotonation.

It is also possible that phenolate anions formed at alkaline pHs contribute to increased visible absorption through their participation in charge transfer complexes. These complexes occur through a transfer of charge from a donor group, such as a phenol, to an acceptor group, such as an aromatic carbonyl, and give rise to electronic transitions with energies different than those of the transitions of the individual constituent groups. Many different charge transfer complexes can be formed with a near-continuum of transition energies, and there is evidence that they can account for a substantial fraction of the visible absorption in both ambient particulate matter[18,19] and humic substances.[20,58] As pH increases, phenolate anions, with lower ionization potentials than corresponding phenols,[59] could act as better electron donors giving rise to both stronger absorption bands as well as bands at longer wavelengths.[21] This effect, however, cannot account for the observed increase in visible absorption at lower pHs (Figures 4.1 and 4.8) where phenols are not deprotonated.

4.5.2 Indirect effect of deprotonation on chromophores: Alteration of a supramolecular assembly

There are many similarities, both chemical and optical, between WS BrC and humic substances.[28] Both are polyacidic with similar functional groups and moieties, including polycyclic ring structures, hydroxyl, carboxyl, and carbonyl groups. They also each have absorption spectra that are broad, featureless, and decrease in intensity with increasing wavelength, and they even display similar fluorescence spectra.[19,28] These similarities suggest that they may share common chemical explanations for the observed increase in absorption with pH, which they also both demonstrate. While

there have been relatively few studies investigating the effect of pH on BrC, there has been substantial research with humic substances and the effect of pH on them. However, there is as yet no comprehensive explanation linking chemical and optical changes accompanying changes in pH.

What is known is that humic substances appear to adopt smaller sizes at low pH, and this has been explained in terms of a supramolecular assembly theory[44,60] in which small molecules form aggregates that are stabilized through a combination of hydrophobic forces and the formation of hydrogen bonds.[38] There is substantial evidence in the literature from size exclusion chromatography,[61] fluorescence quenching,[62] TEM,[60] photon correlation spectroscopy,[60] small-angle X-ray scattering,[63] and NMR,[64] that humic and fulvic acids form such aggregates. At low pH, when most carboxylic acid groups are protonated, hydrophobic dispersive forces, such as van der Waals, $\pi - \pi$, and CH$-\pi$, and hydrogen bonding drive aggregation and provide structural stability.[28,44] As the pH increases, a growing number of carboxylate and phenolate anions are created that repel each other and hydrogen bonds are disrupted. As a result, the assembly adopts a more open configuration as pH is raised, which has been observed with a variety of methods, including diffusivity measurements,[25] small angle neutron scattering,[65] turbidity,[66] scanning electron microscopy,[66] and dynamic light scattering.[24,60,67–69]

Given the many similarities between ambient organic particulate matter and humic substances, we hypothesize that such supramolecular assemblies are formed in ambient aerosols as well. Furthermore, we hypothesize that some of the observed change in absorption of water-soluble brown carbon with changing pH is attributed

to an alteration of the supramolecular assembly of their constituent molecules. We suggest that the increased flexibility accompanying this change can potentially influence the absorption spectrum in three ways: 1) decreased interaction between neighboring aromatic moieties making them absorb UV light more strongly, similar to the observed increase in absorption by DNA upon denaturation,[70] 2) increased flexibility of conjugated polyenes with longer extent of conjugation leading to more absorption at longer wavelengths,[71] and 3) increased number and diversity of charge transfer contacts that can be made between donor moieties (e.g. phenols and phenolate ions) and acceptor moieties (e.g. aromatic ketones and aldehydes) increasing and red-shifting absorption.[18,21] Janot et al.[46] have also suggested that the increase in the broad absorption band of humic substances near 370 nm observed with increasing pH could be associated with such "intrachromophore interactions" (e.g. charge transfer complexes), though they are careful to point out that this is speculative.

The potential link between increased pH and increased absorption by charge transfer complexes is particularly interesting because they may be responsible for a sizeable fraction of WS BrC absorption including well into the visible region where few other potential chromophores absorb.[18,19] Since these complexes are formed through local interactions between electron-donating and electron-accepting groups, it stands to reason that as pH increases and the supramolecular assembly adopts a less compact and less rigid conformation, more charge transfer contacts will be formed and absorption will increase. What is more, this change could occur continuously over a wide range of pHs, beginning at acidic conditions where carboxylic acid groups deprotonate (whose apparent pKas in fulvic acids fall in the range $2 - 3.8$[47])

and extending to alkaline conditions where phenols deprotonate (whose apparent pKas in fulvic acids fall in the range $7.2-10.9$[47]). Alvarez-Puebla and Garrido[67] observed such a continuous increase in charge with increasing pH in humic substances using laser Doppler electrophoresis. Likewise, Brigante et al.[26] observed a continuous increase in the rate of dissolution of humic acid particles over a wide pH range, which they attribute to the continuous increase in charge accompanying deprotonation. Thus, it seems reasonable that at least some of the systematic increase in absorbance observed for WS BrC from pH = 2 to pH = 12 (Figure 4.2) could be explained by conformational changes accompanying increasing charge.

Furthermore, the opening up of the supramolecular assembly with increasing pH would be expected to increase the likelihood of forming all of the different charge transfer complexes with their different absorption bands. In fact, this is exactly what is observed in the normalized differential absorption spectra (Figure 4.9a) at the longer wavelengths ($\lambda > 370$ nm). Here, even as pH increases, the shape of the differential spectrum does not change substantially. There is a slight difference apparent at pH = 3 and pH = 4, but that might be a result of incomplete deprotonation of the carboxylic acids at such low pH values; for pH = 5 and higher the similarity is remarkable. What is more, this region of the spectrum is precisely where Phillips and Smith found charge transfer complexes in WS BrC to contribute the most to absorption, proportionately;[18] they proposed a gradual transition from absorption dominated by independent chromophores at $\lambda < 300$ nm to absorption dominated by charge transfer complexes at $\lambda > 370$ nm with a gradual transition occurring in between. That model is consistent with the uniform spectral response observed in

the normalized DAS spectra of Figure 4.9a if increasing pH affects all of the near-continuum of charge transfer complexes in similar ways. Such a uniform behavior would have to be highly coincidental for a superposition of chromophores, for example nitro-aromatic species. What is more, such a change would be accompanied by a decrease in absorption at shorter wavelengths (see Figure 4.5, for example), which is not observed.

Clearly, the many similarities between WS BrC and humic substances suggest that supramolecular assemblies may be an important part of explaining the pH dependence of light absorption. However, this link is still speculative at this point and requires additional work to establish more firmly.

4.5.3 Atmospheric implications

The systematic increase in absorbance accompanying increases in pH could have implications for the role BrC plays in influencing the radiative balance in the atmosphere. For example, radiative forcing by aerosols may be overestimated in climate models if refractive index values based on measurements made at pH = 7 instead of more representative values, such as pH = 2, are used. Likewise, the climate impact may vary depending on season, location, or particle age to the extent that pH changes with these conditions, too. To explore the potential effect of particle pH on radiative transfer, we have calculated the simple forcing efficiency (SFE, units of W/g) using the formulation of Chen and Bond,[6] (details given in Appendix 1) which is commonly used to estimate climate impacts associated with changing particle properties.[8,72]

We investigated three possible scenarios involving a mixture of black carbon and organic matter (in a 1:10 mass ratio): 1) an external mixture, 2) an internal mixture, and 3) a combination of both internally mixed and externally mixed particles with 50% of the organic mass in each type of particle. For each of these, we set the value of kOA (550 nm) at pH = 2 to either 0.001 (low BrC absorption) or 0.010 (high BrC absorption). These values were chosen to represent a range of possible values for organic particulate material consistent with recent measurements, though we point out that substantial uncertainty remains regarding them.[8] And, since these values are used for all of the organic material, both BrC and non-absorbing, they are best thought of as effective refractive index values. The value of kOA was parameterized as a function of both wavelength and pH based on the results of this study (details given in Appendix 2).

Figure 4.10 shows the percentage increase in SFE calculated for the various scenarios as a function of pH. In all cases SFE increases with pH with the most pronounced effects occurring for completely externally mixed particles, which may be more representative of freshly emitted aerosols that havent yet mixed internally. Such a case could represent newly formed aerosols near biomass burning sources, for example.[7] Clearly, the magnitude of the pH effect is influenced by the magnitude of absorption by the organic fraction, too. Thus, the influence of pH may be more pronounced in particles containing more highly absorbing, extremely low volatility organic compounds (ELVOCs) and thus might be a function of combustion conditions.[8] Figure 4.10 also illustrates that if pH is not accounted for in making bulk aerosol measurements, the impact of BrC absorption on SFE can be overestimated;

for example, measurements made at pH = 7 overestimate SFE by 5% - 49% (depending on kOA(550 nm) and mixing state) compared to pH = 2, a value more representative of ambient aerosol acidity in many locations, including the Southeast U.S.[33] Thus, to the extent that aerosol pH may change in the atmosphere or may vary from sample to sample, its impact on aerosol absorption and radiative forcing should be considered.

4.6 Acknowledgements

The authors gratefully acknowledge support for this research by the National Science Foundation (AGS-1241621) and Prof. Rawad Saleh for providing Matlab code for performing the Mie calculations.

4.7 Appendix 1. Details of simplified forcing efficiency (SFE) calculations

The SFE was calculated at each pH value and mixing state according to the formulation of Chen and Bond[6]:

$$SFE = \int_{300nm}^{800nm} \frac{dSFE}{d\lambda} = \int_{300nm}^{800nm} -\frac{1}{4}\frac{dS}{d\lambda}\tau_{atm}^2(1-F_c)\left[2(1-a_s)^2 \cdot \beta \cdot MSC - 4a_s \cdot MAC\right] \tag{4.3}$$

where a_s is the solar irradiance (taken from the ASTM G173-03 reference spectrum,[73] τ_{atm} is the atmospheric transmission (0.79[74]), F_c is the cloud fraction (0.6[74]), and as is the surface albedo (0.19[74]). The backscatter fraction, β, is taken to be a

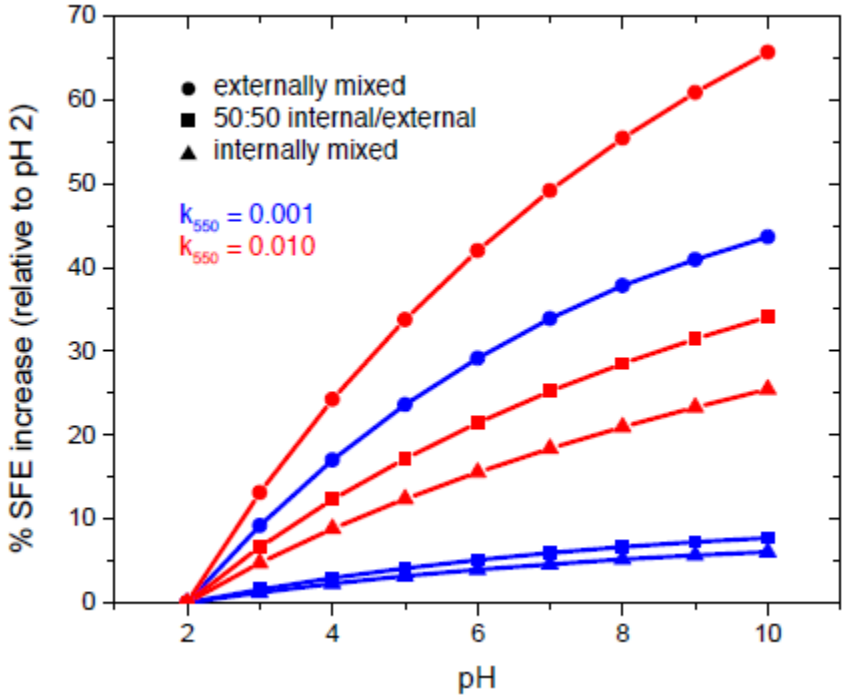

Figure 4.10: Calculated increase in estimated simple forcing efficiency as a function of pH for weakly- and strongly-absorbing organic particulate matter (blue and red points, respectively). Three different mixing states with black carbon are assumed: externally mixed (circles), internally mixed (triangles), and 50:50 in which half the organic matter is internally mixed with black carbon and the other half is externally mixed.

constant value (0.17^8) at all wavelengths and for all particle diameters, and MSC and MAC are the mass scattering and mass absorption cross section of the particles, respectively. The MSC and MAC are calculated from Mie theory for coated spheres consisting of both black carbon and organic material. The value of k_{OA} was parameterized as a function of both wavelength and pH based on the results of this study (see Appendix 2).

4.8 Appendix 2. Details of the parameterization of k_{OA} as a function of λ and pH

The imaginary part of the refractive index for the organic aerosol component, k_{OA}, was parameterized as a function of both λ and pH according to the findings of the present work.

The wavelength dependence of the value of k_{OA} was assumed to follow a power law function:

$$k_{OA}(\lambda, pH) = k_{550}(pH) \cdot \left(\frac{550}{pH}\right)^{w(pH)} \tag{4.4}$$

with k_{550} the value of k_{OA} at $\lambda = 550$ nm and the exponent, w, describing the wavelength dependence. Both k_{550} and w are functions of pH:

$$k_{550}(pH) = k_{550}(pH = 2) \cdot [1 + 0.25 \cdot (pH - 2)] \tag{4.5}$$

which is derived from the spectra shown in Figure 1 in the main text, and:

$$w(pH) = 6.16 - 0.17 \cdot pH \tag{4.6}$$

which is derived from the observed trend of AAE vs. pH (Figure 4.6 in the main text) and the assumption that w = AAE - 1.[8]

Bibliography

[1] Bond, T. C. et al. *Journal of Geophysical Research: Atmospheres* **2013**, *118*, 5380–5552.

[2] Cheng, Y.; He, K.-b.; Du, Z.-y.; Engling, G.; Liu, J.-m.; Ma, Y.-l.; Zheng, M.; Weber, R. J. *Atmospheric Environment* **2016**, *127*, 355–364.

[3] Hammer, M. S.; Martin, R. V.; van Donkelaar, A.; Buchard, V.; Torres, O.; Ridley, D. A.; Spurr, R. J. D. *Atmospheric Chemistry and Physics* **2016**, *16*, 2507–2523.

[4] Kirchstetter, T. W.; Novakov, T.; Hobbs, P. V. *Journal of Geophysical Research: Atmospheres* **2004**, *109*, D21208.

[5] Andreae, M. O.; Gelencsér, A. *Atmospheric Chemistry and Physics* **2006**, *6*, 3131–3148.

[6] Chen, Y.; Bond, T. C. *Atmospheric Chemistry and Physics* **2010**, 1773–1787.

[7] Lack, D. A.; Langridge, J. M.; Bahreini, R.; Cappa, C. D.; Middlebrook, A. M.; Schwarz, J. P. *Proceedings of the National Academy of Sciences of the United States of America* **2012**, *109*, 14802–14807.

[8] Saleh, R.; Robinson, E. S.; Tkacik, D. S.; Ahern, A. T.; Liu, S.; Aiken, A. C.; Sullivan, R. C.; Presto, A. A.; Dubey, M. K.; Yokelson, R. J.; Donahue, N. M.; Robinson, A. L. *Nature Geoscience* **2014**, *7*, 647–650.

[9] Sareen, N.; Schwier, A. N.; Shapiro, E. L.; Mitroo, D.; McNeill, V. F. *Atmospheric Chemistry and Physics* **2010**, *10*, 997–1016.

[10] De Haan, D. O.; Tolbert, M. a.; Jimenez, J. L. *Geophysical Research Letters* **2009**, *36*, L11819.

[11] Updyke, K. M.; Nguyen, T. B.; Nizkorodov, S. a. *Atmospheric Environment* **2012**, *63*, 22–31.

[12] Powelson, M. H.; Espelien, B. M.; Hawkins, L. N.; Galloway, M. M.; De Haan, D. O. *Environmental science & technology* **2014**, *48*, 985–993.

[13] Laskin, A.; Laskin, J.; Nizkorodov, S. A. *Chemical Reviews* **2015**, *115*, 4335–4382.

[14] Desyaterik, Y.; Sun, Y.; Shen, X.; Lee, T.; Wang, X.; Wang, T.; Collett, J. L. *Journal of Geophysical Research: Atmospheres* **2013**, *118*, 7389–7399.

[15] Mohr, C. et al. *Environmental science & technology* **2013**, *47*, 6316–24.

[16] Zhang, X.; Lin, Y.-H.; Surratt, J. D.; Weber, R. J. *Environmental Science & Technology* **2013**, *47*, 3685–93.

[17] Lin, P.; Aiona, P. K.; Li, Y.; Shiraiwa, M.; Laskin, J.; Nizkorodov, S. A.; Laskin, A. *Environmental Science & Technology* **2016**, *50*, 11815–11824.

[18] Phillips, S.; Smith, G. *Environmental Science & Technology Letters* **2014**, *1*, 382–386.

[19] Phillips, S. M.; Smith, G. D. *Journal of Physical Chemistry A* **2015**, *119*, 4545–4551.

[20] Vecchio, R. D.; Blough, N. *Environmental science & technology* **2004**, 3885–3891.

[21] Sharpless, C. M.; Blough, N. V. *Environmental science. Processes & impacts* **2014**, *16*, 654–71.

[22] Ghosh, K.; Schnitzer, M. *Journal of Soil Science* **1979**, *30*, 735–745.

[23] Baes, A. U.; Bloom, P. R. *Soil Science Society of America Journal* **1990**, *54*, 1248–1254.

[24] Pinheiro, J. P.; Mota, A. M.; d'Oliveira, J. M. R.; Martinho, J. M. G. *Analytica Chimica Acta* **1996**, *329*, 15–24.

[25] Wang, Y.; Combe, C.; Clark, M. M. *Journal of Membrane Science* **2001**, *183*, 49–60.

[26] Brigante, M.; Zanini, G.; Avena, M. *Colloids and Surfaces A: Physicochemical and Engineering Aspects* **2007**, *294*, 64–70.

[27] Dryer, D.; Korshin, G.; Fabbricino, M. *Environmental Science and Technology* **2008**, *42*, 6644–6649.

[28] Graber, E.; Rudich, Y. *Atmospheric Chemistry and Physics* **2006**, 729–753.

[29] Fridlind, A. M.; Jacobson, M. Z. *Journal of Geophysical Research: Atmospheres* **2000**, *105*, 17325–17340.

[30] Keene, W. C.; Pszenny, A. A. P.; Maben, J. R.; Sander, R. *Geophysical research letters* **2002**, *29*, 1–4.

[31] Pszenny, A. A. P.; Moldanová, J.; Keene, W. C.; Sander, R.; Maben, J. R.; Martinez, M.; Crutzen, P. J.; Perner, D.; Prinn, R. G. *Atmospheric Chemistry and Physics* **2004**, *4*, 147–168.

[32] Guo, H.; Xu, L.; Bougiatioti, A.; Cerully, K. M.; Capps, S. L.; Hite Jr, J. R.; Carlton, A. G.; Lee, S. H.; Bergin, M. H.; Ng, N. L. *Atmos. Chem. Phys* **2015**, *15*, 5211–5228.

[33] Weber, R. J.; Guo, H.; Russell, A. G.; Nenes, A. *Nature Geoscience* **2016**, *9*, 1–5.

[34] Lee, H. J.; Aiona, P. K.; Laskin, A.; Laskin, J.; Nizkorodov, S. A. *Environmental science & technology* **2014**, *48*, 10217–10226.

[35] Teich, M.; van Pinxteren, D.; Wang, M.; Kecorius, S.; Wang, Z.; Müller, T.; Mocnik, G.; Herrmann, H. *Atmospheric Chemistry and Physics Discussions* **2017**, *17*, 1653–1672.

[36] Ahillen, S. Forest fires burn 119,000 acres in 8 Southeastern states. 2016; `http://www.usatoday.com/story/news/nation-now/2016/11/20/forest-fires-burn-119000-acres-8-southeastern-states/94169774/`.

[37] Hecobian, A.; Zhang, X.; Zheng, M.; Frank, N.; Edgerton, E. S.; Weber, R. J. *Atmospheric Chemistry and Physics* **2010**, *10*, 5965–5977.

[38] Davis, H.; Mott, C. J. B. *Journal of Soil Science* **1981**, *32*, 379–391.

[39] Marshall, S. J.; Young, S. D.; Gregson, K. *European Journal of Soil Science* **1995**, *46*, 471–480.

[40] Heighton, L. P.; Schmidt, W. F. *Journal of Geography and Geology* **2014**, *6*, 214–227.

[41] Claeys, M.; Vermeylen, R.; Yasmeen, F.; Gómez-González, Y.; Chi, X.; Maenhaut, W.; Mészáros, T.; Salma, I. *Environmental Chemistry* **2012**, *9*, 273–284.

[42] Lin, P.; Laskin, J.; Nizkorodov, S. A.; Laskin, A. *Environmental science & technology* **2015**, *49*, 14257–14266.

[43] Avdeef, A. E.; Sofen, S. R.; Bregante, T. L.; Raymond, K. N. *Journal of the American Chemical Society* **1978**, *100*, 5362–5370.

[44] Piccolo, A. *Soil Science* **2001**, *166*, 810–832.

[45] Sutton, R.; Sposito, G. *Environmental science & technology* **2005**, *39*, 9009–9015.

[46] Janot, N.; Reiller, P. E.; Korshin, G. V.; Benedetti, M. F. *Environmental science & technology* **2010**, *44*, 6782–6788.

[47] Milne, C. J.; Kinniburgh, D. G.; Tipping, E. *Environmental Science & Technology* **2001**, *35*, 2049–2059.

[48] Russell, L. M.; Bahadur, R.; Ziemann, P. J. *Proceedings of the National Academy of Sciences of the United States of America* **2011**, *108*, 3516–21.

[49] Havers, N.; Burba, P.; Lambert, J.; Klockow, D. *Journal of Atmospheric Chemistry* **1998**, 45–54.

[50] Bahadur, R.; Uplinger, T.; Russell, L. M.; Sive, B. C.; Cliff, S. S.; Millet, D. B.; Goldstein, A.; Bates, T. S. *Environmental science & technology* **2010**, *44*, 2542–8.

[51] Calvert, J. G.; Pitts, J. N. *Photochemistry*; John Wiley & Songs, Inc: New York, 1966.

[52] Dearden, J. C.; Forbes, W. F. *Canadian Journal of Chemistry* **1959**, *37*, 1294–1304.

[53] Li, C.; Hoffman, M. Z. *The Journal of Physical Chemistry B* **1999**, *103*, 6653–6656.

[54] Achladas, G. E. *Journal of Chromatography A* **1991**, *542*, 263–275.

[55] Simoneit, B.; Rogge, W.; Mazurek, M. A.; Standley, L. J.; Hildemann, L. M.; Cass, G. R. *Environ. Sci. Technol* **1993**, *27*, 2533–2541.

[56] Andjelkovic, T.; Perovic, J.; Purenovic, M.; Blagojevic, S.; Nikolic, R.; Andjelkovic, D.; Bojic, A. *Ecletica quimica* **2006**, *31*, 39–46.

[57] Boyle, E. S.; Guerriero, N.; Thiallet, A. *Environmental Science & Technology* **2009**, *43*, 2262–2268.

[58] Ma, J.; Del Vecchio, R.; Golanoski, K. S.; Boyle, E. S.; Blough, N. V. *Environmental science & technology* **2010**, *44*, 5395–5402.

[59] Ghosh, D.; Roy, A.; Seidel, R.; Winter, B.; Bradforth, S.; Krylov, A. I. *The Journal of Physical Chemistry B* **2012**, *116*, 7269–7280.

[60] Baalousha, M.; Motelica-Heino, M.; Le Coustumer, P. *Colloids and Surfaces A: Physicochemical and Engineering Aspects* **2006**, *272*, 48–55.

[61] Conte, P.; Piccolo, A. *Environmental Science & Technology* **1999**, *33*, 1682–1690.

[62] Kumke, M. U.; Löhmannsröben, H.-G.; Roch, T. *Analyst* **1994**, *119*, 997–1001.

[63] Pranzas, P. K.; Willumeit, R.; Gehrke, R.; Thieme, J.; Knöchel, A. *Analytical and bioanalytical chemistry* **2003**, *376*, 618–625.

[64] Simpson, A. J.; Kingery, W. L.; Hayes, M. H.; Spraul, M.; Humpfer, E.; Dvortsak, P.; Kerssebaum, R.; Godejohann, M.; Hofmann, M. *Naturwissenschaften* **2002**, *89*, 84–88.

[65] Diallo, M. S.; Glinka, C. J.; Goddard, W. A.; Johnson, J. H. *Journal of Nanoparticle Research* **2005**, *7*, 435–448.

[66] Senesi, N.; Rizzi, F. R.; Dellino, P.; Acquafredda, P. *Soil Science Society of America Journal* **1996**, *60*, 1773–1780.

[67] Alvarez-Puebla, R. A.; Garrido, J. J. *Chemosphere* **2005**, *59*, 659–667.

[68] Jovanović, U. D.; Marković, M. M.; Cupać, S. B.; Tomić, Z. P. *Journal of Plant Nutrition and Soil Science* **2013**, *176*, 674–679.

[69] Guo, R.; Ma, J. *RSC Advances* **2014**, *4*, 25880–25885.

[70] D'Abramo, M.; Castellazzi, C. L.; Orozco, M.; Amadei, A. *Journal of Physical Chemistry B* **2013**, *117*, 8697–8704.

[71] Kohler, B.; Woehl, J. *Journal of Chemical Physics* **1995**, *103*, 6253–6256.

[72] Erlick, C.; Abbatt, J. P. D.; Rudich, Y. *Journal of the Atmospheric Sciences* **2011**, *68*, 1845–1852.

[73] *ASTM G173-03, Standard Tables for Reference Solar Spectral Irradiance: Direct Normal and Hemispherical on 37 Tilted Surfaces*; ASTM International: West Conshohocken, PA, 2012.

[74] Chylek, P.; Wong, J. *Geophysical Research Letters* **1995**, *22*, 929–931.

Chapter 5

Spectroscopic comparison of water- and methanol-soluble brown carbon particulate matter[1]

[1]Sabrina M. Phillips, and Geoffrey D. Smith. Submitted to *Aerosol Sci. Technol.*, **2017**

5.1 Abstract

It is now recognized that some organic components of ambient aerosols absorb light with a spectrum distinct from that of other absorbers such as black carbon and mineral components. The most common method for isolating this light-absorbing organic fraction, or "brown carbon", is to collect particulate matter on filters and extract in a solvent, usually water or methanol. Here, we compare the absorption spectra of water-soluble (WS) and methanol-soluble (MS) extracts from ambient samples collected in Athens, Georgia. We find that despite syringe filtering the MS extracts, extinction by suspended particles is evident in the spectra leading to an overestimation of absorption by a factor of two on average. No such particle extinction is evident in the WS extracts. We demonstrate that it is possible to subtract the extinction contribution in the MS extracts by fitting the spectrum to the sum of two power law functions, one describing the absorption spectrum and the other describing the extinction spectrum. With extinction thus removed, we find that integrated absorption (300 - 800 nm) by the MS brown carbon extract is highly correlated with the WS extract and is on average 1.55x larger. The wavelength dependence of the WS and MS spectra are also highly correlated and very similar with average absorption Ångström exponents of 6.1 ($\pm$0.7) and 6.7 ($\pm$1.1), respectively. This study demonstrates that: 1) brown carbon absorption is overestimated if scattering in MS spectra is not accounted for, 2) there is no spectral evidence that the WS and MS chromophores are different, and 3) it may be possible to use WS spectra to represent total brown carbon absorption using a simple scaling factor.

5.2 Introduction

Aerosols in the atmosphere affect the climate both directly by interacting with sunlight (i.e. absorption and scattering) and indirectly by altering cloud properties. The magnitude and even the sign of the impact of particle scattering and absorption, in particular, is not very well constrained, in part because they depend on many factors including particle size, shape, and composition. It is known that black carbon (BC) particles, for example, efficiently absorb solar radiation throughout the UV-visible region of the spectrum with an estimated contribution to positive radiative forcing second only to carbon dioxide.[1] However, internal mixing of organic constituents can alter this effect,[2] and some organic species also absorb light further complicating estimates of radiative transfer in the atmosphere.

This absorbing organic fraction, often termed "brown carbon" (BrC) because of its more pronounced wavelength dependence compared to BC, can contribute significantly to aerosol absorption in the UV and near-UV region of the spectrum. Measurements of both the magnitude and shape of the BrC spectrum have varied substantially making it difficult to correlate with specific types of sources and processes in the atmosphere as well as quantitatively incorporate into radiation transfer modules of climate models. This BrC spectrum is usually derived either by: 1) measuring the absorption spectrum of the entire aerosol (including BC and BrC) and subtracting the BC contribution,[3–7] or 2) extracting collected particulate matter samples in a solvent thereby separating the solvent-extractable BrC fraction from the insoluble BC.[8–11] The latter approach has the advantage that the particle mix-

ing state need not be known to measure the BrC absorption spectrum. Additionally, collection of particulate matter over an extended period of time makes it possible to study aerosols even when loadings are low and makes a variety of offline analyses possible.

Most commonly, water is used as the extraction solvent, but it does not extract all BrC. Organic solvents, and methanol in particular, have been found to extract even more absorption than water does, and it is believed that the water-soluble (WS) fraction of BrC is a subset of the methanol-soluble (MS) fraction.[8,11] Some studies have suggested that differences in the wavelength dependence of the two extracts indicate different classes of chromophores present.[8,12] However, relatively few studies have extracted in both solvents much less compared them systematically. Here, we analyze a collection of ambient particulate matter samples using a split-filter approach in which we extract half of each filter in water and the other half in methanol. Through such direct comparison we find that the WS and MS BrC spectra display many similarities but also with some important differences, including extinction by suspended insoluble particles in MS extracts, which has not previously been reported.

5.3 Materials and Methods

5.3.1 Particulate matter sampling and extraction.

Ambient aerosols were collected out of a window in the Chemistry Building at the University of Georgia (20 m above ground level) in Athens, Georgia (33.9488° N, 83.3747° W) for a total of 22 days during the months of July - October, 2015 and May

- June, 2016. The samples were collected on 47 mm diameter polytetrafluoroethylene (PTFE, Teflon) filters (0.2 μm pore size, Sterlitech) at 16.7 L/min for separate 24 h periods. A Very Sharp Cut Cyclone inlet (BGI, Inc.) was used to size select for particles with diameters less than 2.5 μm. The filters were cut in half for extraction in either water or methanol, thereby allowing a direct comparison of the water-soluble (WS) and methanol-soluble (MS) absorption spectra for the same sample. Figure 5.2 shows an image of a typical split filter after extraction in water (top half) and methanol (bottom half).

Solvent-extractable species were extracted, similarly to Hecobian et al.,[9] by sonication of the filter for 20 minutes in 10 mL of either Milli-Q water ($< 18.2 M\Omega \cdot cm$) or methanol (Sigma Aldrich, $\geq 99.6\%$ purity). Unless otherwise noted, extracted solutions were filtered using a 13 mm, 0.45 μm PTFE disposable syringe filter (VWR 28145-493). Some samples were filtered using a 13 mm, 0.22 μm PTFE disposable syringe filter (Omicron Scientific, SFTF13RB). The syringe filters were pre-wetted with methanol and in the case of the WS extractions were subsequently rinsed with water several times prior to filtering.

UV-visible absorption spectra measurements and fitting.

UV-visible absorption spectra (200 - 800 nm) of the extracts were measured in a 1 cm cuvette on a Cary 60 UV-vis spectrophotometer (Agilent). Spectra were blanked with cuvettes containing the appropriate solvent (water or methanol) and were fit using either a single power law function:

Figure 5.1: Picture of split filter after extraction in water (top) and methanol (bottom). Greater absorption visible on the water half is believed to be associated with insoluble particles remaining on the filter. Note the absence of such absorption on the methanol half. The radial pattern is imposed by the substrate supporting the filter.

$$Abs = a \cdot \lambda^{-AAE} \tag{5.1}$$

or a dual power law function:

$$Abs = a \cdot \lambda^{-AAE} + b \cdot \lambda^{-EAE} \tag{5.2}$$

where a and b are scaling coefficients, AAE is the absorption Ångström exponent, and EAE is the extinction Ångström exponent.

Results and Discussion

5.3.2 Methanol soluble spectra contain extinction by suspended particles.

Extinction by particles can be accounted for with a power law function.

Particulate matter extracted in methanol consistently demonstrated larger absorbance at all wavelengths compared to the corresponding water extracts, similar to observations from other studies.[8,11,13,14] This behavior can be seen in Figure 5.2 in which the average absorbance spectra of all 22 filters analyzed are shown for both solvents. To account for day-to-day variations in absorbance intensity, each day's spectrum has been normalized to the methanol extract value at 300 nm. The long-wavelength ($\lambda > 600$ nm) "tail" evident in the methanol extract is particularly interesting, as BrC is typically not believed to absorb significantly at these wavelengths.[4,10,15] It's possible that this tail is the result of baseline drift, as others have suggested,[9,13]

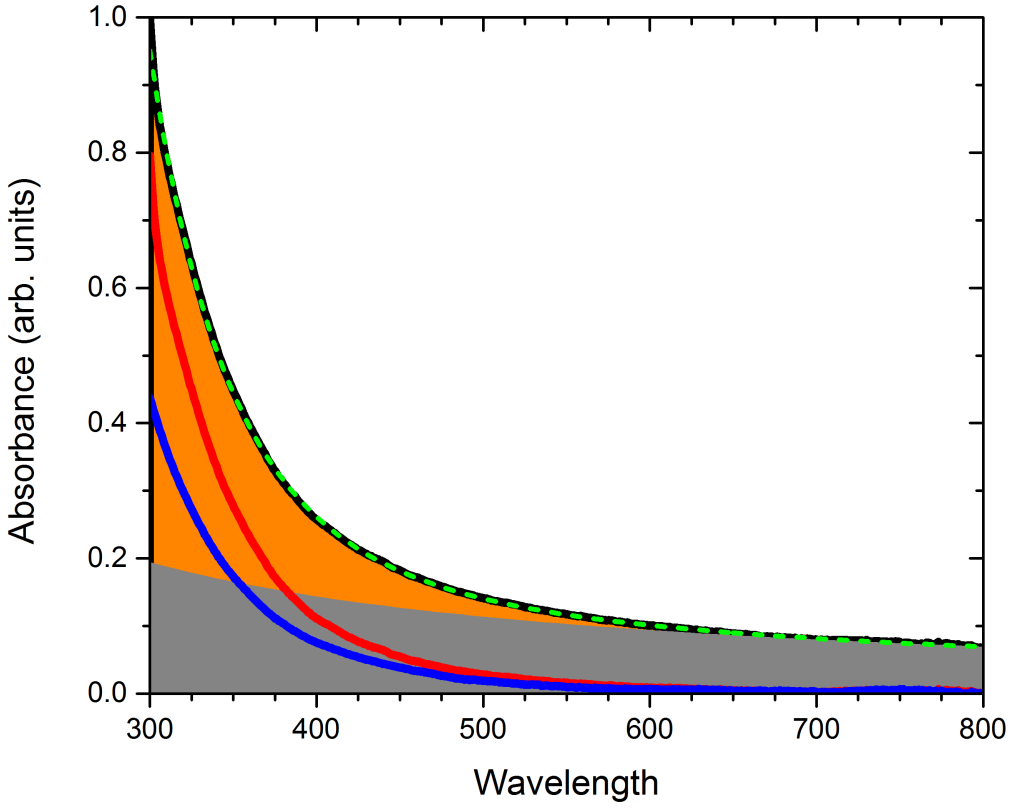

Figure 5.2: Average absorption spectra for MeOH-soluble (black line), H2O-soluble (blue line), and MeOH-soluble BrC with particle extinction removed (red line). The gray area represents extinction by particles in the MeOH extract, while the orange area represents the contribution by BrC absorption.

however it is not clear why the MS spectra would suffer from baseline drift while the WS spectra clearly do not. Furthermore, baseline drift would not be expected to result in systematically positive offsets in the spectra for nearly every filter.

Alternatively, the long-wavelength tail could result from scattering (and possibly absorption) by suspended particles in the extract. Not all of the particulate matter collected on the filter is soluble in water or methanol, so it stands to reason that some particles may remain in the extracts. In fact, the extract is passed through the 0.45 μm syringe filter to remove these particles. Yet, the apparent absorption at long wavelengths suggests that this removal is incomplete. To account for this particle extinction, we performed a non-linear fit of the apparent MS absorption spectrum to a dual power law function (Equation 5.2) in which one power law function describes the soluble extract absorption and the other describes the insoluble particle extinction. Such a fit is similar to fits used by others to separate contributions from BC and BrC.[6,16–18]

This dual power law function (green dashed line in Figure 5.2) fits the MS spectrum well with a coefficient of determination, R^2, of 1.00 and values of AAE = 6.43 and EAE = 1.07. The residual spectrum, which remains after the extinction component (gray area) has been subtracted from the MS spectrum, represents just the MS BrC absorption spectrum (orange area), which is also plotted as the red curve. We point out that we use the term "MS BrC" to distinguish the soluble absorbing component of the entire MS extract, which includes extinction by insoluble particles as well.

The spectra are also plotted in a log-transformed plot in Figure 5.3 in which a single power law function is represented by a straight line. Single power law functions fit the WS (blue line, AAE = 6.07, R^2 = 1.00) and MS BrC (red line, AAE = 6.49, R^2 = 1.00) curves well over the entire range 300 - 700 nm. A single power law does not fit the MS spectrum (black line) as well yielding an AAE = 3.48 (R^2 = 0.96), which clearly reflects the influence of the particle extinction at longer wavelengths.

Also shown in Figure 5.3 is the MS spectrum that would be obtained by subtracting the value at 700 nm to account for a presumed baseline offset (light blue line), as others have done;[9,13] this fit yields an AAE = 5.43 and appears to fit well (R^2 = 1.00), though it systematically underestimates absorption at > 450 nm. And, compared to the MS BrC spectrum it overestimates integrated absorption (300 - 800 nm) by 34%. In essence, the baseline subtraction has served to remove some of the influence of the particle extinction but in doing so assumes that contribution is wavelength independent (i.e. with an equivalent EAE = 0 in the dual power law formalism). Not surprisingly, this helps but does so incompletely.

5.3.3 MS BrC absorption spectra are similar with different degrees of filtration.

To further confirm that extinction by suspended particles is present in the spectra, we applied the dual power law approach to an ambient sample that had been filtered to various degrees. Specifically, we measured the apparent absorption spectra of a single methanol extract that was either unfiltered, filtered using a 0.45 μm pore size syringe filter, or filtered using a 0.22 μm size syringe filter (Figure 5.4a). There should

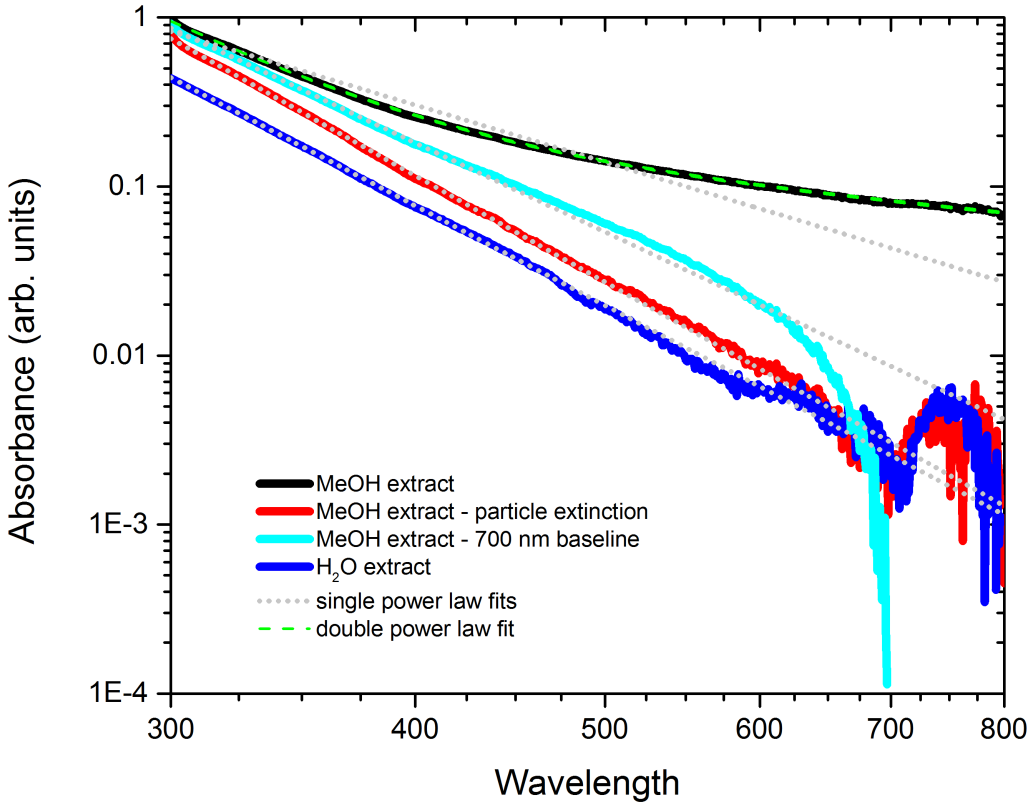

Figure 5.3: Log-transformed plot of absorption spectra for WS and MS extracts. Insoluble particle extinction contributes significantly to apparent MS absorption (black line), but the dual power law fit (green dashed line) accounts for it and the BrC absorption.

be a consistent contribution from the MS BrC absorption in each of these samples despite different particle concentrations and size distributions, thereby providing a good test of the dual power law approach.

Each of the spectra is fit well by the dual power law function (green dashed lines), and the fraction of apparent absorption attributable to particle extinction (gray/black shaded areas) decreases exactly as would be expected from 91% for the unfiltered to 71% and 38% for the 0.45 μm and 0.22 μm syringe filters, respectively (Table 5.1). What is more, the MS BrC absorption spectra in each case appear very similar (Figure 5.4b) with the AAE values obtained nearly indistinguishable (Table 5.1) despite the varying contributions from particle extinction. Importantly, even when the smallest pore size filter (0.22 μm) was used, extinction by suspended particles was evident indicating that fitting to the dual power law function is likely always needed. Since the ability to obtain the MS BrC spectrum relies on an accurate parameterization of the particle extinction spectrum, we recommend that the 0.45 μm syringe filter offers the best compromise between reducing the magnitude of the particle extinction and retaining enough particle extinction to fit well.

By comparison, the spectra from the same sample extracted in water, instead, showed no discernible differences regardless of which syringe filter was used or even if one was used (Figure 5.4c). Clearly, then, the use of the syringe filters is not affecting the soluble BrC spectra. The AAE values from these WS spectra are similar to the values obtained from the MS BrC spectra (Table 5.1) indicating very similar spectral shapes despite the different magnitudes of absorption and presence of particle extinction in the MS extracts. Furthermore, the fact that particle extinction

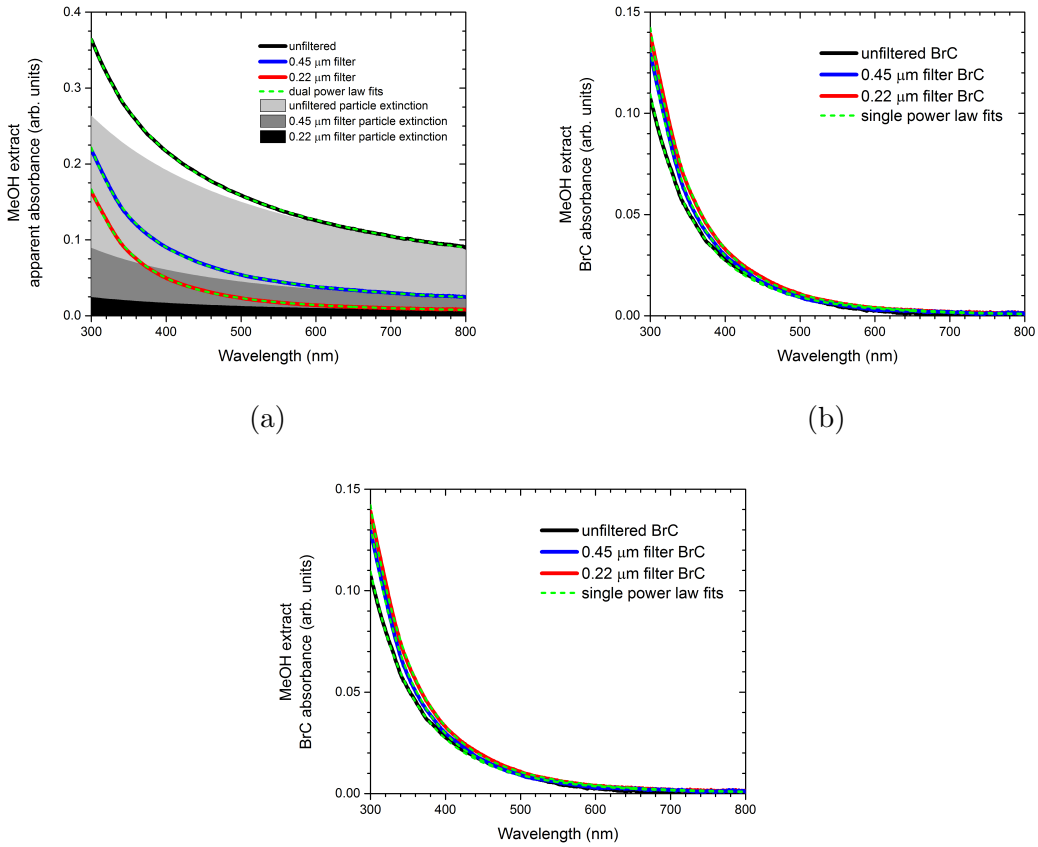

Figure 5.4: Comparison of filtration of a sample collected on June 8, 2016 in Athens, GA. (a) Apparent MS absorption spectra either not filtered (black lines), filtered with a 0.45 μm syringe filter (blue lines), or filtered with a 0.22 μm syringe filter (red lines). Green dashed lines are dual power law fits and gray/black areas represent suspended particle extinction. (b) Residual MS BrC spectra are similar regardless of extent of filtering. Green dashed lines are single power law fits. (c) WS absorption spectra with different extents of filtering, as in (a), showing no evidence of particle extinction.

Table 5.1: Comparison of spectral fits for different extents of particle filtration

Filter	MS AAE[1]	MS EAE[2]	% Area from particle extinction	WS AAE
unfiltered	4.84 (0.19)	1.11 (0.01)	91	5.38 (0.02)
0.45 m	5.20 (+0.19 / -0.09)	1.35 (+0.06 / -0.03)	71	5.20 (+0.04 / -0.03)
0.22 um	5.07 (+0.16 / -0.14)	1.29 (0.21)	38	5.37

[1] AAE = absorption Ångström exponent
[2] EAE = extinction Ångström exponent
error bars indicate 95% confidence intervals from fits

is present only in the MS spectra and decreases as the degree of filtration is increased suggests that particles are only removed from the filter samples when methanol, and not water, is the solvent.

This distinction is corroborated by the observation of a visible difference in the appearance of the filter after extraction in the two solvents (Figure 5.1); the filter half extracted in methanol appears white indicating a substantial removal of particles while the half extracted in water clearly shows visible absorption remaining. It is not clear why the insoluble particles would be removed from the filter in methanol but not in water; perhaps hydrophobic compounds, such as polyaromatic hydrocarbons, present on the particles inhibit their dissolution in water.

5.3.4 MS BrC is more absorbing than WS BrC but correlated with it.

As the average spectra in Figure 5.2 show, MS BrC absorption is greater than that of WS BrC at all wavelengths. Here, we explore the correlation between MS and WS BrC absorption by comparing integrated absorption (300 - 800 nm) for pairs of filter halves each taken from the same original filter. In this way, we can directly compare the effect of the solvent on the spectrum for the same sample.

Figure 5.5 shows the observed relationship between the integrated spectral areas for the two solvents. If particle extinction in the MS extract is not accounted for (open squares), there is a lot of scatter and correlation with WS absorption is weak with an adjusted R^2 of 0.75 and a slope of 4.21 (black dashed line). Despite having used the 0.45 μm syringe filter to remove particles, enough extinction remains that it appears as if the methanol extracts significantly more absorption than does water. Even subtracting the absorption at 700 nm (open triangles), ostensibly accounting for baseline drift, does not change the relationship much; the slope is 3.83 with an adjusted $R^2 = 0.76$ (green dashed line) and the data are still scattered. Once the particle extinction is removed using the dual power law approach (red circles), however, the MS absorption is reduced substantially and the correlation improves, with the adjusted $R^2 = 0.90$ and a slope of 1.81 (red dashed line). Removing the apparent outlier (open red circle) improves the correlation substantially with an adjusted $R^2 = 0.98$ and a slope of 1.55 (red solid line).

The large number of split-filter samples (22) represented in Figure 5.5 allows several important conclusions to be drawn. First, most MS spectra contain particle

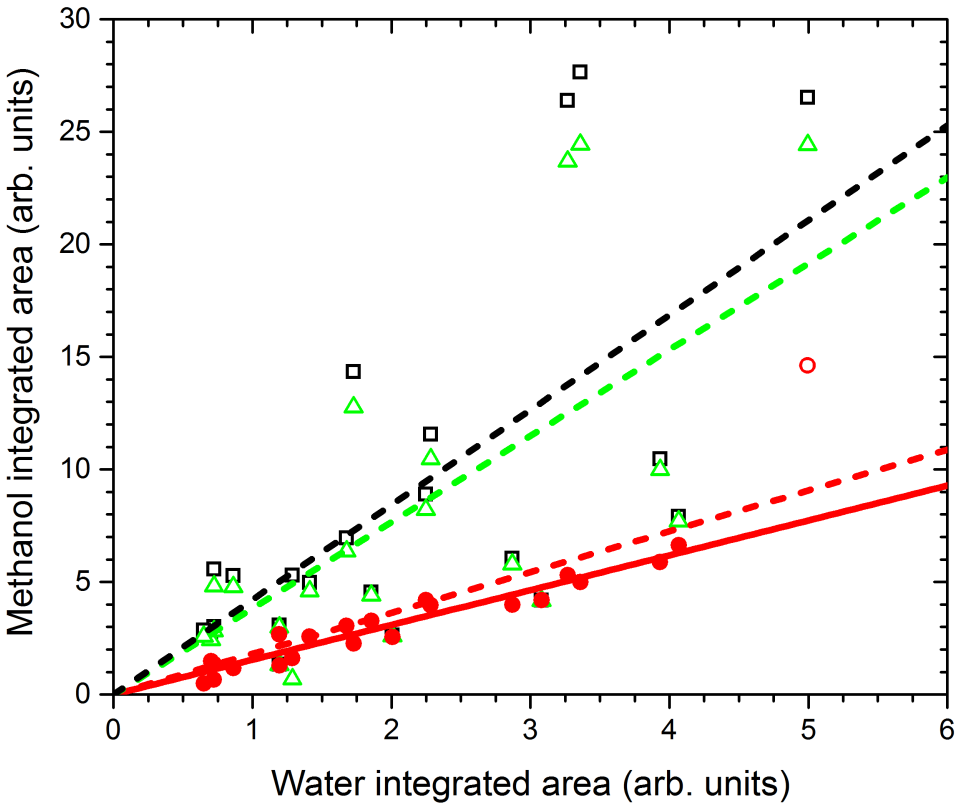

Figure 5.5: Correlation between integrated absorption (300 - 800 nm) for WS and MS BrC extracts (red circles). Insoluble particle extinction has been subtracted using a dual power law function. Linear fits are shown excluding the outlier point (red solid line, point indicated by open red circle) or not (red dashed line). Data without particle extinction subtracted (open squares) and with baseline subtraction (open triangles) and respective fits (black and green dashed lines) are also show for comparison.

extinction as evidenced by the differences in the integrated areas with (red circles) and without (open squares) the use of the double power law approach. In fact, of the 22 samples only three contain no particle extinction, i.e. are fit better by a single power law function. Of the other 19 samples, particle extinction accounted for an average of 56% (± 23%) of integrated apparent absorption (300 - 800 nm) ranging from 13% to 86%. Even though the samples were filtered with the syringe filter, extinction by suspended particles is not insignificant and is present in nearly every sample.

Second, the degree of scatter in the data would suggest that there is not much correlation between MS and WS BrC absorption despite the fact that the initial split filter samples were nearly identical. Such a conclusion would be difficult to rationalize, as it is commonly believed that the WS BrC fraction is a subset of the MS BrC fraction. Indeed, the correlation observed after removing particle extinction (red circles) suggests that the WS BrC fraction may, indeed, be a subset of the MS BrC fraction.

Third, the high degree of correlation observed in the data corrected for particle extinction (red circles) is highly suggestive that the dual power law approach is effective for single filter analysis (i.e. not just for spectra averaged from all filters). The correlation, encompassing samples taken over a whole year, also indicates that the relationship between MS and WS BrC absorption may be universal, at least for the background aerosols sampled at a site such as Athens, Georgia. Furthermore, it may be possible to estimate the magnitude of MS BrC absorption, believed to be more representative of total BrC, from WS BrC absorption (or vice versa).

5.3.5 MS BrC and WS BrC spectral shapes are similar.

We can also take advantage of the split-filter dataset to explore the degree to which the MS and WS BrC spectra are similar. In Figure 5.6 we compare the absorption Ångström exponents (AAE's) derived from power law fits to the MS and WS spectra. We fit the WS spectra to a single power law function (300 - 500 nm), while we fit the MS spectra (300 - 800 nm) using both a single power law function (black squares) and the dual power law function (red circles), for which the AAE represents the absorbing component after particle extinction is removed.

We find that the WS AAE values range from 4.96 to 7.54 with an average of 6.13 ($\pm$ 0.69). This value is typical of WS AAEs reported by many others for particulate matter sampled from a variety of locations, with many falling in the range of 6 - 8.[9,11,13,14,16,19–25] The quality of the single power law fits to the WS spectra is good, with the majority of the R^2 values at least 0.999. We tried to fit the WS spectra to a dual power law function, but none of the 22 samples was fit better than with a single power law function. This finding is highly suggestive that insoluble particles are not liberated from the filters when extracted in water, or if they are they do not scatter and absorb light efficiently.

Fitting the MS spectra to a single power law function (i.e. including particle extinction) is not nearly as good, however, with AAE values ranging from 2.04 to 6.80 (black squares) with an average of 4.00 ($\pm$ 1.66) and most R^2 values well below 0.99. Considerable scatter is evident with little correlation between the MS and WS AAE's; indeed the slope of the linear fit (black line) is 0.63 with a value of R^2 of only 0.80. Conversely, the MS BrC AAE values (i.e. with particle extinction subtracted)

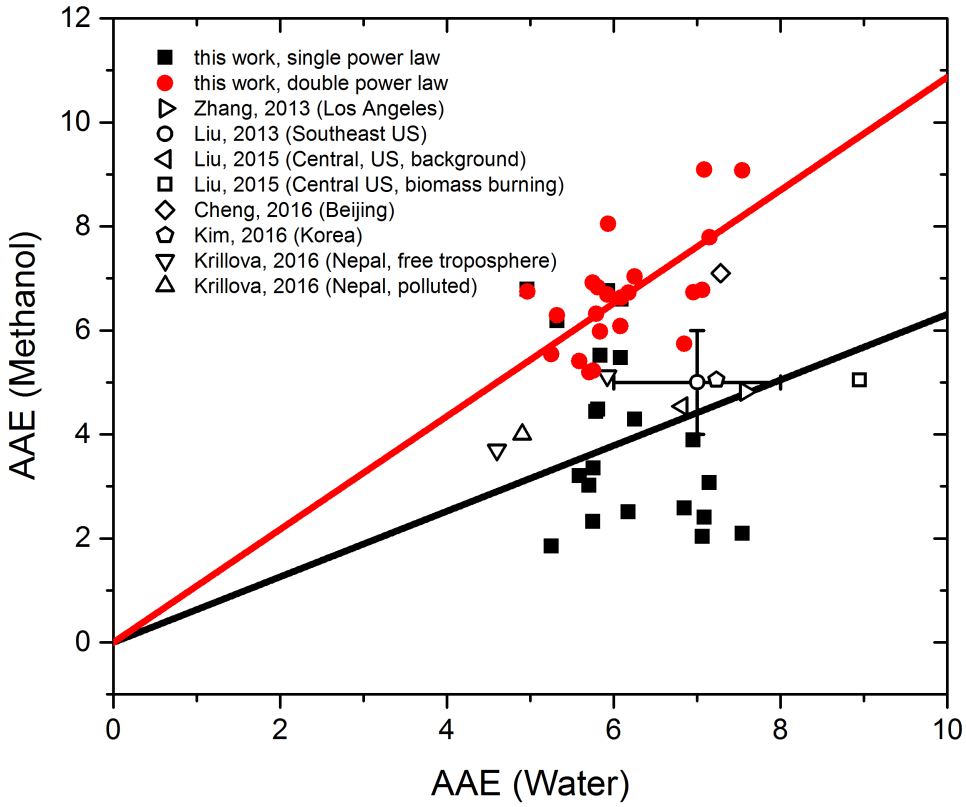

Figure 5.6: Correlation between WS and MS BrC absorption Ångström exponents (AAEs) when insoluble particle extinction is subtracted using a dual power law function (red points). The linear fit (red line) shows a high degree of correlation (R^2 = 0.98) with a slope of 1.09. AAE values for MS spectra fit to a single power law function (black squares) show much lower correlation with WS AAE values (R^2 = 0.80) with a slope of 0.63. Measurements from other studies in which AAE's from both WS and MS are shown for comparison (open symbols).

are much more highly correlated with the WS AAE values (red line) with a slope of 1.09 and $R^2 = 0.98$. These values span a range of 5.20 - 9.09 with an average of 6.68 ($\pm$ 1.07). The average EAE of the particle extinction from these dual power law fits is 1.05 ($\pm$ 0.36), which is in the range of values found for extinction by ambient particles suspended in air (0 - 2).[26–28]

Clearly, fitting the MS spectra to a single power law function inadequately describes the wavelength dependence of the BrC absorption even though it may appear to capture the shape of the spectrum (see Figure 5.3, for example). The consequence of such a fitting is to overestimate absorption at the longer wavelengths thereby erroneously lowering the value of AAE. What is more, this error obscures the correlation between the MS BrC and WS BrC spectral shapes because it originates from particle extinction, which is only present in the MS extracts.

A limited number of studies have measured the absorption spectra of both WS and MS ambient particulate matter, and most have found that the MS AAEs are lower than the corresponding WS AAEs (see open symbols in Figure 5.6). The notable exception is Cheng et al.[20] who report values that are nearly identical (open diamond). Even the laboratory studies of wood combustion aerosols by Chen and Bond[8] (not shown in Figure 5.6) result in WS AAE values that are systematically only 0.63x that of the corresponding MS AAE values. Interestingly, the AAEs from that study and all of the other studies except for Cheng et al.,[20] fall on or near the correlation line (black line) that we obtain if we only fit the MS spectra with a single power law (just as all of the other studies do). This coincidence suggests that

perhaps interference by particle extinction in MS extracts could be widespread and influence how MS BrC spectra are being interpreted.

For example, it has been suggested that the lower AAE values observed for MS extracts arise from long-wavelength absorption attributed to polyaromatic hydrocarbons.[8,12] Though reasonable, the present work illustrates that such an interpretation may be complicated by the presence of particle extinction in the extracts. Upon subtraction of this extinction, there appears to be little evidence for much spectral difference with average WS and MS BrC AAEs of 6.13 and 6.68, respectively.

Nonetheless, the spectral shapes are not identical, as is easily seen in the plot of the average ratio of the MS BrC and WS absorption as a function of wavelength from the 22 individual filters (Figure 5.7). While the MS BrC absorption is greater than the WS absorption at all wavelengths, this enhancement is seen to decrease monotonically with increasing wavelength. This trend illustrates the fact that the MS BrC spectra systematically decrease with wavelength more rapidly (i.e. have a larger AAE) than do WS spectra even though they are more highly absorbing. Such spectral differences could be indicative of chromophores that are more soluble in methanol than in water and which tend to absorb in the UV and near-UV of the spectrum, such as aromatic species. Recognition of this difference, though slight, could be useful for understanding the chemical sources and evolution of BrC and may have implications for how it is implemented in radiative transfer calculations in climate models. This ability, however, requires the ability to resolve the difference in spectral shape, which is only possible because the insoluble particle extinction is removed using the dual power law fit.

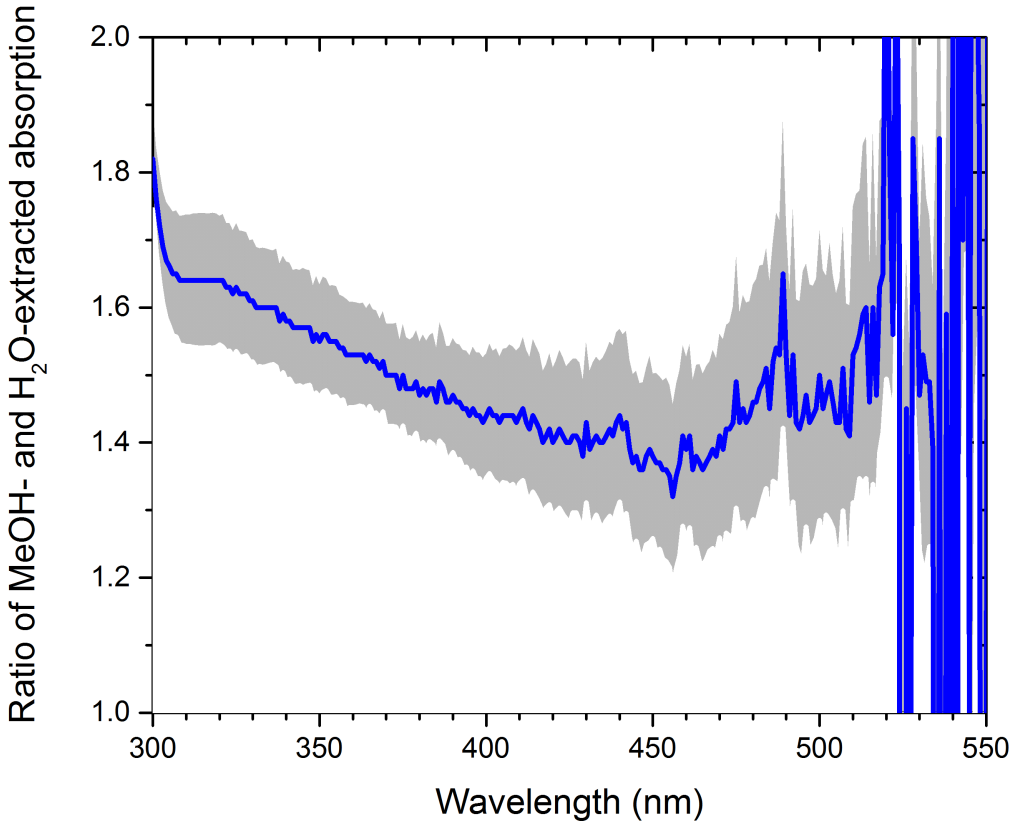

Figure 5.7: Average ratio of MS BrC absorption to WS absorption as a function of wavelength. Gray area represents standard error of the 22 samples. The MS BrC absorbs more strongly at all wavelengths but to a less extent as wavelength increases.

5.4 Conclusions

We have compared split filters of ambient particulate matter extracted in water and methanol and found that most (19 out of 22) MS spectra are significantly impacted by extinction of suspended insoluble particles liberated from the filter even after filtering with a syringe filter. It appears as if particles are not liberated from the filter by water, and thus the WS spectra do not include particle extinction. A dual power law fit to the MS spectra is able to separate the MS BrC absorption from the particle extinction adequately. Comparing the WS and MS BrC spectra we find that:

- WS and MS BrC integrated absorption (300 - 800 nm) is highly correlated
- MS BrC integrated absorption (300 - 800 nm) is a factor of 1.55x larger than WS integrated absorption
- The spectral shapes of WS and MS BrC absorption are similar, with average AAEs of 6.13 and 6.68, respectively
- MS BrC spectra display a slight absorption enhancement at UV and near-UV wavelengths

Based on these findings, we recommend that:

- Methanol is preferable for extracting BrC from particulate matter on filters since the MS extract more completely represents the total BrC absorption spectrum, but ...

- Water could be used for extraction, if more convenient, and the total BrC spectrum be approximated by scaling the WS spectrum (by a factor of 1.55x for background aerosols; perhaps a different factor depending on source and/or location)

- MS spectra **not** be fit using a single power law function since particle extinction overestimates BrC absorption even when using syringe filters

- MS spectra not be baseline corrected by subtracting absorption at 700 nm, which tends to incompletely remove the particle extinction contribution, but instead ...

- MS spectra be fit to a dual power law function from which the MS BrC spectrum can be extracted

5.5 Acknowledgements

Funding was provided by the National Science Foundation through the Atmospheric and Geospace Sciences Division of the Geosciences Directorate (AGS-1241621 and AGS-1638307).

Bibliography

[1] Bond, T. C. et al. *Journal of Geophysical Research: Atmospheres* **2013**, *118*, 5380–5552.

[2] Lack, D. A.; Cappa, C. D. *Atmospheric Chemistry and Physics* **2010**, *10*, 4207–4220.

[3] Guo, R.; Ma, J. *RSC Advances* **2014**, *4*, 25880–25885.

[4] Lack, D. A.; Langridge, J. M.; Bahreini, R.; Cappa, C. D.; Middlebrook, A. M.; Schwarz, J. P. *Proceedings of the National Academy of Sciences of the United States of America* **2012**, *109*, 14802–14807.

[5] Saleh, R.; Robinson, E. S.; Tkacik, D. S.; Ahern, A. T.; Liu, S.; Aiken, A. C.; Sullivan, R. C.; Presto, A. A.; Dubey, M. K.; Yokelson, R. J.; Donahue, N. M.; Robinson, A. L. *Nature Geoscience* **2014**, *7*, 647–650.

[6] Wiegand, J. R.; Mathews, L. D.; Smith, G. D. *Analytical Chemistry* **2014**, *86*, 6049–6056.

[7] Zhang, X.; Kim, H.; Parworth, C. L.; Young, D. E.; Zhang, Q.; Metcalf, A. R.; Cappa, C. D. *Environmental Science and Technology Letters* **2016**, *50*, 1681–1690.

[8] Chen, Y.; Bond, T. C. *Atmospheric Chemistry and Physics* **2010**, 1773–1787.

[9] Hecobian, A.; Zhang, X.; Zheng, M.; Frank, N.; Edgerton, E. S.; Weber, R. J. *Atmospheric Chemistry and Physics* **2010**, *10*, 5965–5977.

[10] Kirchstetter, T. W.; Novakov, T.; Hobbs, P. V. *Journal of Geophysical Research: Atmospheres* **2004**, *109*, D21208.

[11] Liu, J.; Bergin, M.; Guo, H.; King, L.; Kotra, N.; Edgerton, E.; Weber, R. J. *Atmospheric Chemistry and Physics Discussions* **2013**, *13*, 18233–18276.

[12] Zhang, X.; Lin, Y.-H.; Surratt, J. D.; Weber, R. J. *Environmental Science & Technology* **2013**, *47*, 3685–93.

[13] Kim, H.; Kim, J. Y.; Jin, H. C.; Lee, J. Y.; Lee, S. P. *Atmospheric Environment* **2016**, *129*, 234–242.

[14] Kirillova, E. N.; Marinoni, A.; Bonasoni, P.; Vuillermoz, E.; Facchini, M. C.; Fuzzi, S.; Decesari, S. *Journal of Geophysical Research: Atmospheres* **2016**, *121*, 1–19.

[15] Saleh, R.; Hennigan, C. J.; McMeeking, G. R.; Chuang, W. K.; Robinson, E. S.; Coe, H.; Donahue, N. M.; Robinson, A. L. *Atmospheric Chemistry and Physics* **2013**, *13*, 7683–7693.

[16] Liu, J. et al. *Atmospheric Chemistry and Physics* **2015**, *15*, 7841–7858.

[17] Massabò, D. et al. *Atmospheric Environment* **2015**, *108*, 1–12.

[18] Olson, M. R.; Victoria Garcia, M.; Robinson, M. A.; Van Rooy, P.; Dietenberger, M. A.; Bergin, M.; Schauer, J. J. *Journal of Geophysical Research: Atmospheres* **2015**, *120*, 6682–6697.

[19] Bosch, C.; Andersson, A.; Kirillova, E. N.; Budhavant, K.; Tiwari, S.; Praveen, P. S.; Russell, L. M.; Beres, N. D.; Ramanathan, V.; Gustafsson, . *Journal of Geophysical Research, [Atmospheres]* **2014**, *119*, 711–743.

[20] Chen, Q.; Miyazaki, Y.; Kawamura, K.; Matsumoto, K.; Coburn, S.; Volkamer, R.; Iwamoto, Y.; Kagami, S.; Deng, Y.; Ogawa, S.; Ramasamy, S.; Kato, S.; Ida, A.; Kajii, Y.; Mochida, M. *Environmental Science and Technology*; 2016; Vol. 50; pp 10351–10360.

[21] Cheng, Y.; He, K. B.; Zheng, M.; Duan, F. K.; Du, Z. Y.; Ma, Y. L.; Tan, J. H.; Yang, F. M.; Liu, J. M.; Zhang, X. L.; Weber, R.; Bergin, M. H.; Russell, A. G. *Atmos. Chem. Phys.* **2011**, *11*, 11497–11510.

[22] Cheng, Y.; He, K.-b.; Du, Z.-y.; Engling, G.; Liu, J.-m.; Ma, Y.-l.; Zheng, M.; Weber, R. J. *Atmospheric Environment* **2016**, *127*, 355–364.

[23] Du, Z.; He, K.; Cheng, Y.; Duan, F.; Ma, Y.; Liu, J.; Zhang, X.; Zheng, M.; Weber, R. *Atmospheric Environment* **2014**, *89*, 235–241.

[24] Fan, X.; Wei, S.; Zhu, M.; Song, J.; Peng, P. *Atmos. Chem. Phys.* **2016**, *16*, 13321–13340.

[25] Hoffer, a.; Gelencsér, A.; Guyon, P.; Kiss, G.; Schmid, O.; Frank, G.; Artaxo, P.; Andreae, M. O. *Atmospheric Chemistry and Physics Discussions* **2006**, *6*, 3563–3570.

[26] Cappa, C. D.; Kolesar, K. R.; Zhang, X.; Atkinson, D. B.; Pekour, M. S.; Zaveri, R. A.; Zelenyuk, A.; Zhang, Q. *Atmos. Chem. Phys.* **2016**, *16*, 6511–6535.

[27] Hamill, P.; Giordano, M.; Ward, C.; Giles, D.; Holben, B. *Atmospheric Environment* **2016**, *140*, 213–233.

[28] Liu, C.; Chung, C. E.; Zhang, F.; Yin, Y. *Scientific reports* **2016**, *6*.

Chapter 6

Photobleaching of charge transfer complexes in brown carbon aerosols[1]

[1]Sabrina M. Phillips, and Geoffrey D. Smith. To be submitted to *Aerosol Sci. Technol.*, **2017**

6.1 Abstract

The mechanism of light absorption in brown carbon aerosols is still poorly understood. Similarly, photochemical aging during aerosol lifetimes is unknown, and thus ignored in climate models. Photobleaching experiments with a mercury arc lamp were employed to investigate light absorption and emission in ambient brown carbon aerosols. Preliminary absorption spectra were collected before and after irradiation at several wavelengths in the UV and visible region of the spectrum to selectively destroy chromophores. Brown carbon samples responded with absorption loss behavior that is inconsistent with a superposition of independent chromophores. Instead, the violation of consistent absorption loss, the broad absorption loss at long wavelengths, and the coupling between a short wavelength band (∼300 nm) and broad long-wavelength absorption suggest that the spectra arise from a continuum of coupled states. Furthermore, irradiation by the sun shows preliminary evidence that brown carbon would undergo similar photobleaching effects under normal sunlight conditions, which affect both absorption and fluorescence of aerosols. Future work irradiating at additional wavelengths is necessary for a more complete picture.

6.2 Introduction

Light absorption due to chromophores or charge transfer interactions can induce a number of photochemical intermediates and products.[1,2] The formation of these species can lead to the destruction of chromophores, and consequently charge transfer (CT) complexes, thus destroying the absorption associated with them.[3–6] This

'photobleaching' phenomenon can destroy chromophores in light-absorbing aerosols, potentially acting as a sink for brown carbon aerosols in the atmosphere.[7,8] The rate of brown carbon photobleaching has important implications in climate modeling. The absorptivity of these aerosols, and their effect on radiative forcing, can change drastically throughout their atmospheric lifetime. Photobleaching of brown carbon can be assessed through absorbance and fluorescence spectroscopy by measuring the effects of different light sources (monochromatic and polychromatic) on the spectral absorbance and light emission of collected ambient aerosols.

Evidence has been provided in chapters 2 and 3 that the absorption spectra of ambient brown carbon cannot arise from a superposition of the spectra of numerous independent chromophores, based on an analysis of chemical reduction with $NaBH_4$.[9,10] Here, room-temperature absorption spectroscopy and laser photobleaching experiments provide additional evidence. Ambient brown carbon samples were irradiated with a laser to selectively destroy species absorbing at specific wavelengths across the UV-visible wavelengths, using absorption spectroscopy to quantify the extent of photobleaching. The following further corroborates previous findings that absorption spectra of brown carbon cannot arise solely from a simple superposition of spectra of numerous independent chromophores. Instead, the long wavelength absorption tail of brown carbon (>350 nm) appears to arise from a continuum of coupled states, which we attribute to charge-transfer interactions within these materials.

Photobleaching experiments have been conducted on SRFA and SRHA to establish the contribution of charge-transfer complexes in the absorption spectra of HS.[11]

They found that reciprocity of absorption loss was clearly violated for the HS studied. This reciprocity, explained below, can be expressed by the following equation,

$$F' = A_T(t,\lambda)/A_T(0,\lambda) = \sum_i^n f_i(\lambda) \cdot e^{-\sigma_{P_i}(\lambda_{irr})\cdot E(\lambda_{irr})\cdot t} \tag{6.1}$$

where F' is the fraction of original absorbance, $A_T(t,\lambda)$ and $A_T(0,\lambda)$ is the total absorption at observation wavelength λ for irradiation time t and time 0, respectively; $f_i(\lambda)$ is the fractional absorption contribution of the i^{th} chromophore at λ; $\sigma_{P_i}(\lambda_{irr})$ is the photobleaching cross section (cm^2 $photon^{-1}$) of the i^{th} chromophore, and E is the irradiance (photons cm^{-2} s^{-1}) at the irradiation wavelength (λ_{irr}). This equation assumes photobleaching of any one chromophore does not affect the bleaching of another, and that photobleaching does not produce new chromophores that absorb over the spectra range of observations. Both of these assumptions have been demonstrated appropriate with a collection of independent chromophores by Del Vecchio and Blough.[11]

This equation dictates that, for a single chromophore or collection of independent chromophores, the decrease in F' with time will be independent of wavelength. Additionally, for a system undergoing photobleaching, reciprocity must hold between pairs of irradiation and observation wavelengths over the spectral range over which the chromophores absorb. Thus, the fractional absorption losses observed at wavelength 1 when irradiated at wavelength 2 must be equivalent to those observed at wavelength 1 when irradiated at wavelength 1, and vice versa. In other words, the ratio of absorption loss $F'_{\lambda_1}/F'_{\lambda_2}$ resulting from irradiation at wavelength 1 must equal the same absorption loss ratio ($F'_{\lambda_1}/F'_{\lambda_2}$) resulting from irradiation at wavelength 2.

An equivalent ratio of fractional loss demonstrates that the shape of the fractional loss spectrum appears the same, though the magnitude of fractional absorption loss is not necessarily equal at all irradiation wavelengths. This is consistent with the expectation that lower-energy irradiation wavelengths do not photolyze samples as efficiently as the higher-energy irradiation wavelengths.

As previously mentioned, reciprocity of fractional absorption loss was violated in HS samples.[11] Del Vecchio and Blough also observed uniform photobleaching (wavelength-independent loss spectra) at long irradiation times at wavelengths above λ_{irr} ($\geq$355 nm), the same region that is thought to be dominated by charge-transfer absorption. These observations are inconsistent with a superposition model. The interaction model that they proposed, instead, predicts all of these findings. Laser irradiation into the 300 nm band will lead not only to loss of the 300 nm band (either the donor or acceptor in the charge-transfer interaction) but also to the loss of donor-acceptor interactions at longer wavelengths resulting from the destroyed species. In contrast, irradiation into long-wavelength charge-transfer bands (λ_{irr} $\geq$355 nm) initially leads to the destruction of charge-transfer absorption (donor-acceptor interactions) corresponding to the laser wavelength. At longer irradiation times, when photobleaching extends across additional wavelengths, the absorption loss appears due to greater donor-acceptor destruction.

6.3 Materials and Methods

Aerosol collection, extraction, and optical measurements followed same protocol as previous chapters. SRFA was dissolved in Milli-Q water to a concentration of 50

mg/L. The absorption spectra were obtained at timepoints before and during irradiation. Samples were irradiated with a 100 W Hg arc lamp (Optical Building Blocks LPS 100), with bandpass filters to select for the irradiation wavelengths noted in Table 6.1. All bandpass filters are BrightLine single-band (Semrock) with part numbers FF01-315/15-25, FF01-370/36-25, FF01-434/17-25, and FF01-579/34-25, with the first number representing the center wavelength and the second number representing the width at the peak. FWHM values are reported in Table 6.1. Additional details of the setup can be found in Wiegand et al.[12] Brown carbon and SRFA were irradiated at 314 and 436 nm. A nitrophenol solution (25mg/L in Milli-Q water) was irradiated at 314 and 364 nm, because it didn't absorb at 436 nm. Approximately 2 mL of solution (sample and blank) were exposed to the lamp, and absorption spectra were collected as a function of irradiation time. A brown carbon sample was additionally irradiated by sun exposure and its absorption and fluorescence spectra were measured.

SRFA and ambient brown carbon extracts were also dissolved in 90% glycerol/10% Milli-Q water, to recreate the irradiation experiments performed on SRFA by Del Vecchio and Blough,[11] who did so to avoid absorption losses in part from reactions with intermediates produced by the primary photochemistry.[11] An equivalent glycerol/water solution was employed as the blank, and was irradiated in the same way as the samples. Samples in glycerol were irradiated at 314 and 578 nm. Though a blank solution was employed, it was unclear that that losses due to reactions intermediates are irrelevant in atmospheric photochemistry. Additionally, the

Table 6.1: Wavelength bands selected from the Hg arc lamp source

Wavelength (nm)	Power (mW)	FWHM (nm)
314	105.2	25
364	266	41
436	134.5	21
578	178.6	48

irradiation resulted in spectral losses in the glycerol. These results are reported, but the irradiations in water are considered more atmospherically relevant.

6.4 Results and Discussion

6.4.1 Wavelength reciprocity is violated in brown carbon

Brown carbon absorption spectra decrease with increasing wavelength, with no distinct features or absorbing bands (Fig. 6.1a). Similarities in absorption characteristics of brown carbon and SRFA motivated a comparison of spectral responses to irradiation. The following photobleaching data result from very preliminary experiments using just a few irradiation wavelengths. Additional irradiation wavelengths and time points are needed for a more complete picture. Brown carbon and SRFA samples were irradiated at different wavelengths bands in the UV and visible. Samples were irradiated at wavelengths λ_{irr} = 314 and 436 nm for varying lengths of time. These initial irradiation wavelengths were chosen because they lay on either side of the proposed transition from primarily independent chromophore absorption to primarily charge-transfer absorption ($\lambda \sim$350 nm). Absorption loss following

Table 6.2: Wavelength reciprocities for brown carbon irradiations.

Irradiation Wavelength (nm)	% Loss at 314 nm	% Loss at 436 nm	Ratio
314	75	73	0.97
436	7	39	5.6

laser irradiation was measured spectrophotometrically. Spectral loss varied with irradiation wavelength (λ_{irr}) and time (t) (Figures 6.1 and 6.2). At λ_{irr} = 364 nm, absorption was lost in a band centered at or near λ_{irr} and a second band at ∼300 nm. The band at λ_{irr} slightly blue-shifted with increasing irradiation time, however the second absorption loss band remained at a constant 300 nm peak. Irradiation into the 300 nm band (314 nm) produced loss at long wavelengths

Fractional loss was calculated at irradiation wavelengths (Figures figs. 6.1e, 6.1f, 6.2e and 6.2f). If absorption spectra arise from a linear superposition of chromophores the ratio of fractional loss at the two irradiation wavelengths should be equivalent. For brown carbon, irradiation at 314 nm resulted in fractional losses at 314 (75%) and 436 nm (73%) that were equivalent, however irradiation at 436 nm resulted in six times greater fractional loss at 436 nm (39%) than at 314 nm (7%) (Table 6.2). This was similar to the SRFA sample, in which 314 nm irradiation yielded equivalent losses at each wavelength (80% at both) but 436 nm irradiation yielded eight times more fractional loss at the 436 nm than at 314 nm (14% and 1.7%, respectively) (Table 6.3). The discrepancies in fractional loss for brown carbon and SRFA is explained by different irradiation times.

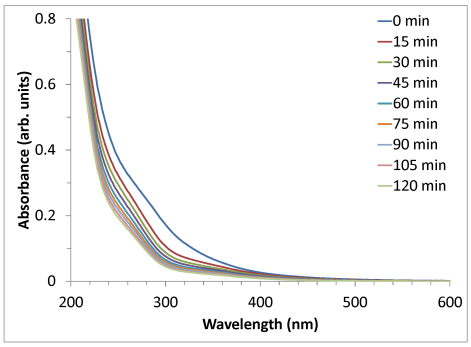

(a)

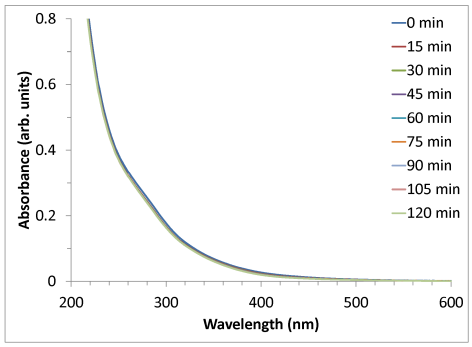

(b)

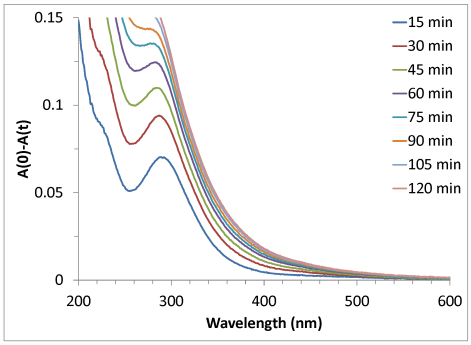

(c)

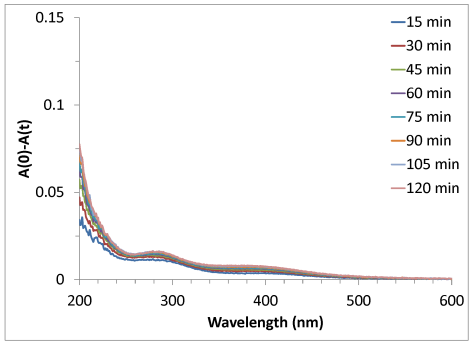

(d)

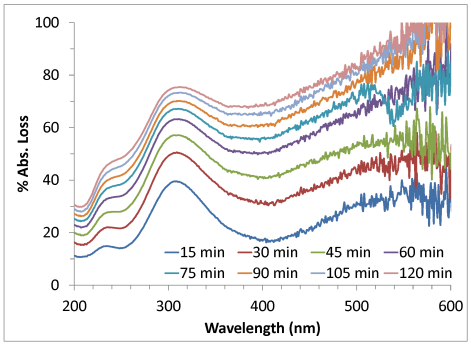

(e)

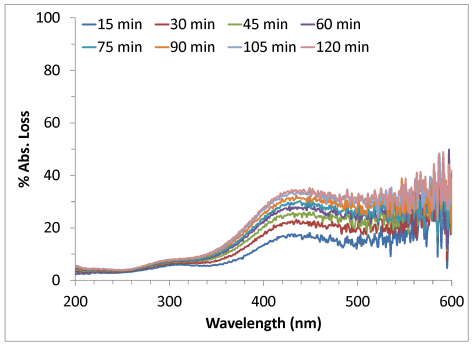

(f)

Figure 6.1: Time dependence of the absorption spectra, total absorption loss, and fractional absorption loss for brown carbon at irradiation wavelengths 314 nm (a, c, e), and 436 nm (b, d, f).

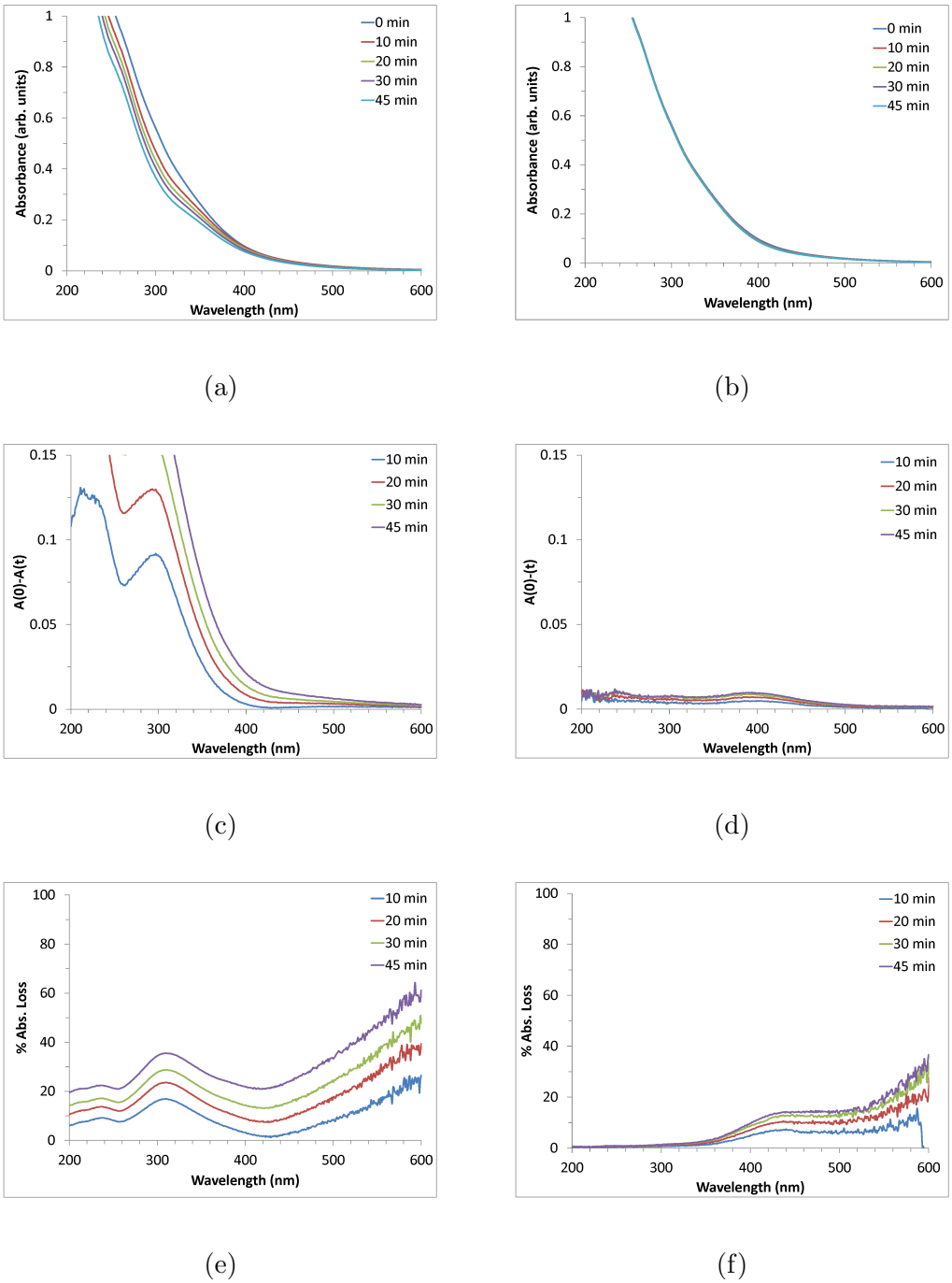

Figure 6.2: Time dependence of the absorption spectra, total absorption loss, and fractional absorption loss for SRFA at irradiation wavelengths 314 nm (a, c, e), and 436 nm (b, d, f).

Table 6.3: Wavelength reciprocities for SRFA irradiations.

Irradiation Wavelength (nm)	% Loss at 314 nm	% Loss at 436 nm	Ratio
314	80	80	1.0
436	1.7	14	8.2

Similar irradations were performed on nitrophenol (Figure 6.3). Nitroaromatic species absorb light at long wavelenghts and have been detected in aerosols[13–16] and been able to attribute as much as 4% of observed brown carbon absorption to them as a class.[15,16] Nitrophenol was irradiated at wavelengths λ_{irr} = 314 and 364 nm, because of little absorbance at 436 nm. At 314 nm irradiation, nitrophenol saw fractional loss of 85% and 65% at 314 and 364nm, respectively, which is a loss ratio of 1.3 for the two wavelengths. At 364 nm irradiation there was a fractional loss of 65% and 50% for the two wavelengths, a loss ratio of 1.3 (Table 6.4). This indicates that, though the two irradiation wavelengths might induce destruction of chromophores more or less efficiently (unsurprisingly, 314 nm yields quicker absorption loss) their affect on the spectrum is identical. This is because a single absorbing species comprises the entire absorption spectrum and would not preferentially display loss at one wavelength over another. A superposition of absorbing species would behave in the same way. This is inconsistent with the way brown carbon and SRFA samples behave, where short-wavelength loss at long irradiation wavelengths is time dependent, and reciprocity of absorption loss at short and long wavelengths is violated. This further corroborates the CT interaction model for brown carbon and SRFA.

Additionally, fractional loss was nearly constant across the photobleaching band observed at ∼320nm. This photobleaching band is a deviation from the photobleaching behavior observed in brown carbon and SRFA, which appear to arise from two distinct sources, independent chromophore absorption and charge transfer absorption, that are coupled together. Though only two irradiation wavelengths have been shown for nitrophenol, the constant fractional loss over more than 100 nm makes it reasonable to assume that similar photobleaching behavior would result from different irradiation wavelengths in that range.

In nitrophenol fractional loss was independent of wavelength across the spectral regions where absorption loss was observed, however absorption can be seen to increase with increasing irradiation time at ∼210 nm and ∼250 nm. This is suggestive of newly absorbing species that were created by photolysis of species at the ∼320nm absorption band. The consistent ratios of fractional loss, the constant loss across the photobleaching band, and the new absorption at short wavelengths all suggest that irradiation of nitrophenol is photolyzing species at long wavelengths, resulting in product absorption bands at shorter wavelengths. This is different from the SRFA and brown carbon samples, in which long-wavelength irradiation actually destroys independent chromophores that already absorb at short wavelengths within the range of UV-visible wavelengths measured in these experiments.

6.4.2 Brown carbon absorption ages in sunlight

To recreate photobleaching effects more relevant to atmospheric particles, brown carbon extracts were measured spectroscopically before and after sun exposure (Figure

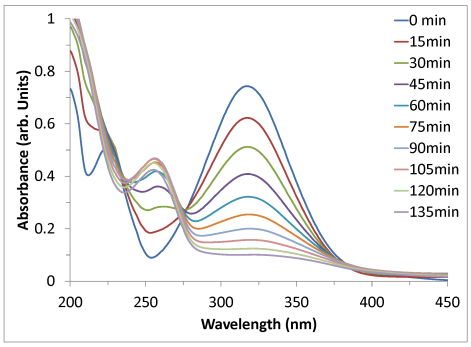

(a)

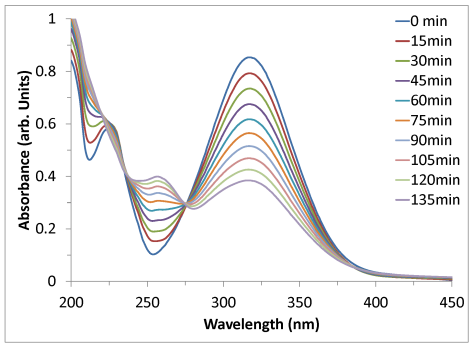

(b)

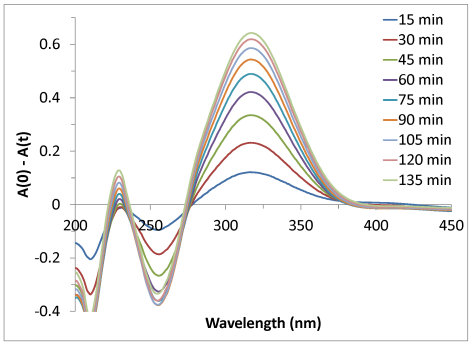

(c)

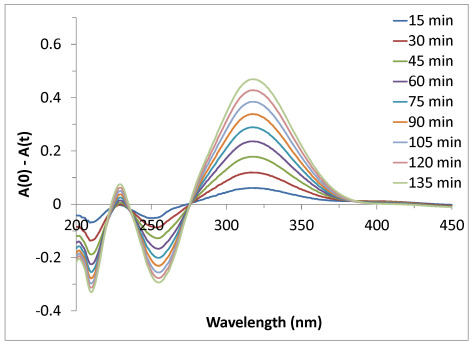

(d)

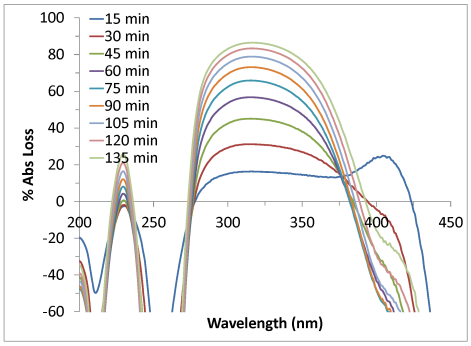

(e)

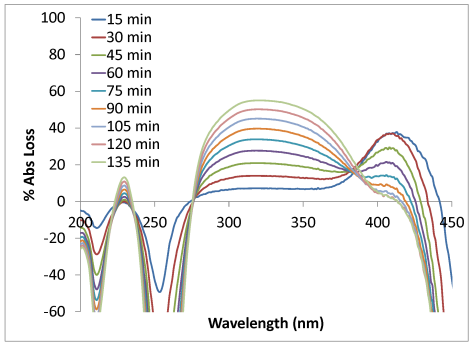

(f)

Figure 6.3: Time dependence of the absorption spectra, total absorption loss, and fractional absorption loss for nitrophenol at irradiation wavelengths 314 nm (a, c, e), and 364 nm (b, d, f).

Table 6.4: Wavelength reciprocities for nitrophenol irradiations.

Irradiation Wavelength (nm)	% Loss at 314 nm	% Loss at 364 nm	Ratio
314	85	65	1.3
364	65	50	1.3

6.4). Roughly eight hours of sun exposure resulted in absorption loss at wavelengths $\geq$280 nm, with a maximum total loss observed at $\sim$325 nm, and a fractional loss of 15-25% at wavelengths 300-600 nm. The effect of sun irradiation on fluorescence was also measured on a brown carbon filter (Figure 6.5). Excitation-emission matrices were collected before and after sun exposure of $\sim$22 hours. The irradiation resulted in a slightly blue-shifted maximum peak of emission that decreased in intensity by 66%. Decreased absorption and emission at short wavelengths ($\sim$300nm), as well as long wavelengths, suggests that sun irradiation is destroying the independent chromophores that absorb at short wavelengths and interact in charge-transfer interactions that give rise to long-wavelength absorption.

Laser irradiations have been performed on humic substances SRFA and SRHA (Suwannee River Humic Acid) previously in 90% glycerol to ensure that absorption losses did not result in part from reactions with intermediates produced by the primary photochemistry.[11] Though it seems that any photobleaching intermediates produced in the lab would be present in the atmosphere, we performed similar experiments on brown carbon and SRFA at irradiation wavelengths 314 and 578 nm (Figures 6.6 and 6.7). Interestingly, though an appropriate glycerol blank solution

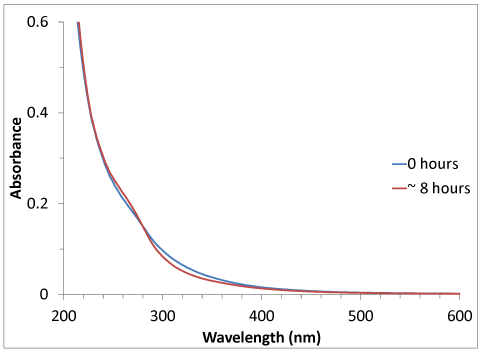

(a)

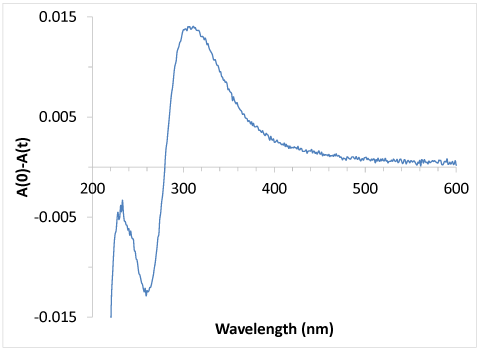

(b)

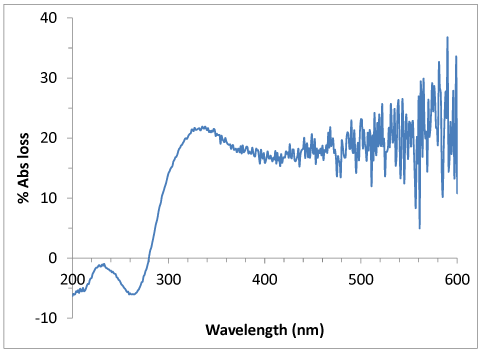

(c)

Figure 6.4: Absorption spectrum, total absorption loss, and fractional absorption loss for brown carbon sun exposure for ∼8 hours.

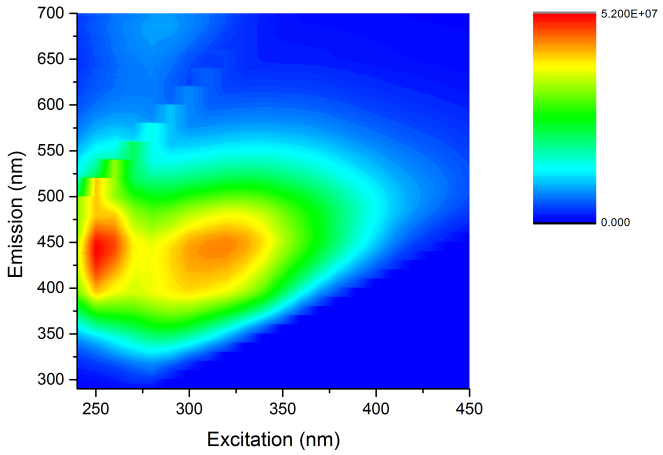

(a)

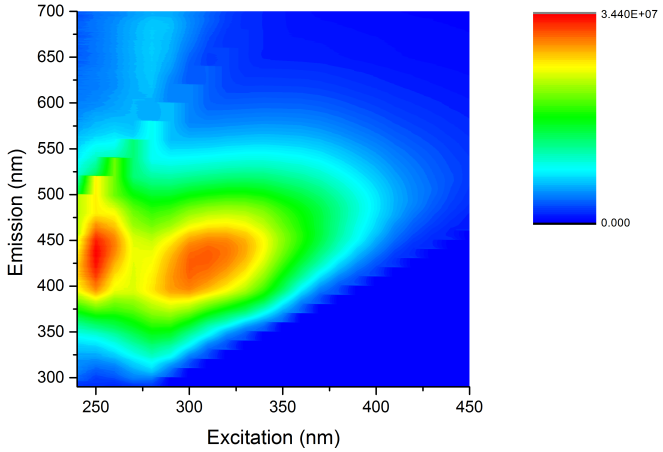

(b)

Figure 6.5: Fluorescence EEM for brown carbon before (a) and after (b) sun exposure for ∼22 hours. EEM's were collected by Jennifer Evans

was irradiated under the same conditions and subtracted from absorption spectra, enhanced losses greater than 100% were observed in both brown carbon and SRFA samples (Figures 6.6e, 6.6f, 6.7e, and 6.7f). Greater than 100% loss suggests an unknown or uninterpretable secondary reaction is occurring. Additionally, irradiations appeared to alter the absorption spectrum of glycerol on its own. This further complicates interpretation of the observed absorption loss, as it is impossible to assume that intermediates arising from photolyzed glycerol are not reacting with the sample. The wavelength reciprocity of fractional loss was violated, as was observed for the samples in water, however little can be concluded from that since the long irradiation wavelength (578 nm) almost always saw more than 100% absorption loss.

The photobleaching results presented above are consistent with an interaction model, such as could arise from intra- or intermolecular electron donor-acceptor interactions within brown carbon and HS. A ground-state association between an electron donor and an electron acceptor can form charge-transfer complexes that exhibit new broad absorption bands that are not shown by the donor or acceptor molecule alone. These arise from the partial or complete promotion of an electron from the donor to the acceptor upon absorption of a photon.[11] The interaction model is also consistent with the electronic scheme shown in Figure 3.8. This model necessitates that fractional absorption loss that increases rapidly and becomes nearly wavelength independent at longer irradiation times requires that the low energy transitions are coupled to those at a higher energy. This is consistent with the appearance of only a single photobleaching band at long wavelengths after short irradiation times ($\lambda_{irr} \geq$ 390 nm, and the appearance of a common 300 nm band at all $\lambda_{irr} \geq 390$ nm fol-

lowing longer irradiation times. Additionally, the violation of reciprocity would only be possible in a scenario where irradiated samples are not either directly connected (i.e. multiple absorption bands in a single chromophore) or a linear superposition of chromophores (i.e. a mixture of completley independent compounds that do not interact).

6.5 Conclusions

The behavior observed upon irradiation of the brown carbon and SRFA samples can arise from the same charge-transfer model proposed in Chapter 2. A transfer of an electron from a phenol to an aromatic ketone or carbonyl moiety would account for the broad, featureless absorption spectra that extends far into the visible, and the photosensitized absorption loss is consistent with an interaction model. What is more, the violation of reciprocity of fractional absorption loss could only be explained with an absorption model much more complex than a linear superposition on non-interacting chromophores. Indeed, there are several mechanisms that could cause this intra- or intermolecular interaction, such as energy transfer, charge migration, structural reorganization, or a combination thereof. However, charge-transfer interactions have been established in humic substances and brown carbon extensively, and the presence of the necessary functional groups is highly likely in organic aerosols in the form of HULIS or biomass burning products. Further study is of great interest, especially at additional irradiation wavelengths that could be provided by the arc lamp, and at a wider range of irradiation times, to differentiate between immediate and long-term photobleaching phenomena. No irradiation experiments have yet

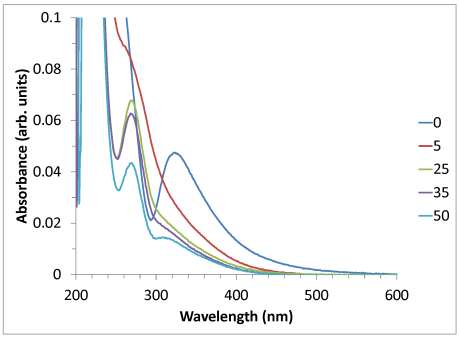

(a)

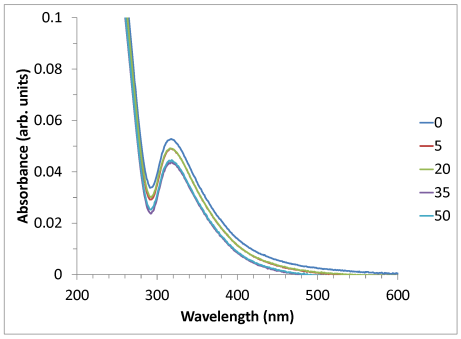

(b)

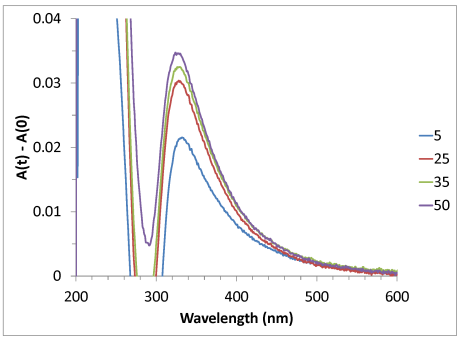

(c)

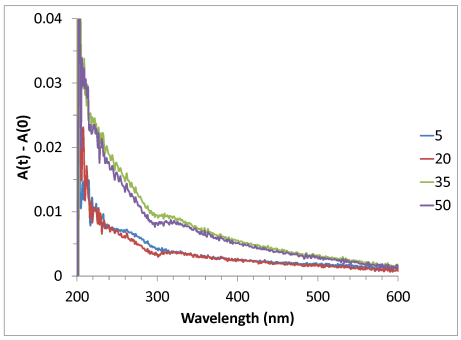

(d)

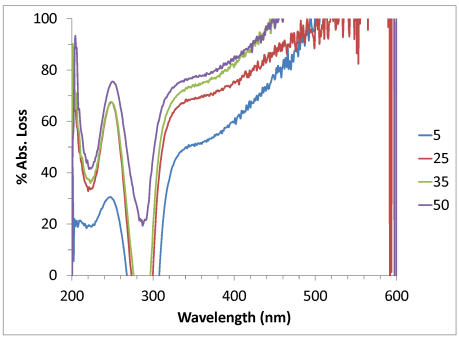

(e)

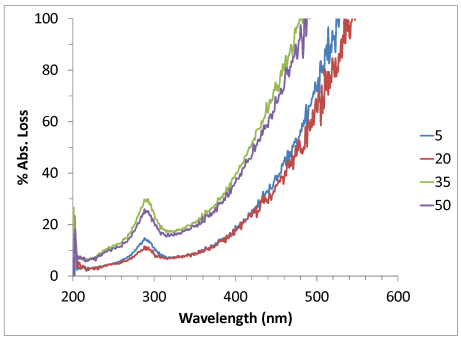

(f)

Figure 6.6: Time dependence of the absorption spectra, total absorption loss, and fractional absorption loss for brown carbon dissolved in 90% glycerol at irradiation wavelengths 314 nm (a, c, e), and 578 nm (b, d, f).

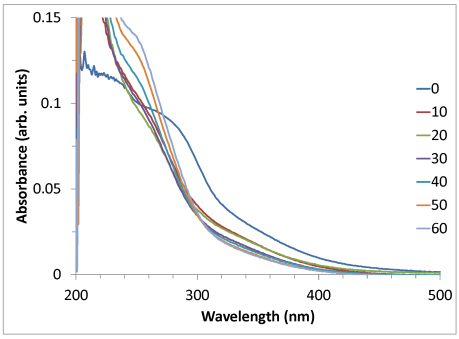

(a)

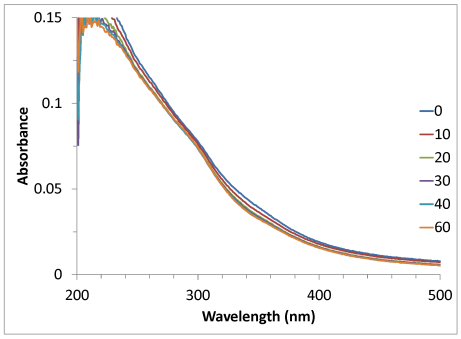

(b)

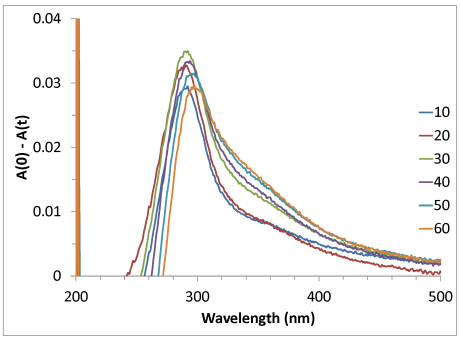

(c)

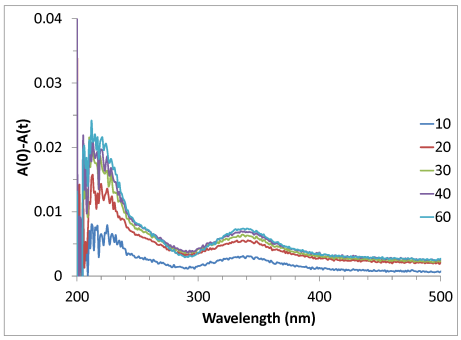

(d)

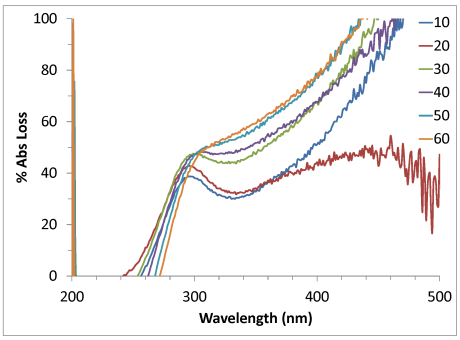

(e)

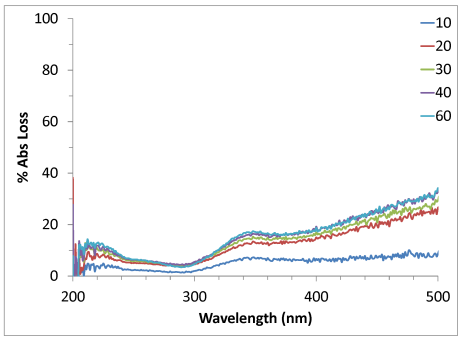

(f)

Figure 6.7: Time dependence of the absorption spectra, total absorption loss, and fractional absorption loss for SRFA dissolved in 90% glycerol at irradiation wavelengths 314 nm (a, c, e), and 578 nm (b, d, f).

been performed on methanol extracts, and this would be of interest in the future as methanol extractions provide more signal.

Bibliography

[1] Moran, M.; Zepp, R. *Limnology and Oceanography* **1997**, *42*, 1307–1316.

[2] Vecchio, R. D.; Blough, N. *Marine Chemistry* **2002**, *78*, 231–253.

[3] Moran, M.; Sheldon, W.; Zepp, R. *Limnology and Oceanography* **2000**, *45*, 1254–1264.

[4] Whitehead, R. F.; de Mora, S.; Demers, S.; Gosselin, M.; Monfort, P.; Mostajir, B. *Limnology and Oceanography* **2000**, *45*, 278–291.

[5] Reche, I.; Pace, M.; Cole, J. *Biogeochemistry* **1999**, 259–280.

[6] Skoog, A.; Wedborg, M.; Fogelqvist, E. *Marine chemistry* **1996**, *55*, 333–345.

[7] De Haan, H. *Limnology and Oceanography* **1993**, *250*, 665–669.

[8] Frimmel, F.; Bauer, H. *Science of the Total Environment* **1987**, *62*, 139–148.

[9] Phillips, S.; Smith, G. *Environmental Science & Technology Letters* **2014**, *1*, 382–386.

[10] Phillips, S. M.; Smith, G. D. *Journal of Physical Chemistry A* **2015**, *119*, 4545–4551.

[11] Vecchio, R. D.; Blough, N. *Environmental science & technology* **2004**, 3885–3891.

[12] Wiegand, J. R.; Mathews, L. D.; Smith, G. D. *Analytical Chemistry* **2014**, *86*, 6049–6056.

[13] Jacobson, M. Z. *Journal of Geophysical Research* **1999**, *104*, 3527–3542.

[14] Desyaterik, Y.; Sun, Y.; Shen, X.; Lee, T.; Wang, X.; Wang, T.; Collett, J. L. *Journal of Geophysical Research: Atmospheres* **2013**, *118*, 7389–7399.

[15] Zhang, X.; Lin, Y.-H.; Surratt, J. D.; Weber, R. J. *Environmental Science & Technology* **2013**, *47*, 3685–93.

[16] Mohr, C. et al. *Environmental science & technology* **2013**, *47*, 6316–24.

Chapter 7

Brown carbon is humic in nature[1]

[1]Sabrina M. Phillips, and Geoffrey D. Smith. To be submitted to *Aerosol Sci. Technol.*, **2017**.

7.1 Abstract

Brown carbon aerosols resemble terrestrial and aquatic humic and fulvic substances in their absorption and fluorescence spectra. Large macromolecular compounds in aerosols appear so similar to humic substances (HS) that they have been termed HUmic-LIke Substances (HULIS). To expand upon comparisons drawn between the two groups of chromophoric organic matter, common absorption and fluorescence humic indices were employed to parameterize and compare the spectral characteristics of brown carbon and HS. Chemical reductions with $NaBH_4$ were performed to determine the fractional absorption loss and estimate relative contribution to absorption by CT complexes, with the goal of creating a new index that corresponded with absorption loss (extent of CT). Preliminary results for established indices are reported here, though a new CT index has yet to be determined.

7.2 Introduction

Atmospheric aerosols perturb the climate by scattering and absorbing incoming solar radiation and through cloud formation as cloud condensation nuclei.[1] These roles in the atmosphere are all influenced by the chemical composition of aerosol particles, and their corresponding spectral characteristics. Organic species in aerosols are diverse and complex; hundreds or thousands of organic compounds in aerosols have been identified by GCMS but these can account for only a small fraction of total organic matter in aerosols.[2–7] A substantial component of organic aerosols comprise polyacidic compounds similar to aquatic and terrestrial humic substances (HS).[8]

In fact, these aerosol species are so similar to HS that they've been called HULIS (humic-like substances). HULIS has been identified in atmospheric aerosols collected in urban[9] and rural[10] sites and in fog samples,[11] and has been characterized by UV, IR, NMR, and fluorescence spectroscopy,[9,12,13] capillary electorphoresis,[9,11] voltammetry,[14] pyrolysis gas chromatography mass spectrometry,[15] elemental analysis,[10] and ultrafiltration LCMS and vapor-pressue osmometry.[16]

All of these studies concluded that the examined organic matter in aerosols resemble fulvic and humic acids, though there are several distinctions. Aerosol HULIS still is distinctive from HS in several ways, namely smaller average molecular weight, lower aromatic moiety content, greater surface activity, and better droplet activation ability.

Humic substance standards have been well studied and categorized by a number of different indices used to describe and differentiate HS by source (microbial or terrestrial) and chemical characteristics of sample.[17–24] Because of the inherent chemical complexity of dissolved organic matter (DOM) in HS, there are historically few simple chemical analyses to readily characterize samples, and consequently the aquatic community has employed absorbance and fluorescence spectra as indicators of general source and chemical characteristic of absorbing species in HS, or chromophoric dissolved organic matter (CDOM).[7,17,19–21,23–25] Variations in HS can arise from differences in precursor organic material and geochemical processes acting on HS, and these indices describe samples in terms of microbial and aromatic content, their relative molecular weight and their level of oxidation and irradiation.

Despite its similarities to HS, atmospheric HULIS has yet to be described by the indices created by the humic community. Below is a preliminary study of how ambient water-soluble brown carbon aerosols from Athens, GA compare to humic and fulvic acid standards for several of the established absorbance and fluorescence indices. Additionally, $NaBH_4$ reductions were performed on all samples to determine relative contribution of charge-transfer complexes to the UV-visible absorption of each sample.

7.3 Materials and Methods

7.3.1 Aerosol Collection

Ambient aerosols were collected out of a window in the Chemistry Building at the University of Georgia (∼20 m above ground level) in Athens, GA (33.9488°N, 83.3747°W). A total of 10 samples were collected on polytetrafluoroethylene (PTFE, Teflon) filters (0.2 μm pore size, Sterlitech) at a rate of 16.7 L/min. A very sharp cut cyclone inlet (BGI, Inc.) was employed to size select for particles with diameters of $< 2.5\mu$m. Water-soluble organic species were then extracted in a manner similar to that described by Hecobian et al.[26] by sonication of the filter for 20 min in 10 mL of Milli-Q water ($< 18.2 M\Omega \cdot cm$). Extracted solutions were filtered using a 0.45 μm PTFE disposable syringe filter and adjusted to pH 7.

7.3.2 Humic Substances

Humic substances were dissolved in Milli-Q water ($< 18.2 M\Omega \cdot cm$) to a concentration of 50 mg/L, were filtered using a 0.45 μm PTFE disposable syringe filter, and

adjusted to pH 7. All humic substance standards, listed in detail in Table 7.1, came from The International Humic Substances Society.

7.3.3 Reduction

Reductions were adapted from the protocol detailed by Ma et al.[27] Extracted aerosol and HS solutions were reduced in a 1 cm quartz cuvette (3 mL) by adding approximately 5 mg of solid $NaBH_4$ and dissolving it by stirring. Reduction proceeded until no further change in absorbance was noticed (25 min). Because of an excess of $NaBH_4$, the pH of the solution increased to 10. The solution was readjusted to pH 7 with HCl before optical absorption spectra were recorded on a Cary 60 spectrophotometer (Agilent) over a range of 200-800 nm. Fluorescence spectra were recorded on a FluoroLog 2 fluorometer (Horiba) over an excitation range of 280-450 nm scanned in 5 nm steps.

Absorbance spectra were used for correction of primary and secondary inner filtering effects in fluorescence measurements.[28] EEM's were compared using the uncorrected matrix correlation (UMC) method, which compares two entire matrices, independent of intensity. A UMC value of 1 indicates that the two matrices are identical and decreases to approach zero with decreasing correlation.[18,29]

7.4 Results and Discussion

7.4.1 Absorption and fluorescence spectra

Figure 7.1 shows absorption spectra obtained for a variety of HS standards (described in Table 7.1) and two representative brown carbon (BrC) extracts. All absorbance

Table 7.1: Sample descriptions and abbreviations of the materials used in this study

Sample Name	Description	Abbreviation
Suwannee River Fulvic Acid	Suwannee River, GA USA Drains the Okeefenokee swamp, a cypress wetland	SRFA
Suwanee River Humic Acid	Suwannee River, GA USA Drains the Okeefenokee swamp, a cypress wetland	SRHA
Pahokee Peat Fulvic Acid	Pahokee soils, Florida Everglades, USA Agricultural peat soil, organic deposits of freshwater marshes	PPFA
Pahokee Peak Humic Acid	Pahokee soils, Florida Everglades, USA Agricultural peat soil, organic deposits of freshwater marshes	PPHA
Pony Lake Fulvic Acid	Pony Lake, Antarctica Eutrophic, saline coastal pond, purely microbially derived	PLFA
Nordic Aquatic Fulvic Acid	Hellrudmyra tarn, Oslo, Norway Isolated water catchment	NAFA

spectra demonstrate the broad, featureless absorption profile that is characteristic of humic substances and BrC aerosols. All spectra decay with increasing wavelength, and absorbance is typically gone at wavelengths greater than ∼600 nm. Absorbance intensity varied among the samples, with the BrC samples being the least absorbing due to lower concentrations of CDOM (chromophoric dissolved organic matter). The absorbance and fluorescence indices described below compare relative values within a spectrum, and thus negate magnitude differences.

Unlike the UV-visible absorption spectra, the fluorescence spectra in HS and BrC have characteristic maxima that may vary by structural characteristics, source

organic material, and chemical environments.[18] Mobed et al. showed that significant differences in EEM's occurred among soil and wetland HS.[18] Coble showed that the position of one humic fluorophore of natural waters was shifted to lower excitation and emission wavelengths for marine compared to riverine and coastal samples.[30]

Fluorescence EEM's for two representative BrC filters are presented in Figure 7.2, and the EEM's for the six HS standards are shown in Figures 7.3 and 7.4. Qualitative analysis of EEM's can be difficult because emission peaks are often broad and unresolved. The EEM's all share two major fluorescence bands, though the specific wavelengths may be shifted depending on sample. The first emission band is the α fluorophore, which materializes as two bands with the excitation and emission maxima typically centered around α : λ_{ex} = 330 - 370 and λ_{em} = 420 - 480 and α' : λ_{ex} = 230 - 260 and λ_{em} = 380 - 480. The α fluorophore is representative of humic material.[23] The second emission band is the β fluorophore, which is typicallly centered near β : λ_{ex} = 310 - 320 and λ_{em} = 380 - 420. The β fluorophore was initially attributed to humic-like material of marine origin.[31] It was later demonstrated that it was responsible for the hypsochromic fluorescence shift between marine and freshwater samples, and that it was related to biological activity in coastal marine environments.[32] The general location of each fluorophore is depicted on the pre-reduction NAFA EEM shows in Figure 7.3e.

In our measurements the α' band is predominant in all samples. Some samples show very little of the α band, like both the BrC samples and the PPFA and PPHA samples. The NAFA EEM shows much greater α band intensity than the β band. The presence of the β fluorophore varies in each sample in intensity and position.

PPFA, PPHA, SRFA, and PLFA show the most intense β peaks, though in the cases of PPFA and PPHA the β and α peaks are not well resolved (Figures 7.4a and 7.4c).

The β fluorophore peaks at longer excitation and emission wavelengths in HS than in BrC samples. There results are in agreement with previous studies.[33–35] A red-shifted fluorescence maximum is attributed, in part, to the presence of higher molecular weight fractions, electron-withdrawing substituents, and higher degree of conjugation in HS.[18] Spectral differences can be quantified by the absorbance and fluorescence indices, and the extent of EEM variation is quantified by the UMC comparisons below.

7.4.2 Absorbance Loss

Chemical reductions with $NaBH_4$ were performed on all BrC and HS samples, as was seen in Chapter 2. The similarities in spectral shape suggests that these substances from very different origins could share a common chemical explanation for light absorption, i.e., CT complex formation. Figure 7.5 shows the average fractional absorption loss (300 - 600 nm). The BrC reductions resulted in a broad range of absorption loss that spanned the extent of absorption loss in HS samples. Among the HS samples, the Pahokee Peat HS (PPFA and PPHA) were least affected by $NABH_4$, and the SRHA and NAFA samples were most affected by $NABH_4$. With the exception of both Pahokee Peat samples showing little absorption loss, it is difficult to determine a trend by sample origin. It does appear that within similar sources the humic acids experience more absorbance loss than the fulvic acids. This is true for the two instances where both samples types were measured, PPFA/PPHA

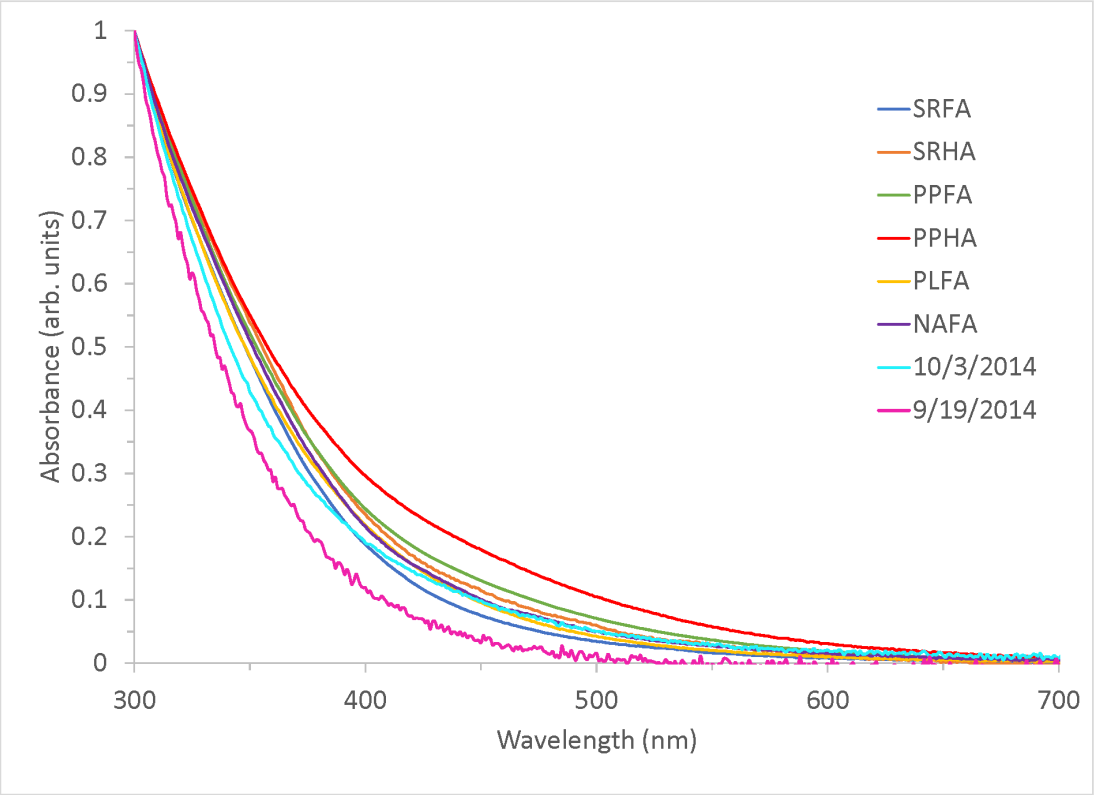

Figure 7.1: UV-visible absorbance of several standard humic and fulvic acids and two representative ambient brown carbon days. All spectra are normalized to their value at 300 nm.

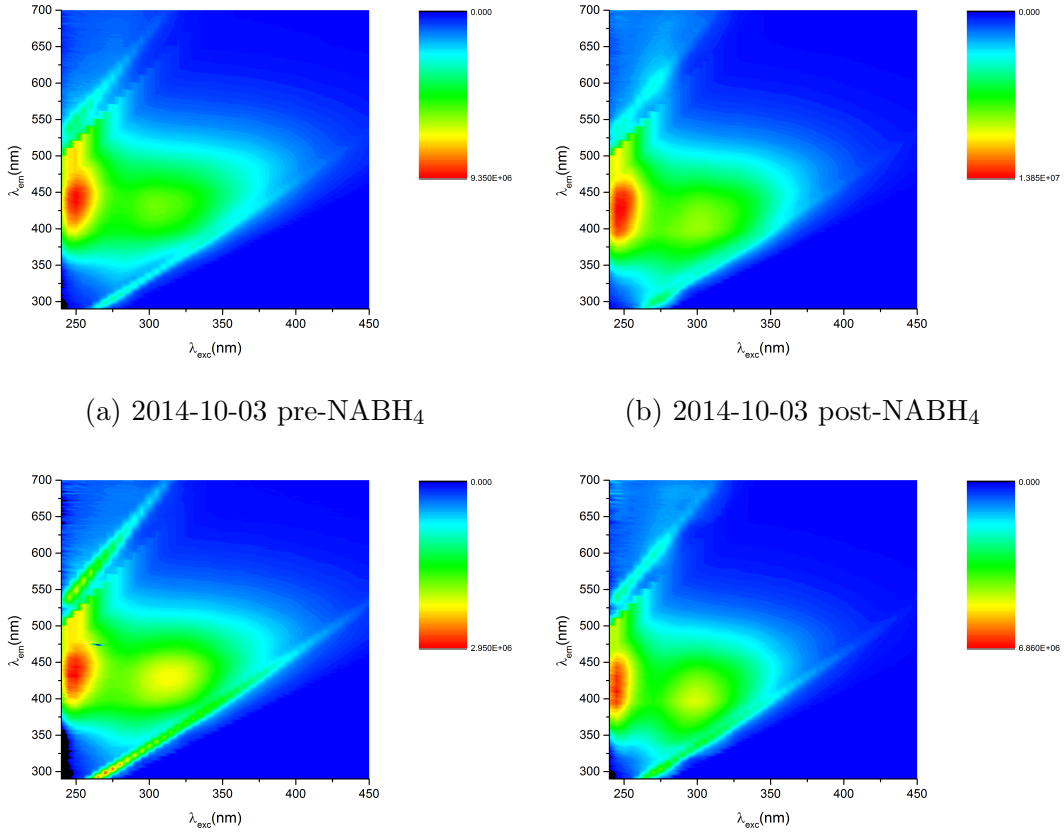

(a) 2014-10-03 pre-$NABH_4$

(b) 2014-10-03 post-$NABH_4$

(c) 2014-09-19 pre-$NABH_4$

(d) 2014-09-19 post-$NABH_4$

Figure 7.2: Representative EEM's for ambient brown carbon extracts

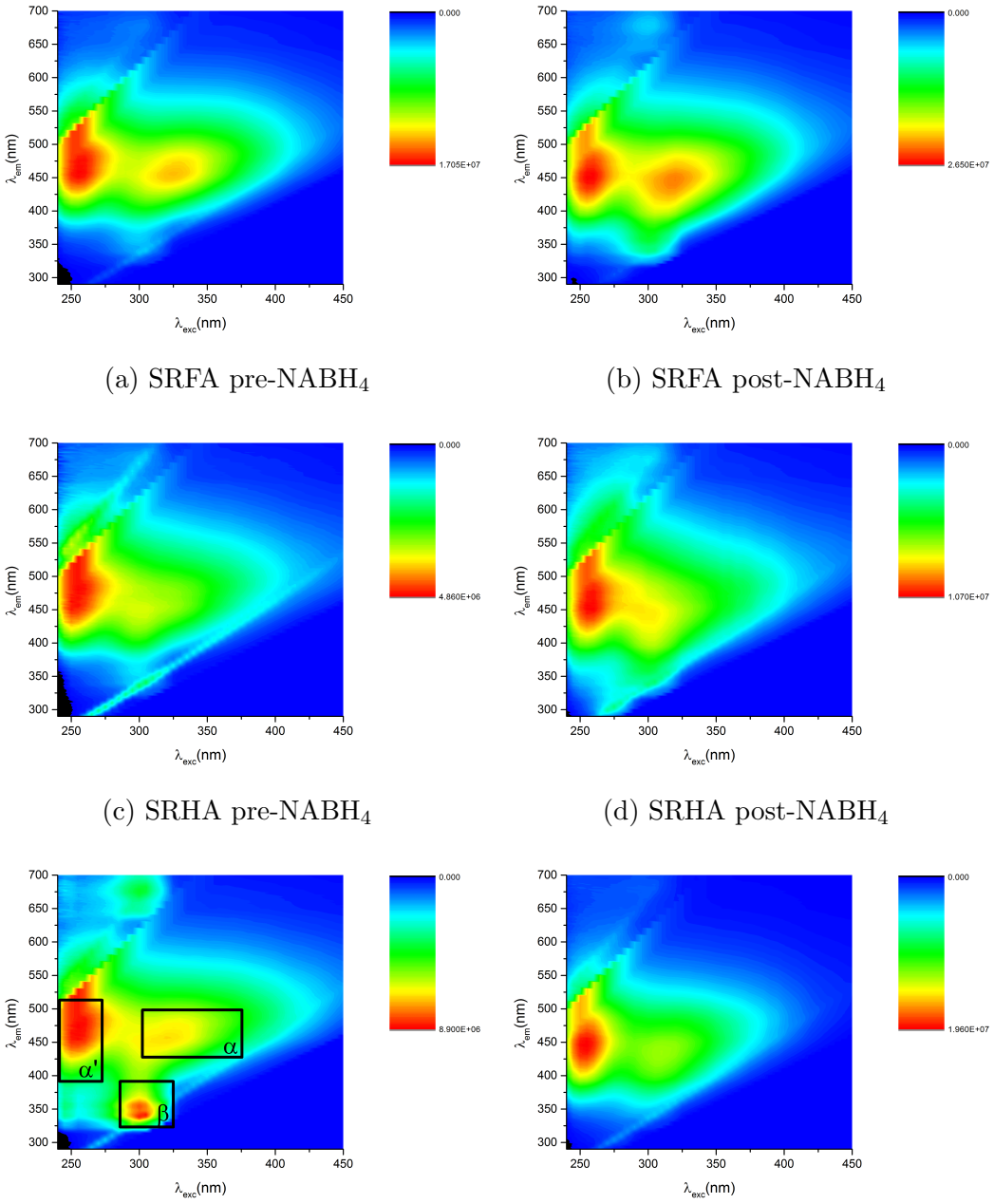

(a) SRFA pre-$NABH_4$ (b) SRFA post-$NABH_4$

(c) SRHA pre-$NABH_4$ (d) SRHA post-$NABH_4$

(e) NAFA pre-$NABH_4$ (f) NAFA post-$NABH_4$

Figure 7.3: EEM's for humic substance standards before and after reduction with $NABH_4$. 7.3e shows general locations of common HS fluorophores.

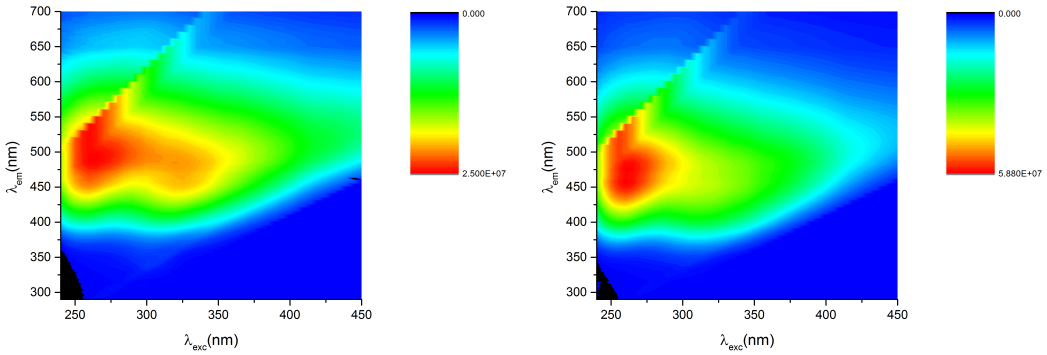

(a) PPFA pre-$NABH_4$

(b) PPFA post-$NABH_4$

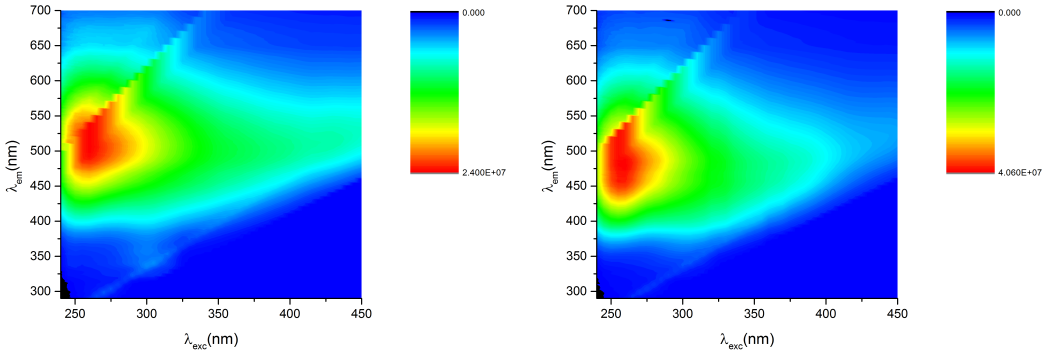

(c) PPHA pre-$NABH_4$

(d) PPHA post-$NABH_4$

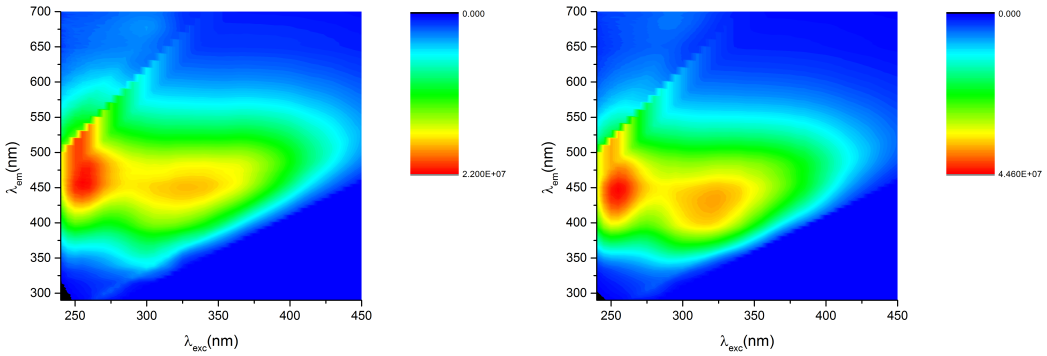

(e) PLFA pre-$NABH_4$

(f) PLFA post-$NABH_4$

Figure 7.4: Additional EEM's for humic substance standards before and after reduction with $NABH_4$.

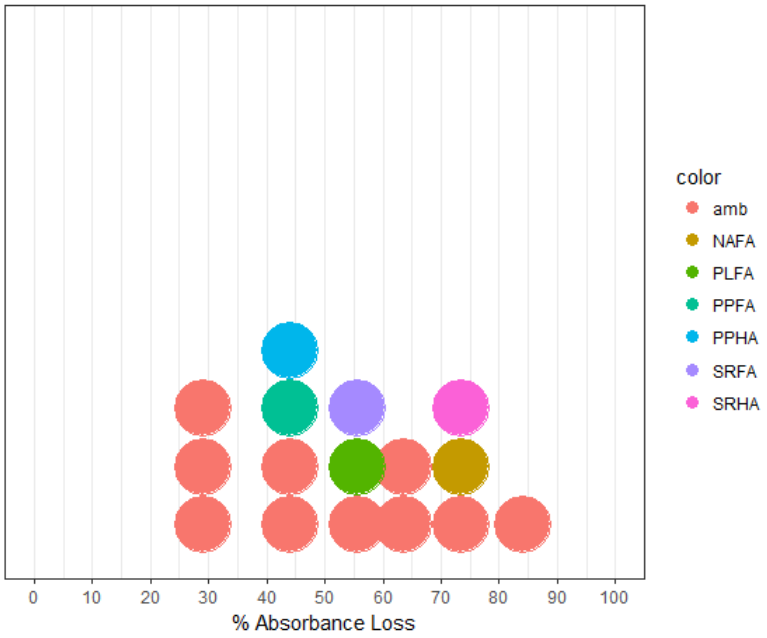

Figure 7.5: Histogram of the fractional absorbance loss after $NaBH_4$ reduction of ambient brown carbon and several standard humic and fulvic acids. Each HS dot represent an average of two reductions for each sample. BrC dots each represent one day.

and SRFA/SRHA. Besides variability among different samples, the HS samples are standardized and thus were extremely reproducible (Figure 2.2). Though the range of BrC loss is large, is can be attributed to variations in ambient collected aerosol source and type.

7.4.3 Fluorescence Index

The fluorescence index (FI) is representative of the origin of HS and is calculated by ratio of emission intensity at $\lambda_{em} = 450/500$ nm at $\lambda_{ex} = 370$ nm. McKnight et al. developed the FI when they found that the α fluorophore displays emission maxima at lower wavelengths in microbially derived HS compared to terrestrially derived HS.[20] They found they could compare the differences in the breadth of the peak by taking the ratio of emission intensity at two different wavelengths from within the same excitation wavelength. Microbial HS samples typically have FI values of $\sim$1.9 whereas FI values for terestrially derived HS are closer to $\sim$1.4. The FI index represents the greater decline in emission with increasing wavelengths for microbially derived samples, and is a simple way to estimate the extent of aromaticity in a HS sample.

The fluorescence EEM's for terrestrially derived humic and fulvic acids are very similar to each other and markedly different from the microbially derived fulvic acid (PLFA), as seen in Figure 7.6. Emission maxima for both the α and β fluorophores occur at the same excitation wavelengths, but much longer emission wavelengths in the terrestrial HS. FI values calculated in the present work were lower than previously observed,[20] however the same trends were observed. Terrestrially derived

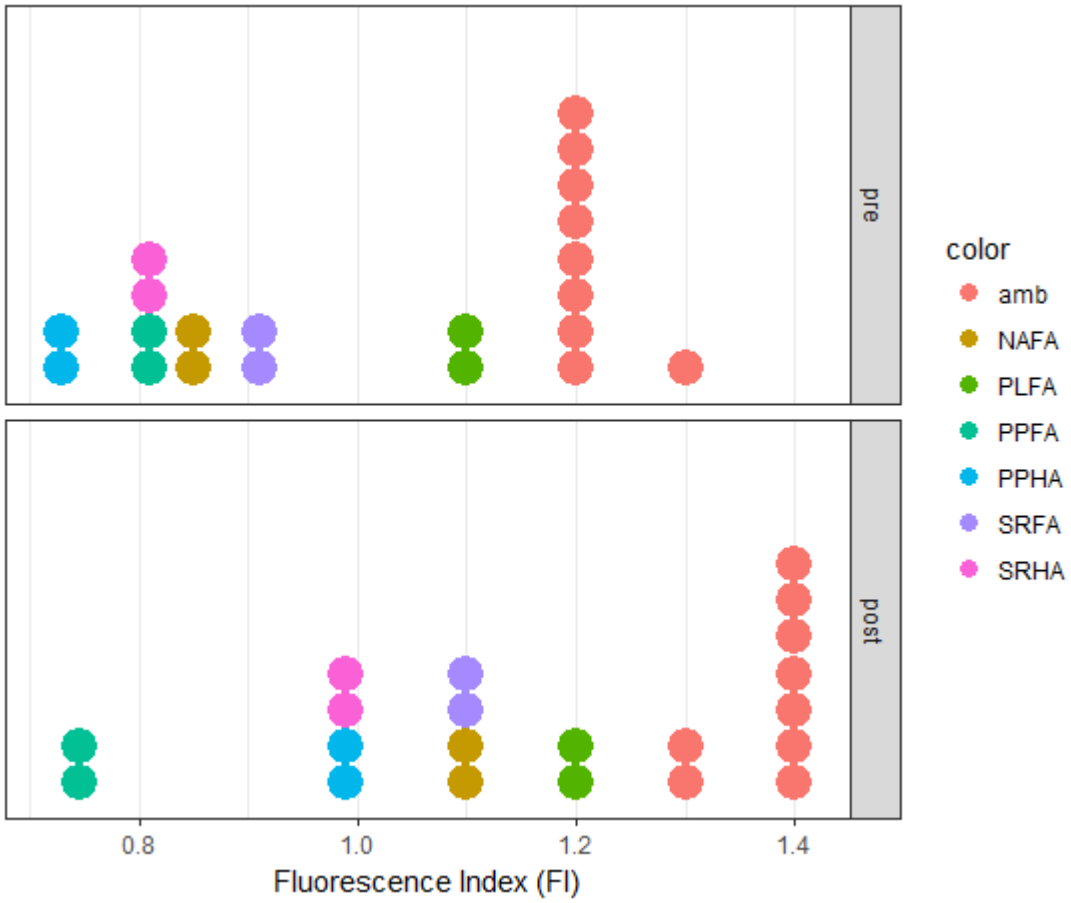

Figure 7.6: Histogram of the fluorescence index (FI) of ambient brown carbon and several standard humic and fulvic acids.

HS had lower FI values (0.7-0.9) compared to microbially derived HS (1.1). Brown carbon FI values were even higher than microbial fulvic acids, with values ranging from 1.2-1.3. These variations in FI reflect the variations in emission maxima. Furthermore, McKnight et al.[20] showed a high correlation ($r^2 = 0.85$) between the FI and aromaticity for isolated fulvic acid samples. However, the authors note that aromaticity should not be estimated based only on a fluorescence measurement without other supporting data such as molar absorptivity at 280 or 254 nm. Aromaticity may be altered by geochemical processes such, as sorption or photobleaching, without causing a change in the fluorescence index. Additionally, a linear relationship could extrapolate to negative aromaticities if some microbially derived fulvic acids had fluorescence indices >2.1.

The high BrC FI values would imply a lower aromatic content in BrC compared to the measured HS. This is consistent with previous measurements by ^{13}C-NMR spectra,[36,37] ^{1}H-NMR, spectra[9,38] and average elemental composition,[13] showing comparatively lower aromaticity values in BrC. $NaBH_4$ reduction caused an increase in FI values for all HS and brown carbon. The would suggest that either the origin of the samples changed, which could not be the case, or that the aromaticity of each sample decreased. As mentioned above, the FI correlation to aromaticity should not be exaggerated, as geochemical processes can alter the relationship. $NaBH_4$ reduces aromatic carbonyls, and it is proposed in Chapters 2 and 3 that shifts in fluorescence maxima is due to a disruption of charge transfer interactions that quench short wavelength fluorescence.

7.4.4 Humification Index

The humification index (HIX), based on the location of the fluorescence emission spectra, comparing the area of two spectral regions from the emission scanned at excitation λ_{ex} = 254 nm. The index is calculated by dividing the long wavelength region λ_{em} = (435 - 480) nm by the area of the short wavelength region λ_{em} = (300 - 445 nm). HIX is used to investigate the extent of humified material in dissolved organic matter. Humification can be associated with a decrease in the H/C ratio[39,40] and with a resulting shift to longer emission wavelengths, thus the HIX index was developed based on emission spectra in order to estimate the degree of maturation of DOM.[21]

When the degree of aromaticity of DOM increases, the emission spectrum (at λ_{ex} = 254) is red shifted, which increases the HIX index. High HIX values ($\sim 10 - 16$) correspond to high fluorescence intensity at long wavelengths and the presence of complex molecules, such as high molecular weight aromatics. Low HIX values (<4) are associated with a low degree of humification, and often times a biological origin.[23] Low HIX values indicate a change in organic matter source and a removal of terrestrial material, which could result from photodegradation.

The present samples were mostly similar with a few outliers (PPFA, and SRFA) that were questionable (values > 40) and were excluded (Figure 7.7). All the samples could be described as moderate to high HIX values, with the BrC samples showing the lowest values (usually $\sim$ 4). SRFA, and PPHA showed the highest HIX nonoutlier-values. Though there are few published comparisons between different HS types, Zsolnay et al.[21] found that aquatic fulvic had a higher degree of humification, by

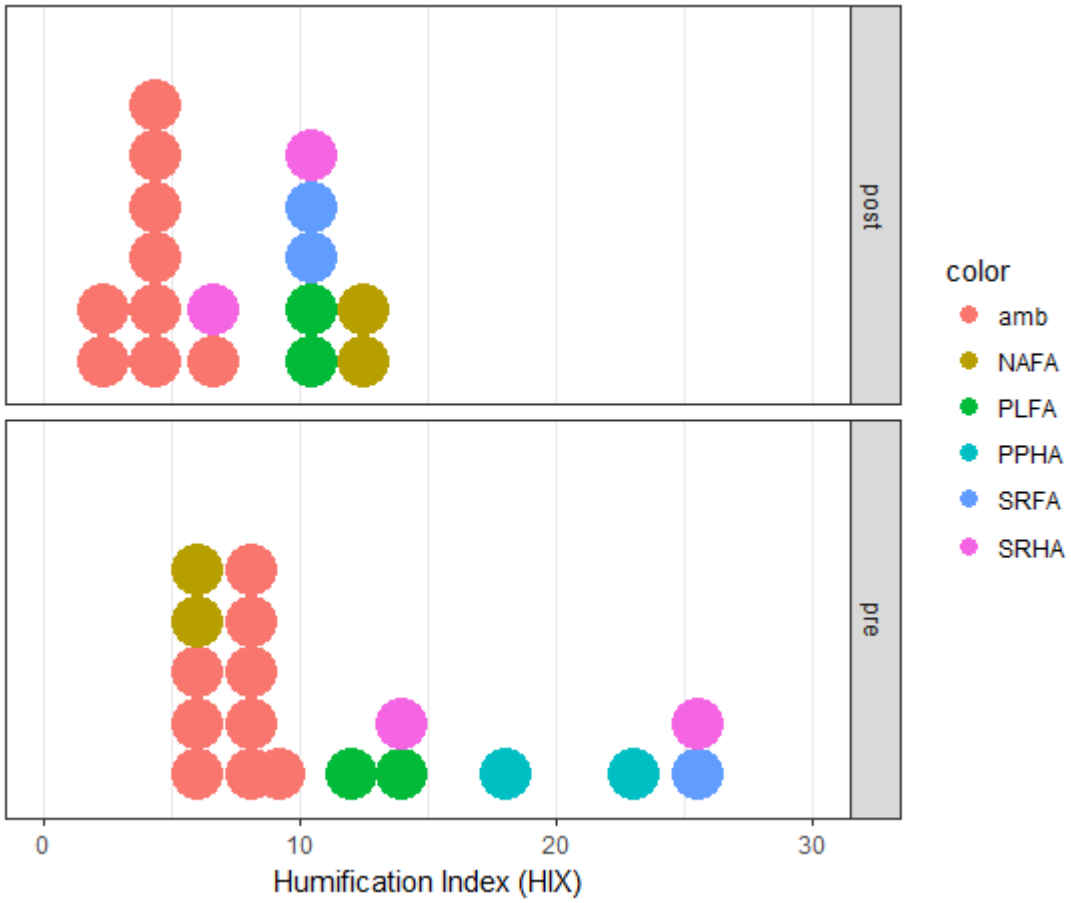

Figure 7.7: Histogram of the humification index (HIX) of ambient brown carbon and several standard humic and fulvic acids. PPFA and SRHA samples were outliers (> 40) and were excluded from the plots.

their index value, than soils. In this study the terrestrial Pahokee Peat samples were all outliers pre-reduction, and thus couldn't be compared in that regard. NAFA and PLFA aquatic samples are much lower than SRFA, which has higher likelihood of terrestrial contribution as the Suwannee River drains the Okeefenokee swamp. The BrC samples are the lowest values observed. This is in line with the high FI values for BrC, suggesting lower levels of aromaticity.

Interestingly, $NaBH_4$ reduction resulted in an increase in HIX values for all samples except NAFA, which decreased from ~ 12 to ~ 6. An increase in HIX suggests a increase in humification, or a blue-shifting of the α' emission peak. Visual assessment of the EEM's suggest that the α' emission peak blue-shifts in all samples, however for many samples this blue-shifting of the peak resulted in the peak moving within the range of the short-wavelength region in the HIX calculation. This results in an increase in the HIX index upon blue-shifting, and thus a perceived increase in extent of humification. This appears to be a shortcoming of the HIX index.

7.4.5 Biological Index

The fluorescence index BIX is used to determine the extent of biological activity in samples. Its calculation is based on the broadening of the emission fluorescence spectrum due to the presence of the β fluorophore. The BIX index is calculated at $\lambda_{ex} = 310$ nm, by dividing emission intensity at 380 nm by the emission intensity at 430 nm.

High BIX values (>1) correspond to a primarily biological origin of DOM and to the presence of fresh organic matter. The HS samples and the BrC samples measured

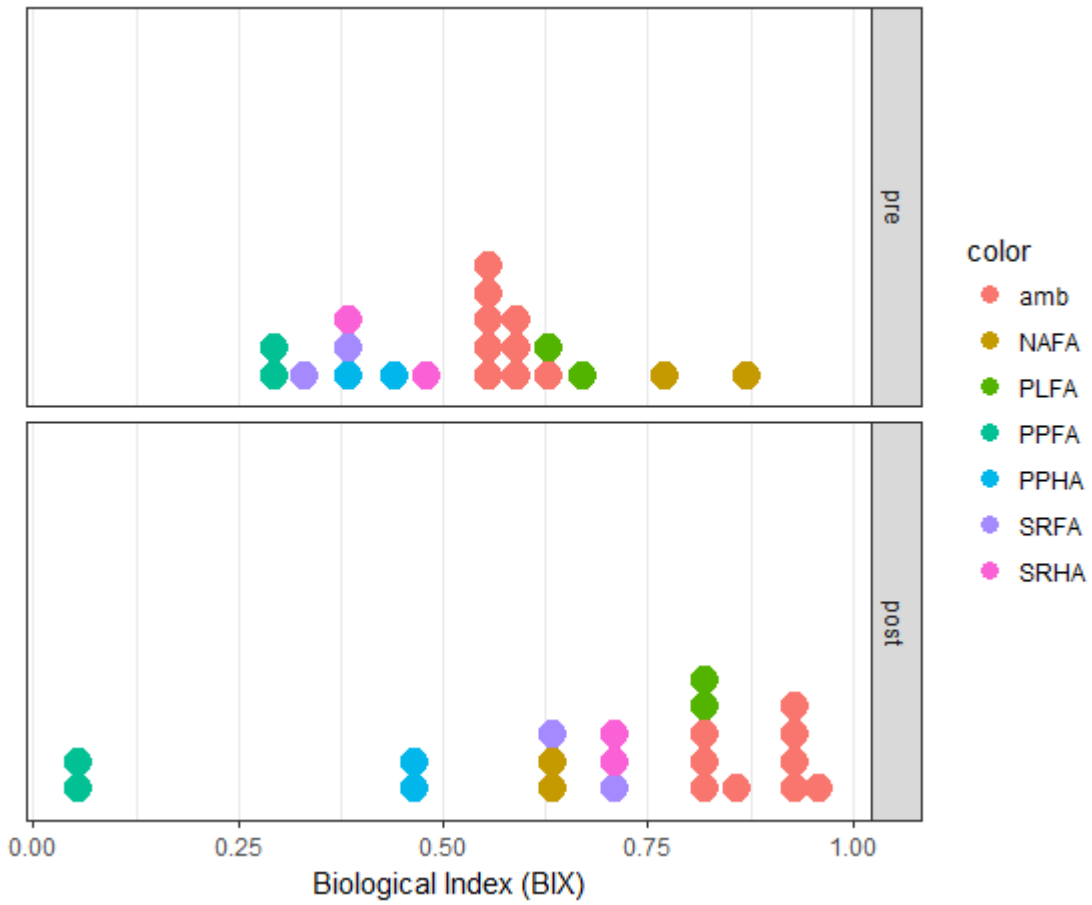

Figure 7.8: Histogram of the biological index (BIX) of ambient brown carbon and several standard humic and fulvic acids.

before and after reduction all resulted in BIX values <1. Prior to reduction the BrC samples were in the middle of the range of HS, with two fulvic acids, PLFA and NAFA, having higher BIX values. This is unsurprising, as NAFA comes from a highly eutrophic Nordic pond, and PLFA is purely microbially derived fulvic acid from a eutrophic, saline coastal pond.[41] Post-reduction BIX values are plotted, however little meaning was assigned to them as reduction does not inherently change the origin or biological content of the samples.

7.4.6 E_2/E_3

BrC and CDOM share UV-visible absorption spectra that increase approximately exponentially with decreasing wavelength.[42,43] To extract information from CDOM spectra, several groups have defined spectral parameters from absorption ratios. These ratios are largely independent of concentration, which is convenient when concentrations are unknown. The E_2/E_3 ratio (A_{250}/A_{365}) has been used to track changes in relative size of DOM molecules[44] because of stronger light absorption by high-molecular-weight CDOM at longer wavelengths.

The brown carbon samples have the highest E_2/E_3 ratio, with SRFA and SRHA values very close to BrC (Figure 7.9). This is consistent with the belief that BrC HULIS is smaller in molecular weight and size than HS. A higher E_2/E_3 ratio corresponds with a faster decrease in absorption, and thus a lower molecular weight. PPFA and PPHA had the lowest E_2/E_3 ratio, which suggests they had the highest molecular weight of the samples measured in this study. $NaBH_4$ resulted in an increase in the E_2/E_3 ratio in almost all samples. This would imply that reduction

decreases the molecular weight or size of samples. Though reduction could disrupt large supramolecular aggregates loosely held together by CT interactions, it is also possible that the decreased absorbance caused by reduction increased the error associated with the measurements. SRFA was the only sample to decrease in value after reduction, however, due to the nature of indices based on single wavelength ratios, it is probable that this shift is within the range of error associated with the index.

7.4.7 E_4/E_6

The E_4/E_6 takes the ratio of absorbance values at 465 nm and 665 nm to provide an estimation of particle size or molecular weight.[17] Secondary relationships are observed between the ratio and pH, O, C, CO_2H contents, and total acidity though it's not directly related to the relative concentration of condensed aromatic rings.[17] However, these secondary relationships are also functions of molecular sizes in HS. For the E_4/E_6, Soil HA's can range from 3.0-5.0 and FA's range between 6.0 and 8.5, though the values vary for humic materials extracted from different soil types.

E_4/E_6 is governed primarily by particle sizes and weights. Surprisingly, the lowest E_4/E_6 belonged to BrC samples, which would suggest that they have higher molecular sizes than the HS (Figure 7.10). Additionally, the highest E_4/E_6 value belonged to SRHA, which suggests that its molecular size is smaller than that of SRFA, and chemical reduction resulted in entirely inconsistent effects, with some samples remaining the same, some increasing, and others decreasing in value. These results are contradictory to other fluorescence and absorbances in the present study as well as published work. The most likely cause for this discrepancy is the weak signals

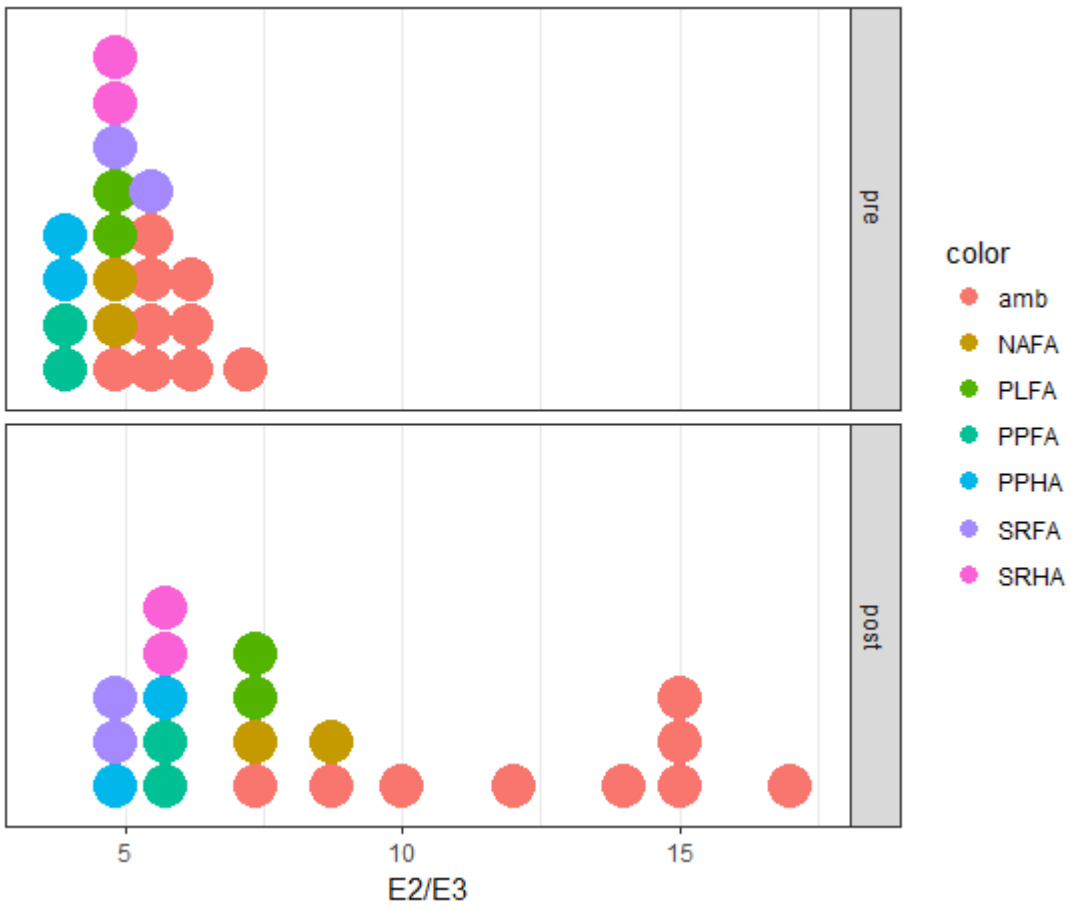

Figure 7.9: Histogram of the E_2/E_3 ratio of ambient brown carbon and several standard humic and fulvic acids.

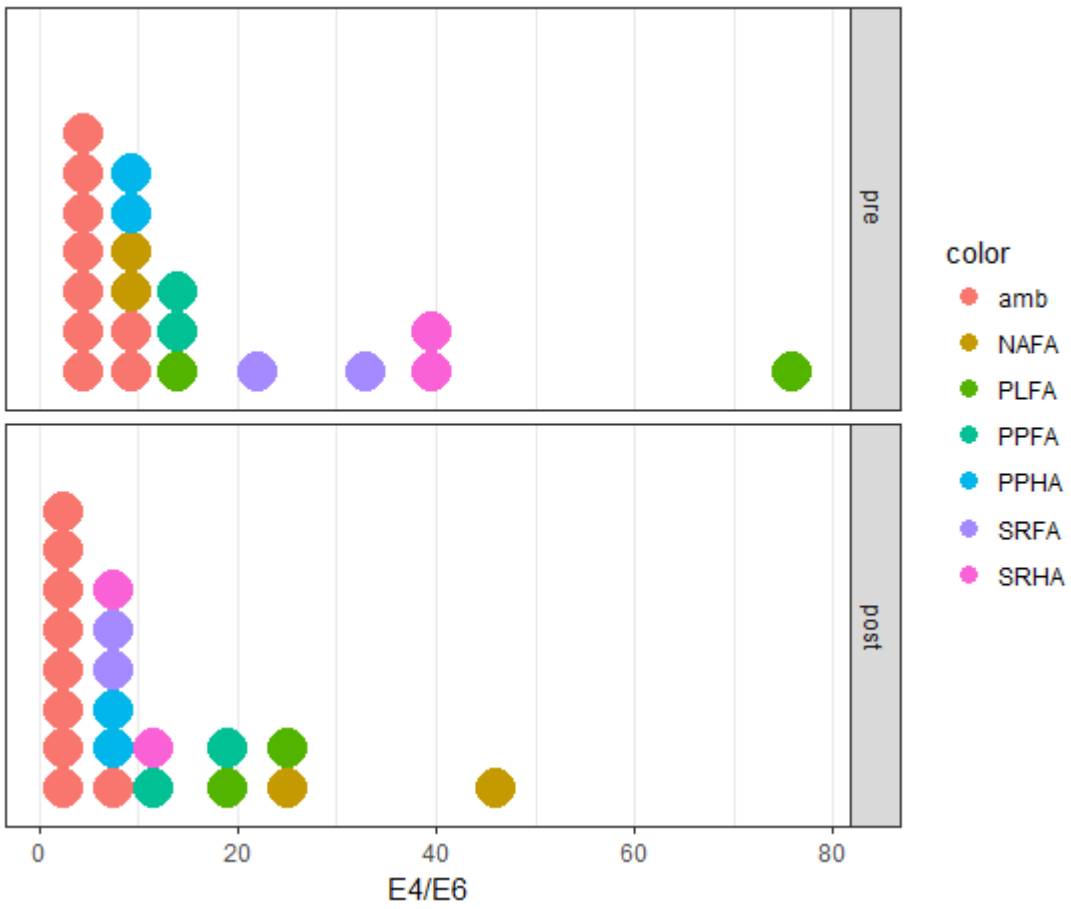

Figure 7.10: Histogram of the E_4/E_6 ratio of ambient brown carbon and several standard humic and fulvic acids.

at both absorbance values used to calculate the index. There is very little signal in BrC and most HS at 465 nm, and no or almost no signal at 665 nm in all the samples. With this is mind, it is surprising that the data are not more scattered, however we nonetheless ascribe little weight to the E_4/E_6 ratio. Since this index was first proposed,[17] several other indices have been created to avoid shortcomings of the E_4/E_6 ratio, and all ratios that rely on single wavelength points. They are described below.

7.4.8 Spectral shape indices

Explanation of indices

S exponential

The spectral slope (S, nm^{-1}) has been derived from CDOM absorption spectra by fitting the absorption data to the equation:

$$a_\lambda = a_{\lambda_{ref}} e^{-S(\lambda - \lambda_{ref})} \tag{7.1}$$

where a = absorption coefficient, λ = wavelength (nm), and λ_{ref} = reference wavelength (nm).[43] Spectral slopes provide more insights into the average characteristics of CDOM than individual wavelengths or wavelength ratios, which are subject to noise error and do not represent overall spectral shape. S correlates strongly with molecular weight of fulvic acids, but is less representative of molecular weight in humic acids.[45,46] S exponential values are discussed below.

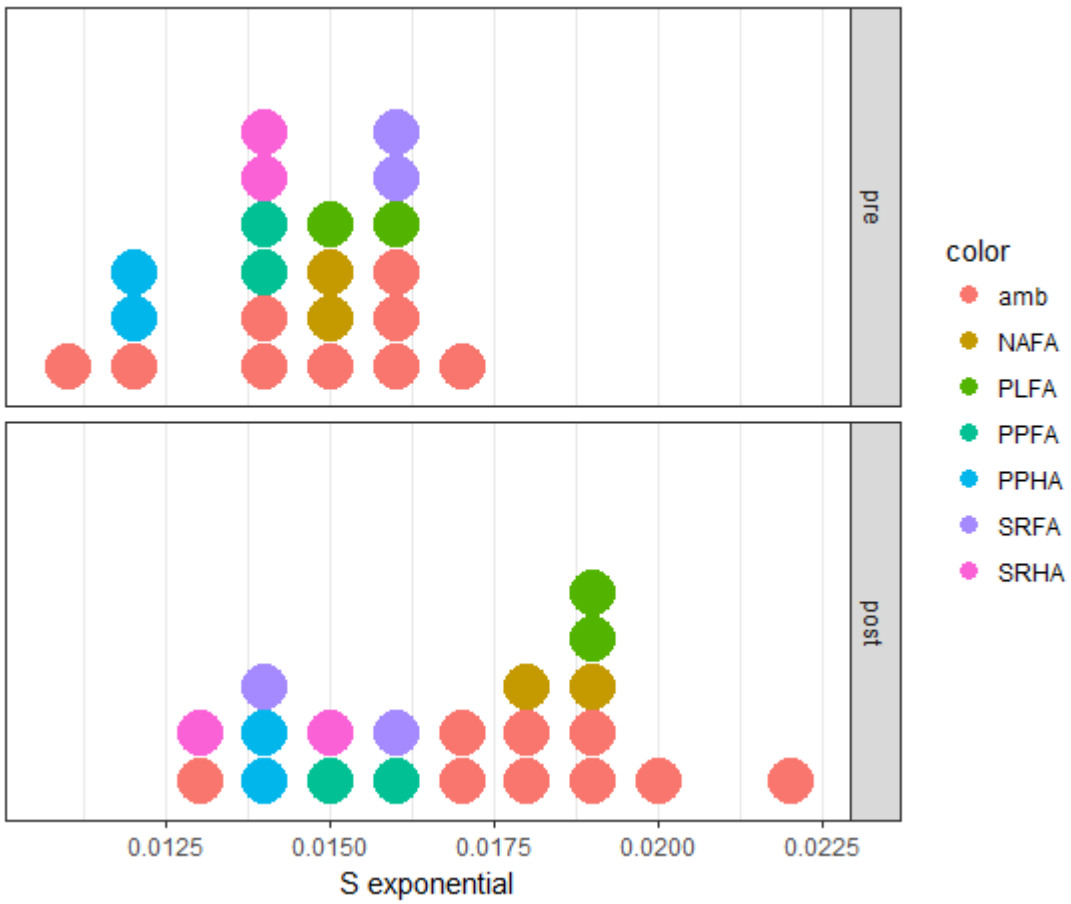

Figure 7.11: Histogram of the S exponential fit of ambient brown carbon and several standard humic and fulvic acids.

AAE

AAE fits are common to the atmospheric community, but are not commonly used to describe HS. AAE is a power law fit, and is defined in Equation 4.1. These fits have been described extensively in Chapters 2-5. AAE values are discussed below.

S_r

Helms et al.[24] developed a slope ratio (S_r) to standardize spectral slope measurements, avoid the use of data near the detection limit of instruments used, and avoid complicated corrections and calculations needed to determine EEM's. They found that the ratio of two spectral slope regions (275-295 nm and 350-400 nm) within log-transformed absorption spectra were related to DOM molecular weight on the basis of size-fractionation studies (ultrafiltration and gel filtration chromatography). These two regions appear applicable to a wide variety of water types, including DOM-rich terrestrial, estuarine, and coastal waters, as well as highly-photobleached, DOM-poor open oceanic water. The short wavelength range (275-295 nm) appears particularly sensitive to shifts in molecular weight and DOM sources, whereas the use of broader wavelength ranges may not be as sensitive to shifts caused by differences in molecular weight of DOM sources.

Discussion of spectral shape indices

The S exponential and AAE fits use different fitting equations (exponential versus power law) however the resulting trends among the HS and BrC samples studied are equivalent. In the S exponential, the BrC samples span the range of HS values, which is true for the AAE fits as well (Figures 7.11 and 7.12). Among the HS samples,

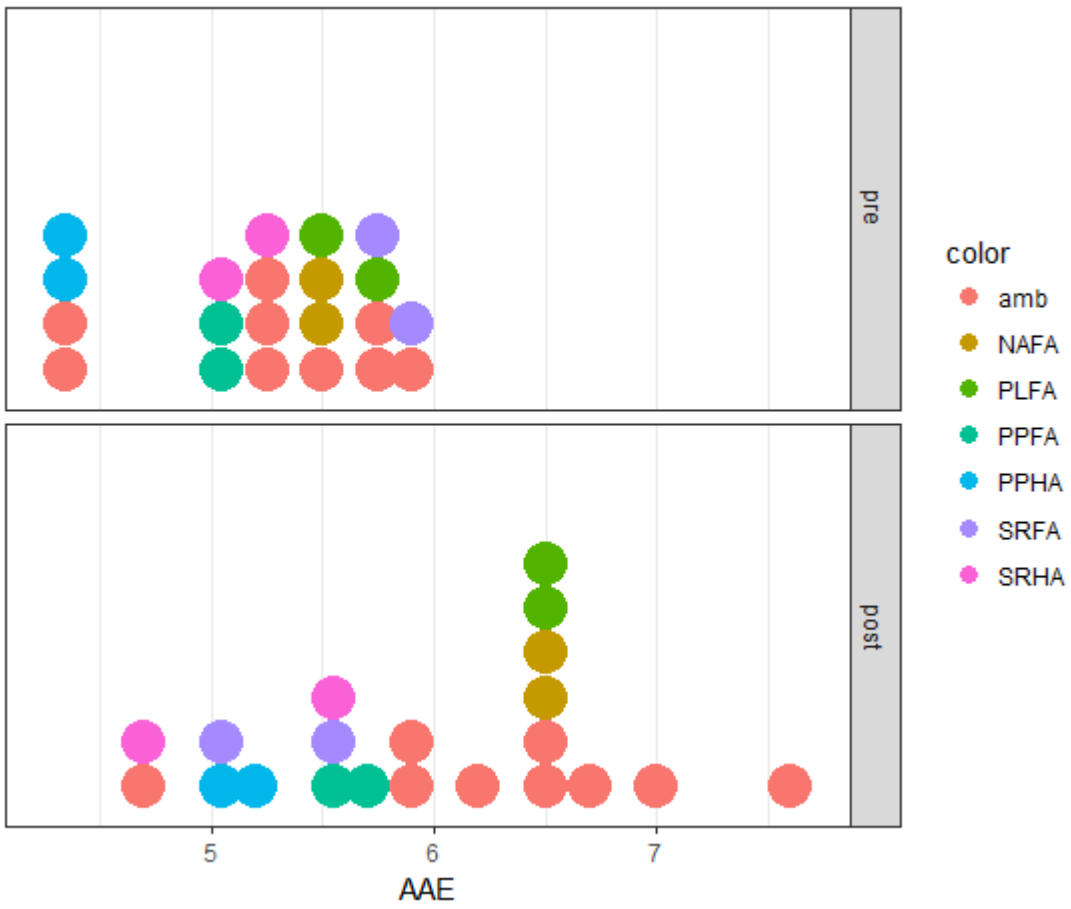

Figure 7.12: Histogram of the AAE fit of ambient brown carbon and several standard humic and fulvic acids.

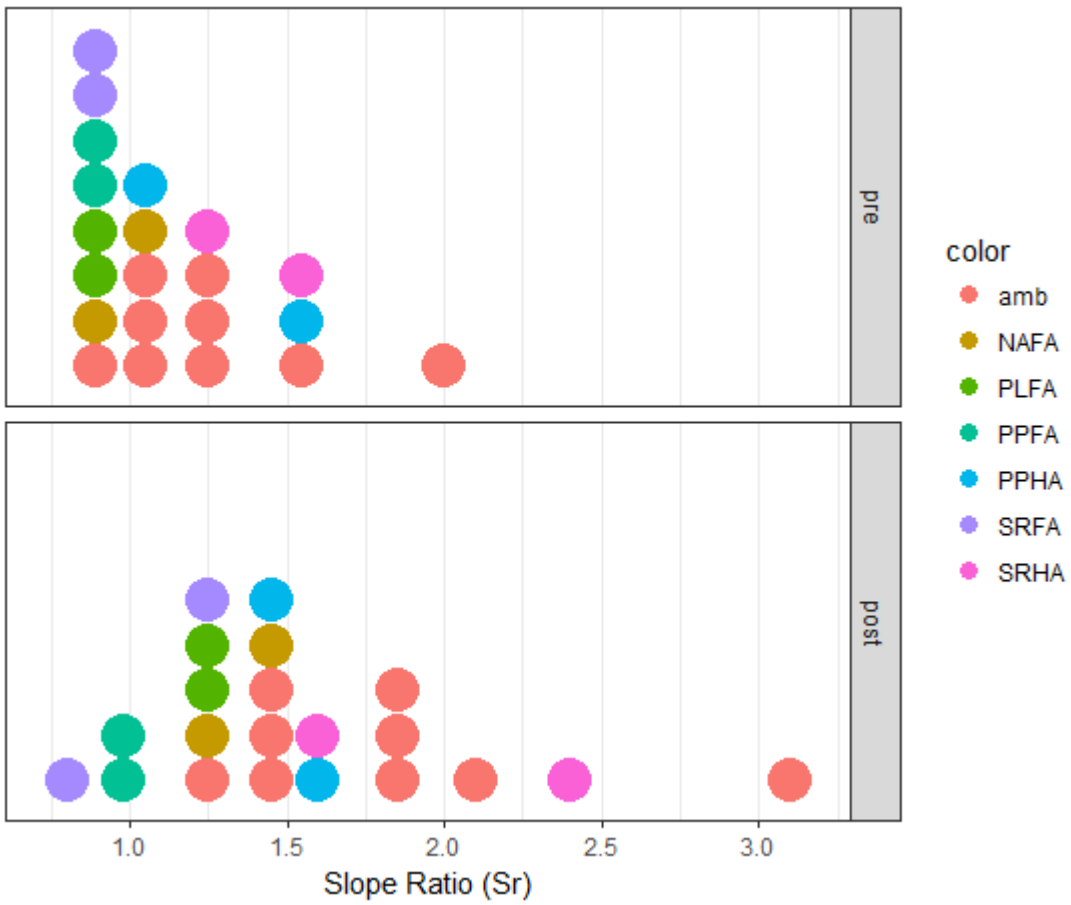

Figure 7.13: Histogram of the slope ratio (S_r) of ambient brown carbon and several standard humic and fulvic acids.

SRFA and PLFA have the highest values for S and AAE. This is indicative of those samples having small molecular weights, as has been observed extensively.[19,47] Low values correspond with high molecular weight in the S and AAE indices, and the lowest values belonged to PPHA and SRHA, the two humic acids studied. This is also consistent with literature values.[47–50] It is surprising that there are BrC values for the S and AAE fits that are as low as PPHA and SRHA. BrC samples are expected to have molecular weight profiles lower than even that of the lowest weight fulvic acids. This most likely can be attributed to the variability in sample for BrC and other differences not reflected in the molecular size.

Similar to the AAE fits that are common in the atmospheric studies, S depends on the wavelength region over which it's fit as well as fitting method (i.e. non-linear fit vs. linear fit of log-transformed data). Lack of standardization has led to a range of published values and contradictory conclusions. Because of this, Helms et al.[24] proposed the S_r approach for parameterizing DOM absorption spectra. They found that S_r was inversely related to the molecular weight of the DOM in a sample over a broad molecular weight range. Though there was a potential for higher sensitivity to change with the S_r index, it appears that the S and AAE are more accurate with regard to molecular weight. Like the S and AAE fits, in the S_r the BrC values spanned the range of HS. Additionally, the lowest S_r values (corresponding to highest molecular weight) belonged to the SRFA, PPFA, and PLFA HS. This is in contradiction to the characteristics of fulvic and humic acids, where fulvic acids are defined as smaller in molecular weight than their counterparts. The SRHA and PPHA samples had the highest values of the HS, which corresponds to low

molecular weight. $NaBH_4$ reduction resulted generally in an increase in all samples for S exponential, AAE, and S_r, however the extent of magnitude was inconsistent within index and even within sample duplicates.

7.4.9 HS indices as a gauge of charge transfer

As mentioned above, $NaBH_4$ reductions were employed to remove contribution of charge transfer complexes in HS and BrC samples, in hopes of finding an index the represents CT. The indices are plotted in relation to % absorbance loss in Figure 7.14 and show the wide range of variability associated with each index. The spread of data in the plots makes it difficult to exclude particular outliers, and more datapoints could potentially fill in gaps, however preliminarily it appears that the FI or the S_r are the most promising indices, assuming that more data be collected to decrease the error and importance of outliers.

7.4.10 Uncorrected Matrix Correlation (UMC)

The UMC values for fluorescence EEM's have been used to investigate the effect of ionic strength, pH, concentration, and sample origin on HS standards.[18] Here, UMC comparisons were used to note the similarity of fluorescing species in HS and BrC, independent of magnitude. Average UMC values comparing HS reproducibility (one HS compared to itself) and HS similarity to BrC (10 averaged UMC values between HS and a BrC sample) are shown in Table 7.2. HS reproducibility of same HS sample comparisons in this study resulted in UMC values 0.998 ± 0.001, which denotes a high level of correlation (a UMC value of 1.0 indicates the two matrices are identical).

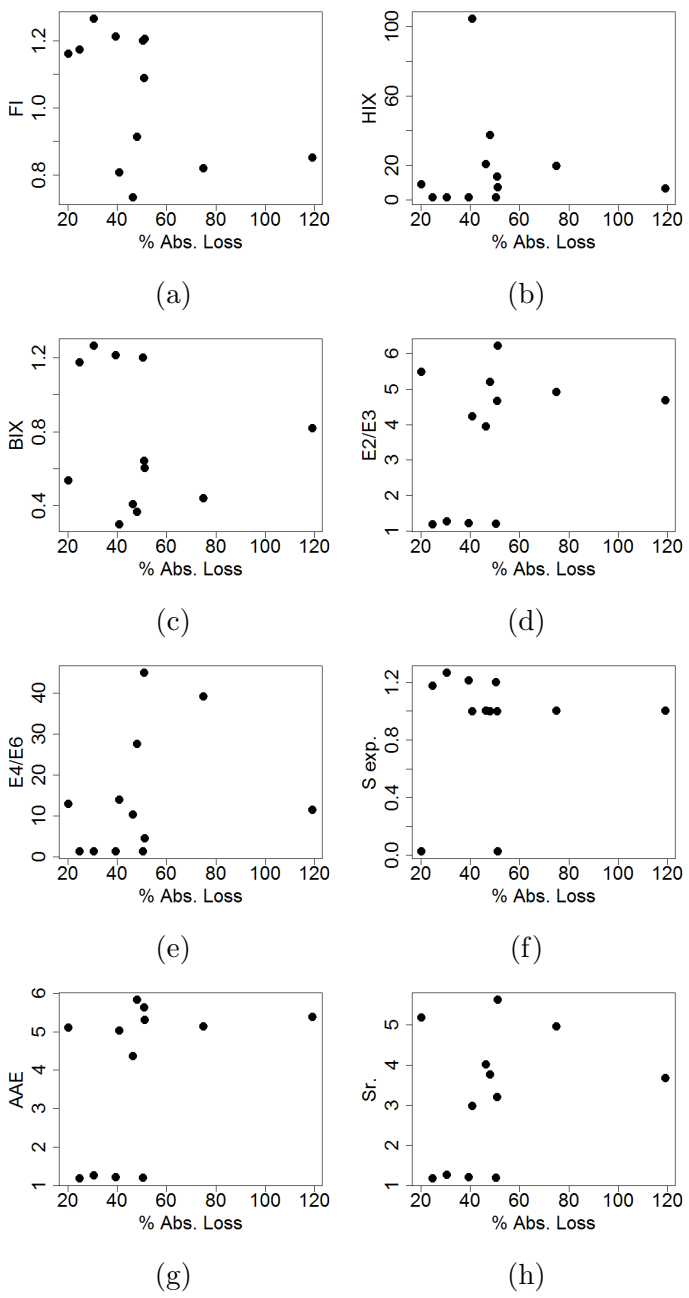

Figure 7.14: Correlation plots comparing each HS index with fractional aborbance loss after reduction with $NABH_4$.

Table 7.2: UMC values for HS sample duplicates (HS sample compared to itself) and averaged UMC values for each HS sample compared to 10 BrC samples. All include UMC's prior to and following reduction with $NaBH_4$.

	HS - HS reproducibility		HS - BrC (10 samples)	
Sample	Pre $NaBH_4$	Post $NaBH_4$	Pre $NaBH_4$	Post $NaBH_4$
NAFA	0.997	0.997	0.901	0.928
PLFA	0.999	1.000	0.935	0.931
PPFA	0.999	0.998	0.846	0.564
PPHA	0.999	0.999	0.790	0.817
SRFA	0.999	0.962	0.910	0.783
SRHA	0.997	0.882	0.911	0.884

Individual comparisons between duplicate HS EEM's as well as a comparison between each HS can be found in Table 7.3.

UMC's were also used to compare each HS standard to each BrC day. The individual values can be seen in Table 7.4. On average, PLFA fluorescence EEM appeared most similar to those of the 10 BrC samples (UMC = 0.935), though the values are clearly much lower than the HS reproducibility, indicating differences in the relative intensities or peak locations in the EEM's. PPFA and PPHA were the two lowest UMC's in comparison to BrC samples (0.846 and 0.790, respectively). This is unsurprising due to the visual differences in the EEM's for the PPFA and PPHA samples (Figures 7.4a and 7.4c). In the Pahokee Peat EEM's the β peak is much more intense relative to the α peaks than in any other samples, and the β peak in the PPHA appears to be blue-shifted in excitation wavelength such that it is almost indistinguishable from the α' peak. UMC individual comparisons between

samples before and after reduction with $NABH_4$ can be found in Tables 7.5 and 7.6, however they were not analyzed in BrC-HS comparisons.

7.5 Conclusions

The absorption and fluorescence indices and the UMC comparisons have been employed as an easy and effective means for comparing HS, as well as quantifying several HS characteristics such as average molecular weight, extent of humification, and sample origin, to name a few. These indices were measured for HS samples and several BrC samples in an attempt to uncover correlations to extent of CT complexes, and to determine where BrC lies in relation to various HS. Discrepancies between published values and measured values in this study were observed for some of the HS for several indices. This most likely can be attributed to inconsistent processing of data. For example, in this study all fluorescence spectra were corrected for inner filter effects. A study of the effects of inner filter corrections has led to an increased use in the field,[18] however some initial published values may be uncorrected. For this reason multiple HS indices were reproduced, instead of comparing BrC values to literature values.

General trends were apparent among the indices, with a few exceptions. The FI, HIX, and E_4/E_6 ratio all showed NAFA as the most similar or one of the most similar HS to BrC, suggesting that NAFA size and origin is similar to BrC. PLFA was very similar to BrC samples for the FI, HIX, and BIX indices, and its EEM was most similar, as evidenced by the UMC values. In almost every index, PPHA or PPFA were the furthest HS value from BrC, including the UMC comparisons. Interestingly,

the non-linear fits, which were supposed to be superior methods of describing spectra due to a greater representation of points and less associated noise, seemed to have the biggest variability with regard to BrC values. In the non-linear fits BrC values spanned the entire range of HS values, making it impossible to make a meaningful comparison to the HS standards.

Much like with humic substances, the fluorescence and absorption spectra and the indices calculated therein could potentially be used in conjunction with other chemical information and air quality data to infer brown carbon characteristics relevant to atmospheric impacts and radiative forcing. In future work, a more exhaustive collection of humic and ambient samples could potentially aid in better correlation between a few indices, namely FI and S_r, and contribution of charge transfer. Secondly, further work and additional indices could provide insight to create a new index that represents the relative amount of charge transfer contribution to light absorption. If successful, an absorption or fluorescence index with high correlation to fractional absorption loss after reduction could provide insight into extent of charge transfer without the need for chemical reductions.

Table 7.3: UMC values for IHSS samples (50 mg/L, pH 7.0)

Sample	NAFA1	NAFA2	PLFA1	PLFA2	PPFA1	PPFA2	PPHA1	PPHA2	SRFA1	SRFA2	SRHA1	SRHA2
NAFA1	1	0.996966	0.944468	0.95058	0.889293	0.885075	0.881478	0.892464	0.920041	0.938076	0.94964	0.964637
NAFA2	0.996966	1	0.963308	0.968582	0.915223	0.911891	0.89954	0.910482	0.944252	0.959162	0.966429	0.978632
PLFA1	0.944468	0.963308	1	0.9988	0.94445	0.942129	0.904887	0.912238	0.987838	0.991588	0.980727	0.981378
PLFA2	0.95058	0.968582	0.9988	1	0.940315	0.939528	0.896753	0.906258	0.984359	0.989435	0.976861	0.980209
PPFA1	0.889293	0.915223	0.94445	0.940315	1	0.998676	0.975346	0.98101	0.9671	0.964672	0.969123	0.960769
PPFA2	0.885075	0.911891	0.942129	0.939528	0.998676	1	0.965782	0.973669	0.965401	0.962797	0.963022	0.956247
PPHA1	0.881478	0.89954	0.904887	0.896753	0.975346	0.965782	1	0.998593	0.918774	0.920178	0.951286	0.941453
PPHA2	0.892464	0.910482	0.912238	0.906258	0.98101	0.973669	0.998593	1	0.924507	0.926775	0.954959	0.948048
SRFA1	0.920041	0.944252	0.987838	0.984359	0.9671	0.965401	0.918774	0.924507	1	0.998681	0.984369	0.978096
SRFA2	0.938076	0.959162	0.991588	0.989435	0.964672	0.962797	0.920178	0.926775	0.998681	1	0.987958	0.984432
SRHA1	0.94964	0.966429	0.980727	0.976861	0.969123	0.963022	0.951286	0.954959	0.984369	0.987958	1	0.996702
SRHA2	0.964637	0.978632	0.981378	0.980209	0.960769	0.956247	0.941453	0.948048	0.978096	0.984432	0.996702	1

Table 7.4: UMC values for comparison between different IHSS samples and ambient brown carbon samples (pH 7.0)

Sample	amb103	amb829	amb909	amb910	amb912	amb915	amb916	amb919	amb922	amb924
amb103	1	0.996824	0.973212	0.972239	0.995686	0.990435	0.977401	0.907783	0.908416	0.908784
amb829	0.996824	1	0.983301	0.980679	0.997664	0.995802	0.985171	0.903674	0.901848	0.904736
amb909	0.973212	0.983301	1	0.994688	0.979963	0.993646	0.996614	0.910516	0.884498	0.898671
amb910	0.972239	0.980679	0.994688	1	0.982485	0.992531	0.996813	0.900036	0.866066	0.878855
amb912	0.995686	0.997664	0.979963	0.982485	1	0.994819	0.984392	0.8893	0.884649	0.886814
amb915	0.990435	0.995802	0.993646	0.992531	0.994819	1	0.995477	0.907334	0.890958	0.899016
amb916	0.977401	0.985171	0.996614	0.996813	0.984392	0.995477	1	0.910448	0.881066	0.893525
amb919	0.907783	0.903674	0.910516	0.900036	0.8893	0.907334	0.910448	1	0.976896	0.983876
amb922	0.908416	0.901848	0.884498	0.866066	0.884649	0.890958	0.881066	0.976896	1	0.996547
amb924	0.908784	0.904736	0.898671	0.878855	0.886814	0.899016	0.893525	0.983876	0.996547	1
NAFA1	0.930715	0.935054	0.924081	0.919573	0.932462	0.931247	0.917327	0.814912	0.815818	0.82371
NAFA2	0.944099	0.94869	0.932338	0.928857	0.946793	0.942991	0.927703	0.832312	0.837802	0.842633
PLFA1	0.97417	0.972582	0.93667	0.939793	0.976382	0.960438	0.940454	0.860459	0.879178	0.873868
PLFA2	0.977606	0.976943	0.942033	0.942497	0.978022	0.964155	0.944419	0.872402	0.891459	0.886637
PPFA1	0.868601	0.872258	0.843702	0.844742	0.877863	0.862574	0.842995	0.79029	0.819343	0.811593
PPFA2	0.869114	0.872523	0.84422	0.842405	0.875731	0.862057	0.842668	0.805248	0.837329	0.829264
PPHA1	0.81265	0.822242	0.806863	0.812789	0.834145	0.819699	0.801006	0.695916	0.712911	0.711275
PPHA2	0.824528	0.834547	0.819885	0.822454	0.843649	0.831291	0.812684	0.717489	0.736223	0.734895
SRFA1	0.945553	0.941391	0.899039	0.905954	0.947648	0.927739	0.907258	0.847125	0.872571	0.862775
SRFA2	0.95357	0.950541	0.911582	0.916818	0.955518	0.937817	0.917943	0.852027	0.874962	0.867252
SRHA1	0.940255	0.941752	0.920692	0.929803	0.950474	0.938987	0.925201	0.832946	0.835548	0.834383
SRHA2	0.950418	0.952632	0.93428	0.939021	0.958376	0.950145	0.936249	0.846175	0.848369	0.849106

Table 7.5: UMC values for IHSS samples after reduction with $NaBH_4$ (50 mg/L, pH 7.0)

Sample	NAFA1	NAFA2	PLFA1	PLFA2	PPFA1	PPFA2	PPHA1	PPHA2	SRFA1	SRFA2	SRHA1	SRHA2
NAFA1	1	0.996578	0.980743	0.984004	0.682526	0.674733	0.951569	0.954239	0.755566	0.893485	0.888101	0.996993
NAFA2	0.996578	1	0.988663	0.990598	0.661685	0.654024	0.939526	0.939972	0.78517	0.909819	0.897851	0.991258
PLFA1	0.980743	0.988663	1	0.999631	0.652988	0.645705	0.919023	0.916411	0.843026	0.940274	0.925572	0.971974
PLFA2	0.984004	0.990598	0.999631	1	0.663224	0.655926	0.924645	0.922665	0.830802	0.933353	0.919763	0.975703
PPFA1	0.682526	0.661685	0.652988	0.663224	1	0.997899	0.717126	0.724808	0.402865	0.513319	0.525289	0.673943
PPFA2	0.674733	0.654024	0.645705	0.655926	0.997899	1	0.70851	0.716284	0.395645	0.504989	0.516475	0.665941
PPHA1	0.951569	0.939526	0.919023	0.924645	0.717126	0.70851	1	0.999028	0.706004	0.85213	0.871976	0.957799
PPHA2	0.954239	0.939972	0.916411	0.922665	0.724808	0.716284	0.999028	1	0.686661	0.839776	0.859509	0.961204
SRFA1	0.755566	0.78517	0.843026	0.830802	0.402865	0.395645	0.706004	0.686661	1	0.962248	0.941499	0.734434
SRFA2	0.893485	0.909819	0.940274	0.933353	0.513319	0.504989	0.85213	0.839776	0.962248	1	0.985679	0.879753
SRHA1	0.888101	0.897851	0.925572	0.919763	0.525289	0.516475	0.871976	0.859509	0.941499	0.985679	1	0.882347
SRHA2	0.996993	0.991258	0.971974	0.975703	0.673943	0.665941	0.957799	0.961204	0.734434	0.879753	0.882347	1

Table 7.6: UMC values for comparison between different IHSS samples and ambient brown carbon samples after reduction with $NaBH_4$ (pH7.0)

Sample	amb103	amb829	amb909	amb910	amb912	amb915	amb916	amb919	amb922	amb924
amb103	1	0.993623	0.988593	0.988976	0.997256	0.995853	0.888691	0.987159	0.997808	0.996102
amb829	0.993623	1	0.972174	0.981775	0.994612	0.994256	0.853084	0.980562	0.99292	0.989162
amb909	0.988593	0.972174	1	0.992872	0.985729	0.986715	0.930428	0.984935	0.985165	0.989283
amb910	0.988976	0.981775	0.992872	1	0.988388	0.992496	0.925091	0.991145	0.986218	0.989937
amb912	0.997256	0.994612	0.985729	0.988388	1	0.99858	0.884965	0.981524	0.993723	0.993776
amb915	0.995853	0.994256	0.986715	0.992496	0.99858	1	0.891446	0.985994	0.992665	0.993955
amb916	0.888691	0.853084	0.930428	0.925091	0.884965	0.891446	1	0.890596	0.872292	0.883531
amb919	0.987159	0.980562	0.984935	0.991145	0.981524	0.985994	0.890596	1	0.990891	0.99361
amb922	0.997808	0.99292	0.985165	0.986218	0.993723	0.992665	0.872292	0.990891	1	0.997909
amb924	0.996102	0.989162	0.989283	0.989937	0.993776	0.993955	0.883531	0.99361	0.997909	1
NAFA1	0.953576	0.958135	0.921281	0.923157	0.963747	0.957162	0.790912	0.913236	0.948811	0.945578
NAFA2	0.957805	0.963158	0.922618	0.92313	0.964985	0.957534	0.78771	0.914003	0.952887	0.945801
PLFA1	0.961734	0.963334	0.928031	0.926147	0.964426	0.9555	0.793515	0.915843	0.956384	0.946396
PLFA2	0.961607	0.964616	0.927166	0.926438	0.965671	0.956988	0.791502	0.915825	0.956039	0.946744
PPFA1	0.586014	0.614963	0.53914	0.56672	0.619673	0.615439	0.443769	0.536247	0.571357	0.577043
PPFA2	0.579234	0.60874	0.532253	0.560304	0.612929	0.608812	0.437281	0.530144	0.564769	0.570458
PPHA1	0.839889	0.848715	0.803966	0.80865	0.860937	0.85482	0.692662	0.779064	0.826891	0.825405
PPHA2	0.844134	0.852897	0.809459	0.814426	0.865911	0.860228	0.697092	0.786547	0.831814	0.832142
SRFA1	0.760729	0.735849	0.747545	0.719143	0.745773	0.728027	0.679156	0.691733	0.75026	0.726857
SRFA2	0.868938	0.850868	0.850203	0.827146	0.8629	0.847641	0.751276	0.805611	0.861145	0.844923
SRHA1	0.861886	0.840055	0.853772	0.834804	0.859446	0.848569	0.79697	0.802219	0.849283	0.838003
SRHA2	0.951711	0.955635	0.924172	0.927814	0.962445	0.958758	0.802627	0.917331	0.946907	0.945982

Bibliography

[1] Ramanathan, V.; Crutzen, P. J.; Kiehl, J. T.; Rosenfeld, D. *Science* **2001**, *294*, 2119–2124.

[2] Liu, J.; Scheuer, E.; Dibb, J.; Ziemba, L. D.; Thornhill, K.; Anderson, B. E.; Wisthaler, A.; Mikoviny, T.; Devi, J. J.; Bergin, M. *Geophysical Research Letters* **2014**, *41*, 2191–2195.

[3] Jacobson, M. Z. *Journal of Geophysical Research* **1999**, *104*, 3527–3542.

[4] Desyaterik, Y.; Sun, Y.; Shen, X.; Lee, T.; Wang, X.; Wang, T.; Collett, J. L. *Journal of Geophysical Research: Atmospheres* **2013**, *118*, 7389–7399.

[5] Zhang, X.; Lin, Y.-H.; Surratt, J. D.; Weber, R. J. *Environmental Science & Technology* **2013**, *47*, 3685–93.

[6] Mohr, C. et al. *Environmental science & technology* **2013**, *47*, 6316–24.

[7] Lee, H. J. J.; Laskin, A.; Laskin, J.; Nizkorodov, S. a. *Environmental science & technology* **2013**, *47*, 5763–70.

[8] Graber, E.; Rudich, Y. *Atmospheric Chemistry and Physics* **2006**, 729–753.

[9] Havers, N.; Burba, P.; Lambert, J.; Klockow, D. *Journal of Atmospheric Chemistry* **1998**, 45–54.

[10] Kiss, G.; Varga, B.; Galambos, I.; Ganszky, I. *Journal of Geophysical Research: Atmospheres* **2002**, *107*, D21.

[11] Krivácsy, Z. *Atmospheric Environment* **2000**, *34*, 4273–4281.

[12] Decesari, S.; Fuzzi, S.; Facchini, M. C.; Mircea, M.; Emblico, L.; Cavalli, F.; Maenhaut, W.; Chi, X.; Schkolnik, G. **2006**, 375–402.

[13] Krivácsy, Z.; Gelencsér, A.; Kiss, G. *Journal of Atmospheric Chemistry* **2001**, 235–259.

[14] Gelencsér, A.; Hoffer, A.; Molnár, A.; Krivácsy, Z.; Kiss, G.; Mészáros, E. *Atmospheric Environment* **2000**, *34*, 823–831.

[15] Gelencsér, A.; Meszaros, T.; Blazsó, M. *Journal of Atmospheric Chemistry* **2000**, 173–183.

[16] Kiss, G.; Tombacz, E.; Varga, B.; Alsberg, T.; Persson, L. *Atmospheric Environment* **2003**, *37*, 3783–3794.

[17] Chen, Y.; Senesi, N.; Schnitzer, M. *Soil science society of america journal* **1977**, *41*, 352–358.

[18] Mobed, J.; Hemmingsen, S.; Autry, J.; McGown, L. *Environmental science & technology* **1996**, *30*, 3061–3065.

[19] Mignone, R. a.; Martin, M. V.; Vieyra, F. E. M.; Palazzi, V. I.; de Mishima, B. L.; Mártire, D. O.; Borsarelli, C. D. *Photochemistry and photobiology* **2012**, *88*, 792–800.

[20] McKnight, D. M.; Boyer, E. W.; Westerhoff, P. K.; Doran, P. T.; Kulbe, T.; Andersen, D. T. *Limnology and Oceanography* **2001**, *46*, 38–48.

[21] Zsolnay, A.; Baigar, E.; Jimenez, M.; Steinweg, B.; Saccomandi, F. *Chemosphere* **1999**, *38*, 45–50.

[22] Korak, J. a.; Dotson, A. D.; Summers, R. S.; Rosario-Ortiz, F. L. *Water research* **2014**, *49*, 327–38.

[23] Huguet, a.; Vacher, L.; Relexans, S.; Saubusse, S.; Froidefond, J.; Parlanti, E. *Organic Geochemistry* **2009**, *40*, 706–719.

[24] Helms, J. R.; Stubbins, A.; Ritchie, J. D.; Minor, E. C.; Kieber, D. J.; Mopper, K. *Limnology and Oceanography* **2008**, *53*, 955–969.

[25] Birdwell, J. E.; Valsaraj, K. T. *Atmospheric Environment* **2010**, *44*, 3246–3253.

[26] Hecobian, A.; Zhang, X.; Zheng, M.; Frank, N.; Edgerton, E. S.; Weber, R. J. *Atmospheric Chemistry and Physics* **2010**, *10*, 5965–5977.

[27] Ma, J.; Del Vecchio, R.; Golanoski, K. S.; Boyle, E. S.; Blough, N. V. *Environmental science & technology* **2010**, *44*, 5395–5402.

[28] Tucker, S.; Amszi, V.; Acree, W. *Journal of Chemical Education* **1992**, *69.1*, A8.

[29] Burdick, D. S.; Tu, X. M. *Journal of Chemometrics* **1990**, *4*, 15–28.

[30] Coble, P. G. *Marine Chemistry* **1996**, *51*, 325–346.

[31] Coble, P. G.; Green, S. A.; Blough, N. V.; Gagosian, R. B. *Nature* **1990**, *348*, 432–435.

[32] Parlanti, E.; Wörz, K.; Geoffroy, L.; Lamotte, M. *Organic Geochemistry* **2000**, *31*, 1765–1781.

[33] Phillips, S.; Smith, G. *Environmental Science & Technology Letters* **2014**, *1*, 382–386.

[34] Phillips, S. M.; Smith, G. D. *Journal of Physical Chemistry A* **2015**, *119*, 4545–4551.

[35] Senesi, N.; Rizzi, F. R.; Dellino, P.; Acquafredda, P. *Soil Science Society of America Journal* **1996**, *60*, 1773–1780.

[36] Malcolm, R. L.; MacCarthy, P. *Environ. Sci. Technol.;(United States)* **1986**, *20*, 904–911.

[37] Duarte, R. M. B. O.; Pio, C. A.; Duarte, A. C. *Analytica Chimica Acta* **2005**, *530*, 7–14.

[38] Tagliavini, E.; Moretti, F.; Decesari, S.; Facchini, M. C.; Fuzzi, S.; Maenhaut, W. *Atmospheric Chemistry and Physics* **2006**, *6*, 1003–1019.

[39] Stevenson, F. J. *Humus Chemistry*; Wiley: New York, 1982.

[40] Lűttig, G. In *Peat and Water: Aspects of water retention and dewatering in peat*; Fuchsman, C. H., Ed.; Springer Science & Business Media, 1986; p 9.

[41] Source Materials for IHSS Samples. 2016; `http://www.humicsubstances.org/sources.html`.

[42] Andreae, M. O.; Gelencsér, A. *Atmospheric Chemistry and Physics* **2006**, *6*, 3131–3148.

[43] Twardowski, M. S.; Boss, E.; Sullivan, J. M.; Donaghay, P. L. *Marine Chemistry* **2004**, *89*, 69–88.

[44] De Haan, H.; De Boer, T. *Water Research* **1987**, *21*, 731–734.

[45] Hayase, K.; Tsubota, H. *Geochimica et Cosmochimica Acta* **1985**, *49*, 159–163.

[46] Carder, K. L.; Steward, R. G.; Harvey, G. R.; Ortner, P. B. *Limnology and oceanography* **1989**, *34*, 68–81.

[47] Palmer, N.; von Wandruszka, R. *Fresenius' Journal of Analytical Chemistry* **2001**, *371*, 951–954.

[48] Piccolo, A. *Soil Science* **2001**, *166*, 810–832.

[49] Boyle, E. S.; Guerriero, N.; Thiallet, A. *Environmental Science & Technology* **2009**, *43*, 2262–2268.

[50] Chen, H.; Kenny, J. E. *Annals of Environmental Science* **2007**, *1*, 1–9.

Chapter 8

Conclusions

8.1 Summary of discussed work

Here, we identify for the first time charge transfer (CT) complexes as a significant source of light absorption by organic compounds in aerosols. A dense manifold of these complexes, formed from interactions between alcohol and carbonyl moieties, accounts for approximately 50% of the absorption (300 nm - 600 nm) observed for water-extracted ambient particulate matter. Corresponding fluorescence emission spectra with broad, overlapping long-wavelength tails are consistent with efficient energy transfer amongst a near-continuum of such coupled excited states. We postulate that a wide variety of CT complexes are formed as a result of a supramolecular association of self-assembling, smaller molecules, just as they are in natural humic substances, and that this gives rise to absorption that extends to red wavelengths where no other potential chromophores absorb. The absorption measurements in Chapter 2 imply that light absorption by organic aerosols is governed by a combi-

nation of independent as well as interacting chromophores and that both must be included in an accurate representation of aerosol optical properties.

Spectral characteristics of brown carbon fluorescence are also consistent with a model consisting of individual chromophores and a densely-populated ensemble of coupled charge transfer states, as seen in Chapter 3. In this model, short-wavelength light primarily excites the individual chromophores that transfer energy to and excite charge transfer complexes while longer-wavelength light excites the charge transfer complexes directly. In both cases, a cascade of energy transfer amongst the near-continuum of charge transfer states populates a range of complexes that are responsible for the broad fluorescence emission observed. The overlapping tails of the fluorescence spectra, the observed wavelength dependence in the emission maxima and the quantum yields, and the more intense and blue-shifted emission after reduction all substantiate the hypothesis that charge transfer complexes are a major contributor to light absorption and fluorescence in brown carbon aerosols. Furthermore, reduction by $NaBH_4$ results in incomplete removal of the charge transfer complexes suggesting that they may be responsible for even more than the 53% of UV-visible light absorption by water-soluble brown carbon that we reported previously.

Chapter 4 demonstrates that changing pH affects absorption spectra of water-soluble BrC from ambient particulate matter. Absorption increases 10% per pH unit from pH = 2 to pH = 12 with a broad, featureless tail at visible wavelengths where the largest fractional increase is also observed. The resulting change in the spectral shape causes the absorption Ångström exponent to decrease by 0.18 per unit increase in pH. Strikingly similar behavior with humic substances suggests that they

and BrC share a common physicochemical link between pH and absorption, which we propose is a consequence of changes in the supramolecular assemblies formed from organic molecules. Specifically, it is hypothesized in Chapter 4 that a wider variety and larger number of absorbing charge transfer complexes are formed as carboxylic acid and phenol moieties in these molecules become deprotonated. These findings suggest that: 1) the pH of ambient particulate matter samples should be measured or controlled, and 2) radiative forcing by aerosols could be overestimated if pH dependent BrC absorption is not accounted for.

The systematic increase in absorbance accompanying increases in pH could have implications for the role BrC plays in influencing the radiative balance in the atmosphere. If pH is not accounted for in making bulk aerosol measurements, the impact of BrC absorption on SFE can be overestimated; for example, measurements made at pH = 7 overestimate SFE by 5% - 49% (depending on kOA(550 nm) and mixing state) compared to pH = 2, a value more representative of ambient aerosol acidity in many locations, including the Southeast U.S.[1] Thus, to the extent that aerosol pH may change in the atmosphere or may vary from sample to sample, its impact on aerosol absorption and radiative forcing should be considered.

Split filters of ambient particulate matter were extracted in water and methanol in Chapter 5, and found that most methanol-soluble (MS) spectra are significantly impacted by extinction of suspended insoluble particles liberated from the filter even after filtering with a syringe filter. It appears as if particles are not liberated from the filter by water, and thus the WS spectra do not include particle extinction. A dual power law fit to the MS spectra is able to separate the MS BrC absorption

from the particle extinction adequately. Comparing the WS and MS BrC spectra demonstrated that water-soluble (WS) and MS BrC integrated absorption is highly correlated, MS BrC integrated absorption is a factor of 1.55x larger than WS integrated absorption, the spectral shapes of WS and MS BrC absorption are similar, with average AAEs of 6.13 and 6.68, respectively, and MS BrC spectra display a slight absorption enhancement at UV and near-UV wavelengths. These results furthermore suggest that a MS spectra fit using a single power law function most likely overestimates BrC absorption due to particle extinction, even when using syringe filters.

In Chapter 6, Irradiation of BrC at specific wavelength ranges resulted in photobleaching behavior similar to SRFA. These photobleaching patters can arise from the same charge-transfer model proposed in Chapter 2. A transfer of an electron from a phenol to an aromatic ketone or carbonyl moiety would account for the broad, featureless absorption spectra that extends far into the visible, and the photosensitized absorption loss is consistent with an interaction model. What is more, the violation of reciprocity of fractional absorption loss could only be explained with an absorption model much more complex than a linear superposition on non-interacting chromophores. Indeed, there are several mechanisms that could cause this intra- or intermolecular interaction, such as energy transfer, charge migration, structural reorganization, or a combination thereof. However, charge-transfer interactions have been established in humic substances and brown carbon extensively, and the presence of the necessary functional groups is highly likely in organic aerosols in the form of HULIS or biomass burning products.

Absorption and fluorescence indices were measured for HS samples and several brown carbon samples in Chapter 7, in an attempt to uncover correlations to extent of CT complexes, and to determine where BrC lies in relation to various HS. General trends were apparent among the indices, with a few exceptions. The FI, HIX, and E_4/E_6 ratio all showed NAFA as the most similar or one of the most similar HS to BrC, suggesting that NAFA size and origin is similar to BrC. PLFA was very similar to BrC samples for the FI, HIX, and BIX indices, and its EEM was most similar, as evidenced by the UMC values. In almost every index, PPHA or PPFA were the furthest HS value from BrC, including the UMC comparisons. Interestingly, the non-linear fits, which were supposed to be superior methods of describing spectra due to a greater representation of points and less associated noise, seemed to have the biggest variability with regard to BrC values. In the non-linear fits BrC values spanned the entire range of HS values, making it impossible to make a meaningful comparison to the HS standards.

8.2 Future work

Further study of photobleaching effects is of great interest, especially at additional irradiation wavelengths that could be provided by the arc lamp, and at a wider range of irradiation times, to differentiate between immediate and long-term photobleaching phenomena. Additionaly study of solar irradiation would contextualize the laboratory irradiations and possible provide insight into atmospheric lifetimes. No irradiation experiments have yet been performed on methanol extracts, and this would be of interest in the future as methanol extractions provide increased signal.

Much like with humic substances, the fluorescence and absorption spectra and the indices calculated therein could potentially be used in conjunction with other chemical information and air quality data to infer brown carbon characteristics relevant to atmospheric impacts and radiative forcing. In future work, a more exhaustive collection of humic and ambient samples could aid in creating a new index that represents the relative amount charge transfer contribution to light absorption. If successful, an absorption of fluorescence index with high correlation to fractional absorption loss after reduction could provide insight into extent of charge transfer without the need for chemical reductions.

In continuation of the investigation of local environment on brown carbon light absorption, ionic strength effects are of particular interest. Previous studies on varying ionic strength in HS have observed changes in electrostatically controlled interactions. Specifically, Na^+ cations are important for such aspects of DOM chemistry due to the supramolecular properties of DOM molecules and their aggregation.[2,3]

All of the future work detailed here could also benefit from chemical and structural information provided by high-resolution mass spectrometry. MS data has provided a wealth of information regarding structure and functionality of HS, as well as origin of sample. MS information would be particularly useful in conjunction with the above mentioned studies, for example the chemical effect of photobleaching BrC, and the aggregation effects caused by varying ionic strength.

Bibliography

[1] Weber, R. J.; Guo, H.; Russell, A. G.; Nenes, A. *Nature Geoscience* **2016**, *9*, 1–5.

[2] Baalousha, M.; Motelica-Heino, M.; Le Coustumer, P. *Colloids and Surfaces A: Physicochemical and Engineering Aspects* **2006**, *272*, 48–55.

[3] Gao, Y.; Yan, M.; Korshin, G. V. *Environmental Science & Technology* **2015**, 150421121845002.